KEMIAN LAITOS
JYVÄSKYLÄN YLIOPISTO

Photoresponsive low molecular weight gels

Master's thesis

University of Jyväskylä

Department of Chemistry

20.5.2024

Iida Nikkilä

Abstract

This master's thesis is about photoresponsive low molecular weight gels (LMWGs) formed by the self-assembly of small gelator molecules. These gels utilize weak intermolecular interactions that can be manipulated by light stimulation. Photoresponsivity is achieved by incorporating chromophoric units into the gelator molecules. Based on the type of the photoresponsive unit, the gels can undergo different kinds of photoreactions upon light irradiation, causing changes in the gel properties. The literature part focuses on useful photoreactions that can be exploited in photoresponsive LMWGs. In addition, the properties, design, characterization, and applications of these gels are discussed.

The experimental part deals with the synthesis of possible photocleavable peptide-based LMWGs functionalized with boron dipyrromethene (BODIPY). The BODIPY moiety was aimed at being linked to a peptide-based gelator *via* a carbamate bond. As a result of several attempts, one possible product was obtained. However, based on the NMR spectroscopy and HR-MS measurements, the formation of the desired compound could not be fully proven.

Tiivistelmä

Tämä pro gradu-tutkielma käsittelee valoresponsiivisia alhaisen molekyylipainon geelejä (low molecular weight gels, LMWGs), jotka muodostuvat kevyiden gelaattorimolekyylien itsejärjestäytyessä. Kyseiset geelit muodostuvat molekyylien välisten heikkojen vuorovaikutusten seurauksena, joihin voidaan vaikuttaa valostimulaation avulla. Valoresponsiivisuus saadaan aikaiseksi liittämällä gelaattorimolekyyleihin erilaisia kromoforisia yksiköitä, joiden tyypistä riippuen geeleissä tapahtuu erilaisia valoreaktioita niitä säteilytettäessä. Säteilytyksen seurauksena saadaan aikaiseksi erilaisia vasteita, jotka vaikuttavat geelien ominaisuuksiin. Kirjallisuuskatsauksessa keskitytään erityisesti erilaisiin valoreaktioihin, joita voidaan hyödyntää valoresponsiivisissa alhaisen molekyylipainon geeleissä. Lisäksi perehdytään kyseisten geelien ominaisuuksiin, suunnittelemiseen, karakterisointiin and sovelluksiin.

Kokeellisessa osassa keskitytään mahdollisten valokatkeavien BODIPY-pohandisten alhaisen molekyylipainon geelien synteesiin. Tavoitteena oli valmistaa yhdisteitä, joissa BODIPY-osa olisi liitettynä peptidipohjaisiin gelaattorimolekyyleihin vihreän valon avulla katkeavan karbamaattisidoksen välityksellä. Useiden yritysten seurauksena saatiin aikaiseksi yksi mahdollinen tuote. Mitattujen NMR- and HR-MS-spektrien perusteella halutun yhdisteen muodostumista ei kuitenkaan voitu täysin todistaa.

Preface

The experimental part of this master's thesis was started in September 2023 and completed in December 2023. The experimental work was carried out at the Nanoscience Center at the University of Jyväskylä. The literature part was written during spring 2024 and the thesis was completed in May 2024. The literature search was done using Web of Science and Google Scholar databases. Professor Maija Nissinen supervised this master's thesis, and doctoral researcher Elsa Korhonen supervised the experimental part. I would like to thank my supervisors for instructing and helping me throughout the process. I would also like to thank Kaisa Helttunen for acting as the second reviewer of my thesis.

Table of contents

Abbreviations

Ala	Alanine
Arg	Arginine
Asp	Aspartic acid
Boc	*tert*-butyloxycarbonyl
BODIPY	Boron dipyrromethene, 4,4-difluoro-4-bora,3a,4a,diaza-s-indacene
CDI	Carbonyl diimidazole
DCM	Dichloromethane
DIPEA	*N,N*-diisopropylethylamine
DMF	Dimethylformamide
DMSO	Dimethyl sulfoxide
dsDNA	Double-stranded deoxyribonucleic acid
ESI	Electrospray ionization
EtOAc	Ethyl acetate
GdL	Glucono-d-lactone
Gln	Glutamine
Gly	Glycine
H-H COSY	H-H correlated spectroscopy
HMBC	Heteronuclear multiple bond correlation
HR-MS	High-resolution mass spectrometry
HSQC	Heteronuclear single quantum coherence
IR	Infrared
LED	Light-emitting diode
Leu	Leucine
LMWG	Low molecular weight gel

Lys	Lysine
MC	Merocyanine
MeOH	Methanol
MGC	Minimum gelation concentration
***n*-hex**	*n*-hexane
NMR	Nuclear magnetic resonance
PEG200	Polyethylene glycol 200
Phe	Phenylalanine
PPG	Photoremovable protection group
RT	Room temperature
SEM	Scanning electron microscopy
Ser	Serine
SP	Spiropyran
***t*Bu**	*tert*-butyl
***t*BuOAc**	*tert*-butyl acetate
TBTU	2-(1H-benzotriazole-1-yl)-1,1,3,3-tetramethylaminium tetrafluoroborate
TEA	Triethylamine
TEM	Transmission electron microscopy
TFE	2,2,2-Trifluoroethanol
THF	Tetrahydrofuran
TLC	Thin-layer chromatography
Tyr	Tyrosine
UV	Ultraviolet
VIS	Visible light

LITERATURE PART

1 Introduction

Gels can be found in many different forms in our everyday lives. They can come across in commercial products such as toothpaste, soap, shampoo, hair gel and other cosmetics. Traditionally, these gels are derived from polymeric compounds. For many decades, polymeric gels have been utilized in applications in fields such as the food industry, medicine, and material science. During the past few decades, supramolecular gels derived from low molecular mass compounds have been studied extensively, and their suitability for applications similar to those of polymeric gels has been envisioned.[1]

In general, gels are viscoelastic soft materials consisting of immobilized solvent molecules encapsulated by entangled three-dimensional cross-linked structures. Classification of gels depends on their composition, the type of cross-linking that forms their three-dimensional network and the medium they comprise.[2] Unlike traditional gels consisting of covalently cross-linked polymeric chains, supramolecular gels are formed by non-covalent intermolecular interactions. This category includes low molecular weight gels (LMWGs) formed by the self-assembly of small gelator molecules. Self-assembly may be driven by a combination of weak interactions, such as hydrogen bonding, π–π stacking, metal coordination, hydrophobic interactions, and van der Waals interactions, to name a few. One of the main advantages of LMWGs is their dynamic nature, which enables reversible tunability with various external stimuli, such as pH, temperature, mechanical stress, and light.[3]

Light as a stimulus has attracted a lot of attention in designing soft “smart” materials due to its capability of remote manipulation and inherent spatial and temporal control. Photoresponsive LMWGs contain a photoresponsive unit that absorbs light, leading to a photoreaction. Interaction of photoresponsive LMWGs with light can result in various responses, some of which can be observed with the naked eye. These responses include gel-to-sol and gel-to-gel phase transitions, photochromic switching, and changes in morphology and electronic properties.[4] Useful photoreactions in these gels include isomerization, ring opening and closing, dimerization and polymerization, and bond cleavage.

2 Low molecular weight gels

2.1 Classification of gels

IUPAC defines a gel as a "non-fluid colloidal network or polymer network that is expanded throughout its whole volume by a fluid."[5] In other words, gels consist of immobilized solvent molecules entangled by a three-dimensional solid network. The composition of gels is mainly liquid, although they exhibit many properties of a solid, and are therefore classified as semi-solid systems. Gels can be defined as hydrogels or organogels based on what kind of medium they comprise; organogels consist of organic liquids and hydrogels of water or aqueous solutions.[2]

Gels can be formed through chemical cross-linking or supramolecular interactions (Figure 1).[4] In polymeric gels, the cross-links are formed through permanent covalent bonds. Such gels are thermally irreversible and cannot be redissolved. Supramolecular gels form three-dimensional entangled networks in a given solvent by employing non-covalent interactions. The network can be composed of entangled polymeric gelators (supramolecular polymeric gels) or self-assembled small gelators (low molecular weight gels, LMWGs).[1] The gelator molecules self-assemble into ordered aggregates, such as fibres, tapes and tubes, through weak intermolecular interactions. The most exploited interactions in these gels are hydrogen bonding, π–π stacking, metal coordination, hydrophobic interactions and van der Waals interactions. The dynamic nature of gels that form by self-assembly enables their manipulation with various external stimuli, such as light, pH or temperature.[3]

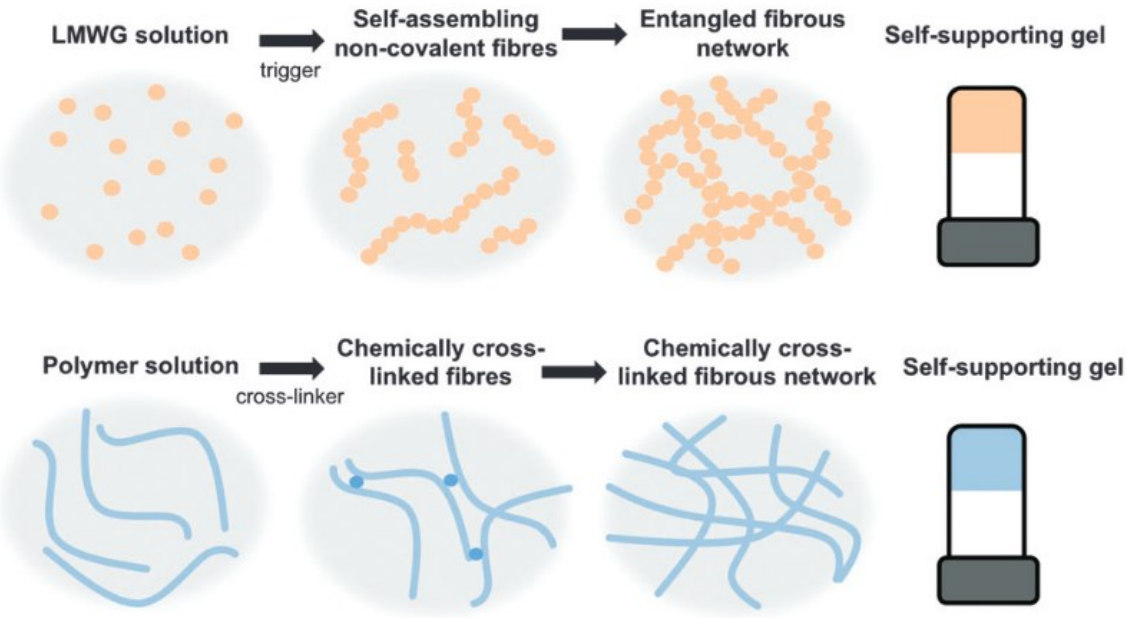

Figure 1. Gelation of low molecular weight gels formed by self-assembly (top) and polymers that form cross-links by permanent chemical bonds or entanglements (bottom). Reproduced from ref. 4 with permission from the Royal Society of Chemistry.

2.2 Photoresponsivity

Photoresponsive LMWGs are particularly interesting due to their remotely controllable nature, enabling high spatial and temporal resolution and relatively fast response times. Moreover, light is a non-invasive stimulus that does not require any additional reagents. These are important benefits over other triggers, such as pH, temperature, and chemical reactions, that usually have longer response times. Typical photoresponsive gelators are constructed from photoresponsive chromophores attached to other functional groups that promote or facilitate gelation.[4] Many photoresponsive units incorporated in these gelator molecules are conjugated systems that can promote self-assembly by π–π stacking or, in water, by hydrophobic interactions.

Photoresponsive units absorb light at specific wavelengths that provide the activation energy for photoreactions. Depending on the type of the photoresponsive unit, photoresponsive LMWGs can undergo various photoreactions, such as isomerizations (e.g. azobenzenes and stilbenes), ring opening and closing reactions (e.g. dithienylethenes and spiropyrans), dimerizations (e.g. coumarins and anthracenes), polymerizations (e.g. diacetylenes), and bond cleavage (e.g. coumarins and 2-nitrobenzyl groups). Many of these photoreactions are

reversible and can be repeated over several cycles. In most cases, the photoreactions can be initiated with UV light, allowing the formation of high-energy intermediates that could not be achieved thermally. However, the reversed reaction often occurs upon longer wavelengths or by heating.

Upon light irradiation, the gels exhibit different responses, some of which can be observed with the naked eye. These responses include gel-to-sol and gel-to-gel phase transitions, photochromic switching, changes in morphology and electronic properties. The versatility of photo-induced responses enables the photoresponsive LMWGs to be used for many applications.[4]

2.3 Designing and preparation

Although low molecular mass gelators were reported much earlier, there was a lack of understanding of the supramolecular nature of these materials. The study of low molecular weight gels was highly neglected until the end of the twentieth century.[6] Interestingly, a recurring theme among the researchers studying LMWGs is that their work often began with an unintentional finding of a specific molecule that forms a gel in a solvent. At present, several structurally diverse classes of molecules known to act as gelators have been discovered. Based on the knowledge gained on the aggregation of gelator molecules, new gelators are often designed by utilizing information about structural features known to promote gelation. For example, the incorporation of hydrogen bonding motifs, such as amides, ureas, and hydrocarbons, is very common.[1,6] Moreover, a large proportion of gelators are composed of amino acids or peptides.[7]

Although there has been development in the area, one of the biggest challenges in designing LMWGs is that the self-assembly of the gelator molecules is still poorly understood. Predicting whether a molecule will form gels can be very difficult; even structurally similar molecules can have very different propensities to form gels. To form gels, the compounds need to be soluble enough to dissolve, but insoluble enough to form suitable aggregates that can eventually entangle. Therefore, while it is clear that non-covalent interactions are a prerequisite for gelation, they are not sufficient to result in gelation. In addition to weak interactions, a balance of solubility is required. To overcome the problem of predicting gelation, various libraries and computational models have been developed.[8] Although these approaches have been

successfully used in the discovery of new gelators, they cannot be used to explain why some molecules form gels while others do not.

To form LMWGs, the gelators are initially dissolved or suspended in a highly soluble state, such as at a high temperature or in a good solvent. The self-assembly can then be initiated using a suitable trigger, such as decreased temperature, bringing the gelators to a more poorly soluble state. In addition to this heating-cooling method, the self-assembly can be triggered by sonication, a change in pH or the addition of a specific salt, to name a few.[3,4] When the gelators become less soluble, they aggregate into long fibres to minimize their interactions with the surrounding solvent. The fibres can then interact further with each other by making cross-links and entanglements, resulting in the formation of a three-dimensional network that can immobilize the solvent through surface tension and capillary forces. Low molecular weight gelators are known for their ability to form gels in relatively low concentrations. The gelation ability is usually described with minimum gelation concentration (MGC), which refers to the critical concentration at which gelation is induced. For typical LMWGs, the MGC is below 1 wt-%.[8]

2.4 Characterization

Gelation can be studied across many different length scales. To understand the gelation process, information on the molecular interactions and the three-dimensional structures formed by the aggregates is needed. Depending on the desired information, gel structures can be analyzed with a variety of techniques (Figure 2).

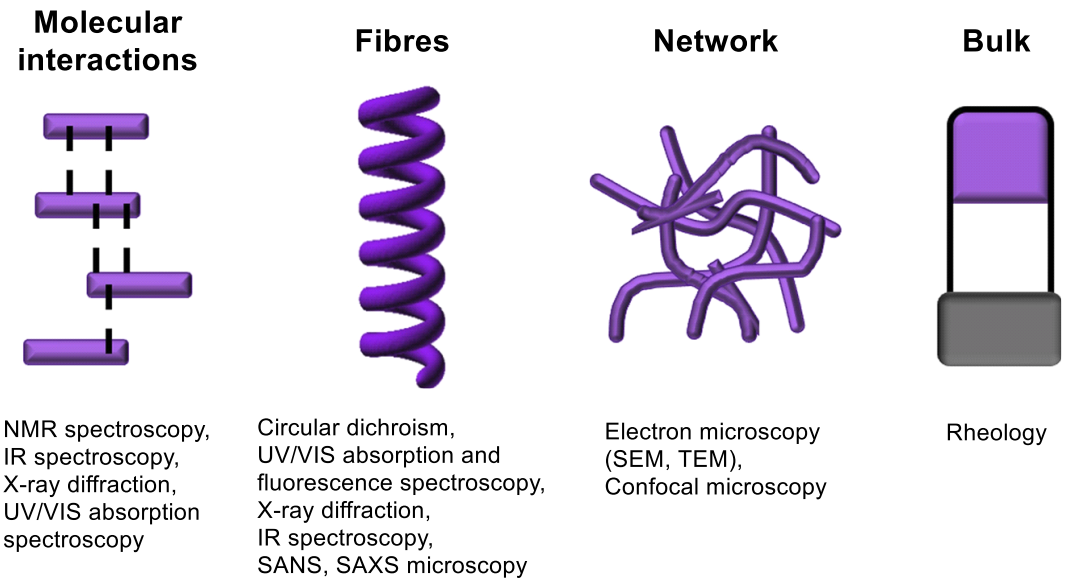

Figure 2. Examples of different techniques used for analyzing gel structures at different length scales. Reproduced from ref. 8. with permission.

2.4.1 Visual inspection

Gel formation can be visually inspected by a tube inversion test.[6] In this simple assay, the gel is prepared in a small tube, and its physical state is observed by inverting the tube upwards and determining whether the material flows under its own weight. Based on the observations, intuitive conclusions can be made about the shapes and strengths of the materials. However, this assay cannot be used to prove gel formation since viscous liquids can also be stable to invertion, though for relatively brief periods.[8] In fact, there have been studies where assumed gels have been self-supporting, but rheological measurements have shown that they are not true gels.[9]

2.4.2 Rheology

Rheology is a common method in studying the mechanical properties of gels since rheological experiments provide useful information about the structure and dynamics of the self-assembled networks. In a rheometer, the sample is applied between two plates or cylinders. Upon applying a given oscillatory strain to one of the plates, the induced movement of the other plate is resolved into in- and out-of-phase components. For soft materials that exhibit both elastic and viscous responses, parameters such as storage modulus G' and loss modulus G" are used to describe the solid- or liquid-like behavior. The energy stored during a strain cycle is measured by the storage modulus G', and the energy lost during a strain cycle is measured by the loss modulus G". For example, when G' > G" the sample behaves more like an elastic solid. In contrast, when G' < G", the sample behaves more like a viscous liquid.[10]

Typical rheological experiments of gels start with the evaluation of yield stress and linear viscoelastic region. To determine the yield stress and linear viscoelastic region, an increasing cyclic stress level is applied to the sample at a constant frequency. Yield stress is the critical stress above which the material undergoes crucial structural changes and starts to flow. The region before that is the linear viscoelastic region, where the strain varies linearly with stress. Other rheological experiments are usually conducted within this region. For instance, it is often customary to perform frequency sweep experiments to study the gel structures further. In a frequency sweep, measurements are made at a constant oscillation amplitude and temperature throughout various oscillation frequencies. In these circumstances, G' should be relatively high and should exceed G" by at least an order of magnitude for a typical structurally robust LMWG.[10]

2.4.3 Microscopy

Microscopic techniques are commonly used to study the morphology of micro- and nanostructures from which the gel networks are constructed. Most studies utilize electron microscopy techniques, such as transmission (TEM) and scanning (SEM) microscopy, with a resolution of up to a nanometer.[6] These techniques require drying of the samples, which may interfere with the original self-assembled arrangements and cause artefacts. However, these disadvantages may be tackled using cryogenic techniques, such as cryo-TEM, which eliminates

the artefacts by making high-resolution images of the gels in their original states.[6] Another disadvantage of electron microscopy techniques is that the three-dimensional networks of gels can only be imaged in two dimensions. Confocal microscopy can be used in three-dimensional imaging to get details of the microstructures and spatial distribution of fibres.[8] Moreover, some studies use techniques such as atomic force microscopy (AFM) and scanning force microscopy (SFM) that can be used to achieve a resolution on the order of fractions of a nanometer.[6] The use of AFM enables the analysis of hydrated samples *in situ* under high humidity conditions or even without dehydration. It is also possible to measure the roughness of a sample surface, which may be useful in defining the mechanical properties of a gel.

2.4.4 Spectroscopy

Other frequently utilized techniques are UV/VIS absorption, fluorescence, NMR and IR spectroscopy. These techniques provide information about the molecular arrangements and intermolecular interactions. Spectroscopy is especially useful in studies involving photoresponsive materials. For example, UV/VIS absorption is often measured to investigate the stacking of the molecules, whilst fluorescence measurements can be useful in studying the aggregation of aromatic groups. Furthermore, NMR spectroscopy can be used to identify changes in chemical shifts that occur in the gelation process or different kinds of photoreactions. It can also be used to probe the molecular interactions and the assembly rate. Molecular interactions can also be investigated by IR spectroscopy, which can provide information on hydrogen bonding.[6,8]

3 Photoisomerization

In photoisomerization, the molecules change reversibly between *cis* and *trans* isomers by using the absorption of light. Photoisomerizable compounds typically have a double bond incorporated between two atoms with substituents that can be found in either *trans* or *cis* form. The *cis*-*trans* isomerization of molecules causes changes in their polarity, size, steric hindrance, and electrical properties, affecting their gelation abilities. Usually, the *trans*-isomers can act as LMWGs, whereas the *cis*-isomers do not gelate due to change in polarization and their inefficient packing into one-dimensional structures. Therefore, photoisomerization is particularly useful in phase transition (gel-to-sol or sol-to-gel) applications. There are several examples of photoresponsive compounds that can be used in photoisomerizable LMWGs. The most common examples are the aromatic azobenzenes and stilbenes (Scheme 1), which efficiently absorb UV light. It has also been shown that photoisomerizable LMWGs based on alkenes behave similarly, but these kinds of studies are much rarer.[4,11]

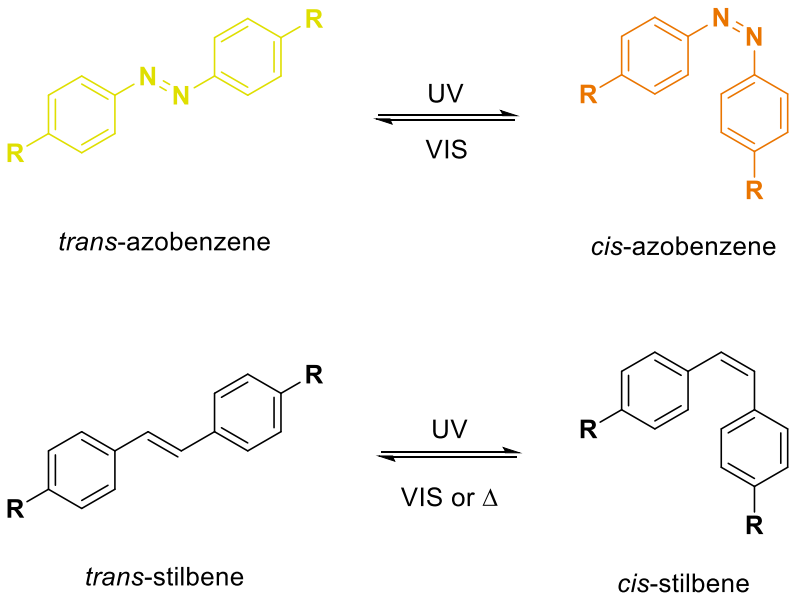

Scheme 1. Photoisomerizations of azobenzene and stilbene.

3.1 Azobenzenes

Azobenzenes (Scheme 1) are a class of photoswitchable compounds with two phenyl rings connected with N=N double bond. Typically, the compounds are intense yellow or orange in colour. Azobenzenes have been extensively utilized as dyes and incorporated in many biomedical and material science applications.[11] Their photoisomerization properties were first discovered in the late 1930s', and since then, they have become one of the most extensively studied stimuli-responsive molecules. There are many commonly known methods to synthesize azobenzene compounds, such as coupling reactions, Mills reactions and Wallach reactions.[12] In addition, a wide range of different kinds of azobenzenes are commercially available.

The first photoresponsive organogel reported in 1994 was based on azobenzene.[13] Nowadays, azobenzenes are probably the most common components of photoresponsive LMWGs due to their extensively studied photoisomerization properties. Generally, azobenzene compounds have two absorption peaks, a high-intensity peak in the UV region and a lower intensity peak in the visible light region. The absorption of UV light (λ=340-380 nm) triggers the photoisomerization of an apolar *trans* isomer to a polar *cis* isomer. The photoisomerization can be reversed by storing the azobenzene in the dark or irradiating it with visible light (λ=420-490 nm). As usual, the *trans* isomer is thermodynamically more favored; thus, the re-isomerization from *cis*-to-*trans* form can be very quick. This problem is often overcome by adding substituents to the azobenzene core to increase the lifetime of the *cis* isomer.[4,12]

Photoisomerization can be studied using UV/VIS spectroscopy. For example, Yang *et al*.[14] designed a low molecular weight organogel C_8-Azo-TPC (**1**) constructed from an alkyl chain, a photoresponsive azobenzene unit, and benzoyl chloride moiety (Figure 3). The gel was irradiated with UV light at λ=365 nm for 20 minutes at 20 °C, upon which the gel gradually collapsed and finally turned into a solution. The *trans*-to-*cis* transition was demonstrated by the gradual decay of the maximum absorption band around λ=350 nm and the formation of a new absorption band at λ=446 nm. The photoisomerization could be reversed within a few minutes by irradiation of visible light or more slowly in the dark. The reversibility was also confirmed by rheological experiments, showing that the viscosity was restored close to the initial state after the photoisomerization process and that the phase transition could be repeated many times.

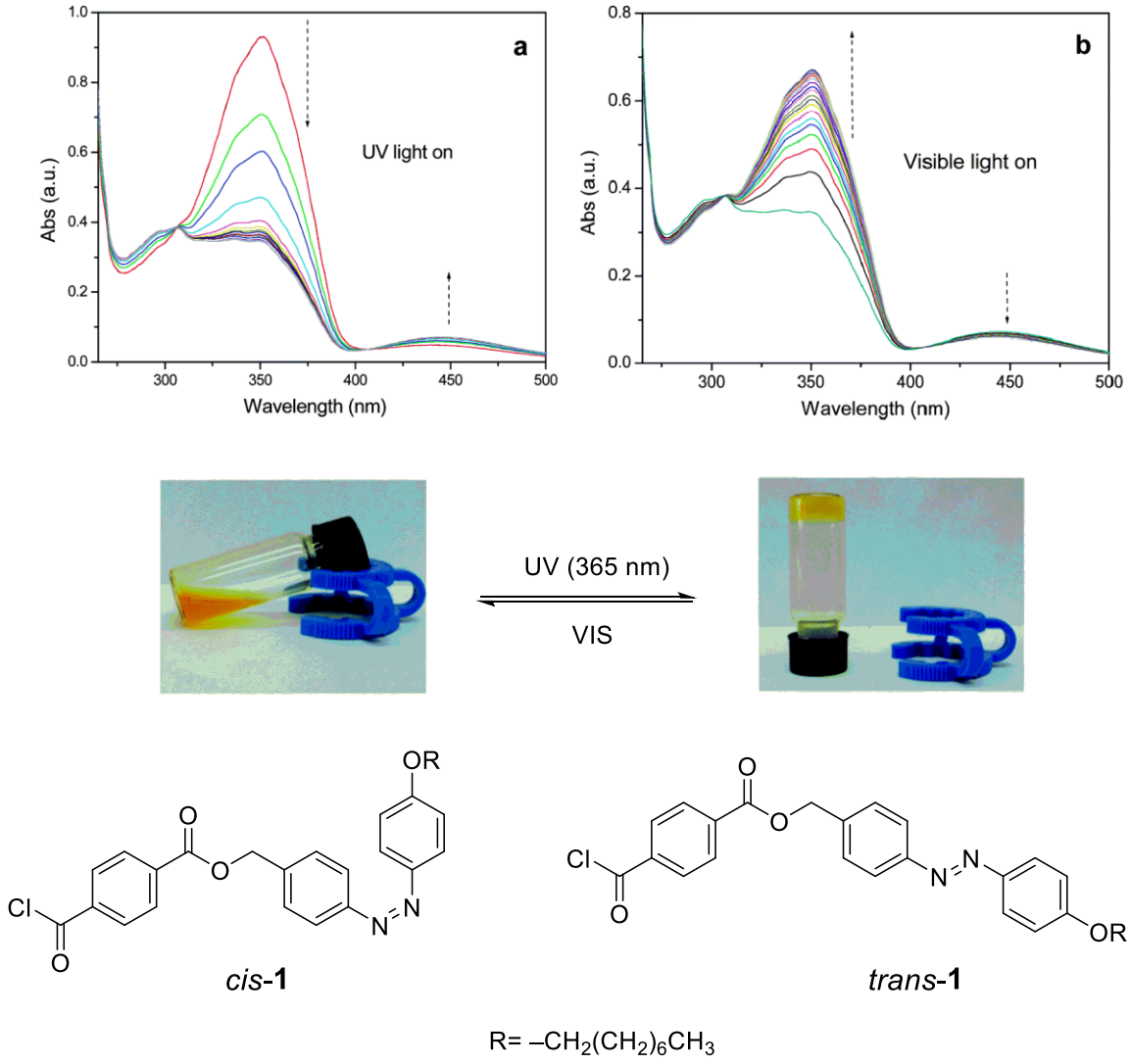

Figure 3. Top: Compound **1** in *n*-dodecane at 20 °C (0.002 wt%) absorption spectra measured within different time intervals during (a) irradiation with UV light (λ=365 nm); (b) irradiation with visible light. Middle: Reversible photoinduced phase transitions of **1**. Bottom: Molecular structure of C8-Azo-TPC (**1**). Reproduced from ref. 14 with permission from the Royal Society of Chemistry.

Fatás *et al.*[15] reported peptide-based organogels with an azobenzene moiety that were responsive to several stimuli, with light being one of them. In the study, a library of tetrapeptides containing a *p*-(phenylazo)-L-phenylalanine unit (azoPhe) was synthesized (Figure 4), and their gelation properties and responsiveness were investigated. The tetrapeptides were constructed from three Asp(OBzl) units and an azoPhe unit with differentiating positions in the peptide backbone. The analogous tetrapeptides without the Boc-protecting group were also studied. In addition, the low molecular weight peptides bearing two peptide chains

connected by azoPhe units (bisazoPhe) and their unprotected analogues were also studied. The studied peptides were found to form gels in various organic solvents. Moreover, it was demonstrated that the minimum gelation concentration, thermal stability, and mechanical strength of the gels could be altered by regulating the position of the azobenzene-containing units. Regarding the responsiveness to light, the photoinduced *trans*-to-*cis* photoisomerization was observed in the solution of all peptides bearing an azoPhe or bisazoPhe unit. However, the photoinduced reversible gel-to-sol transition was observed only for the unprotected peptides with a free amino terminus. The reason for this was presumed to be the Boc-protecting group affecting the sterically hindered spatial conformations of the aggregates that complicate the *trans*-to-*cis* isomerization.

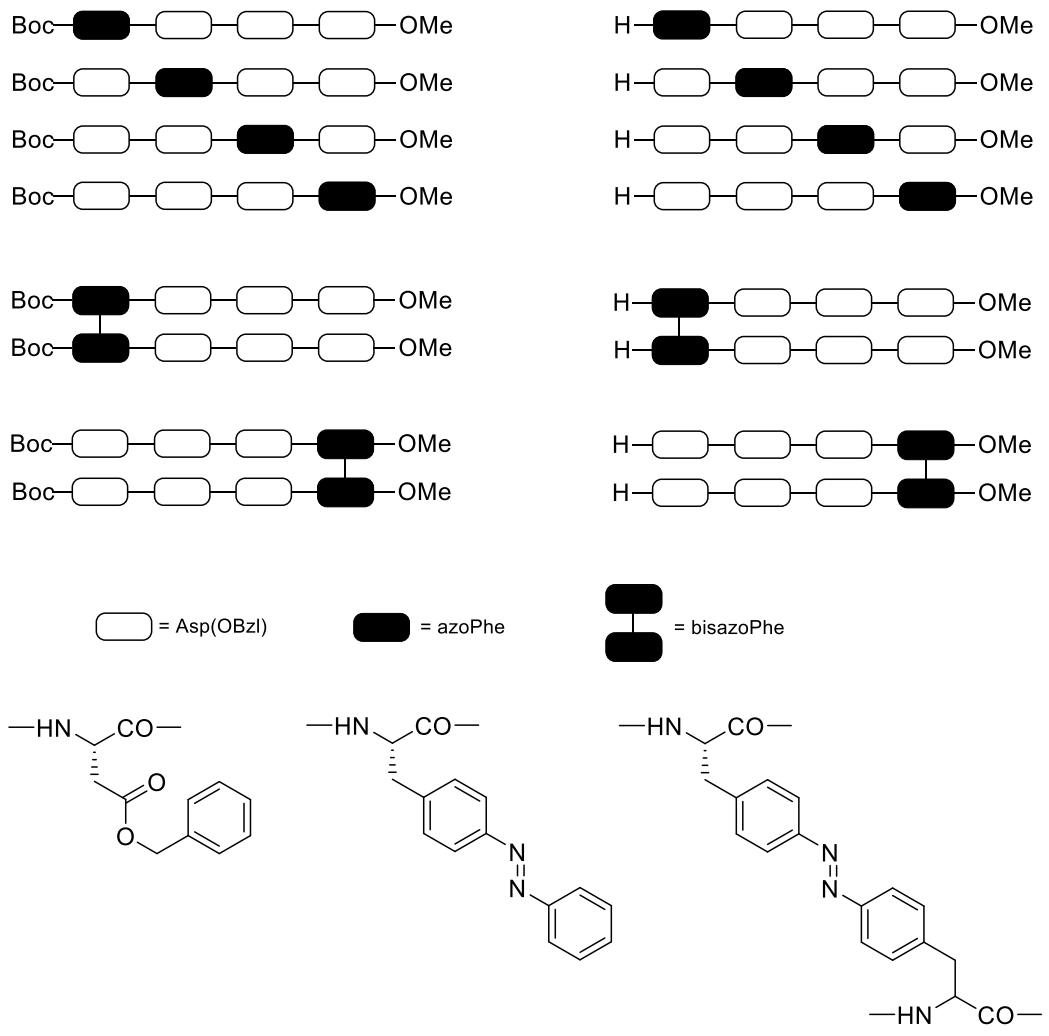

Figure 4. Some of the azoPhe-bearing tetrapeptides studied by Fatás *et al*.[15]

Indeed, the photoinduced gel-to-sol transition is sometimes difficult to achieve, and the time required for the *trans*-to-*cis* isomerization can be very long. For some azobenzene-based LMWGs, the light-controlled gel-to-sol transition may be within a timescale of hours.[16] The azobenzenes in the solid or assembled state are known to be remarkably more restricted than in the solution state, slowing down the kinetics of the organized systems. This is because the azobenzenes in the *trans* configuration tend to be tightly packed by π–π interactions, creating a lot of steric hindrance that should be overcome in the *trans*-to-*cis* isomerization.[13] Nevertheless, some studies of gels made from azobenzene dendrons and aliphatic amide units have exhibited rapid responsiveness to light stimulation.[17,18]

Although azobenzene-based organogels are commonly documented in the literature, there are not as many examples of water-based LMWGs containing azobenzenes. This is due to the hydrophobic nature of the azobenzenes, which affect their solubility in water. Velema *et al*.[19] developed a system based on non-amphiphilic dichromonyl moiety incorporated with photoisomerizable azobenzene (**2**) (Figure 5). The self-assembly of the dichromonyl compounds into fibrous network could be triggered with light, inducing the formation of hydrogels. It was reasoned that the *cis*-**2** cannot form self-assembled aggregates due to its non-planar configuration, which decreases the interactions between the molecules. The planar *trans*-**2**, on the other hand, forms self-assembled fibres that are stacked on top of each other through non-covalent interactions. Although the light-induced hydrogelation took place, the system was found to be irreversible.

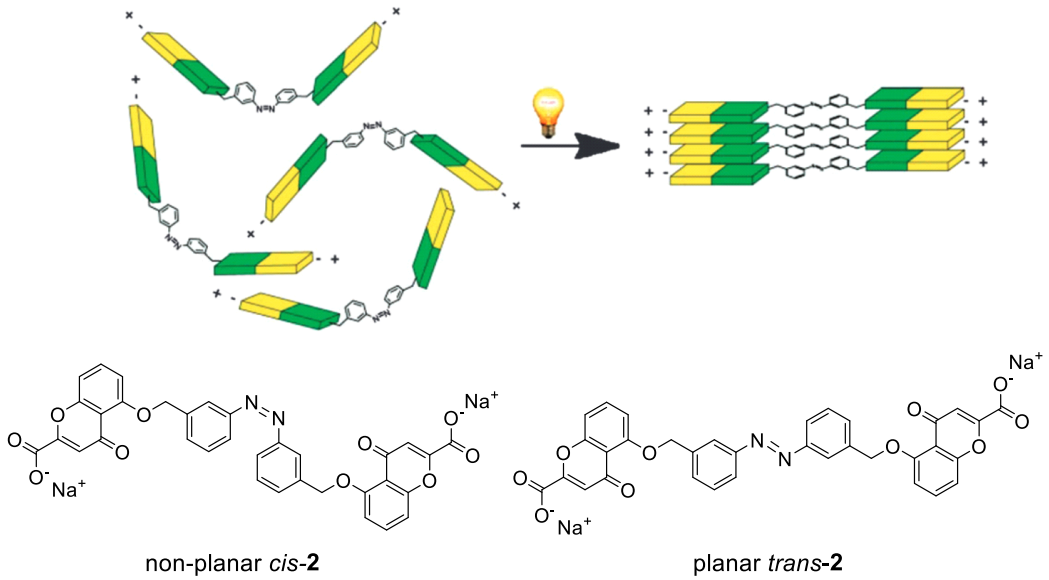

Figure 5. Photoinduced self-assembly of compound **2**. Reproduced from ref. 19 with permission from the Royal Society of Chemistry.

Another example of azobenzene-based hydrogels is from a study by Salzano de Luna *et al.*[20] The team designed and synthesized a hydrogel based on hexadecyltrimethylammonium bromide (CTAB) and azobenzene-4,4'-dicarboxylic acid. The CTAB/AZO (**3**) (Figure 6) hydrogels were found to respond to several stimuli, including light. Spectroscopic experiments were performed to study the kinetics of the AZO photoisomerization. The UV/VIS spectrum of the *trans*-to-*cis* transition was recorded while irradiating the sample with UV light, and the *cis*-to-*trans* transition was recorded subsequently by exposing the sample to visible light at room temperature. The experiment proved that the photoisomerization was fully reversible. The isomerization kinetics were also investigated by increasing the AZO concentration in the sample. It was shown that the UV irradiation times needed for the photoisomerization were significantly longer with higher concentrations. Although the CTAB addition might influence the photoisomerization kinetics, the results provide estimations of the UV irradiation times for the photoisomerization of the CTAB/AZO hydrogels.

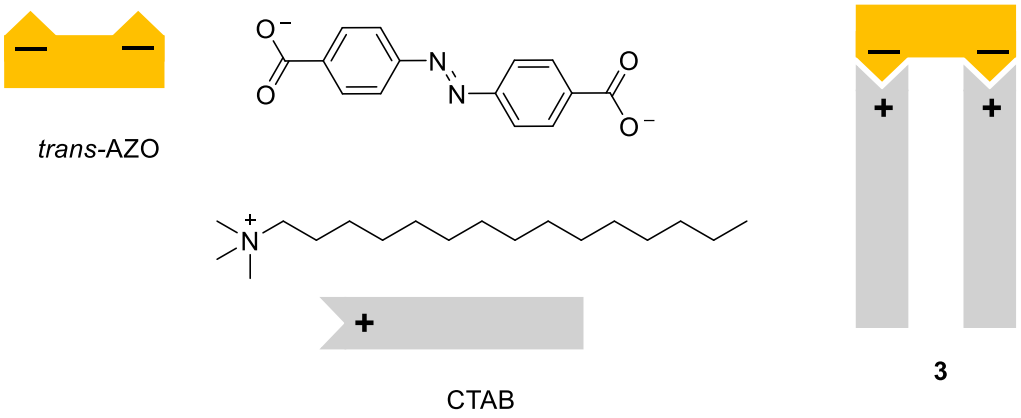

Figure 6. Schematic illustration of CTAB/AZO (**3**).[20]

Huang *et al.*[21] studied the effect of pH and salt on the hydrogelation properties of short peptides linked with photoswitchable azobenzene. The azobenzene was linked to the N-terminal of the short peptides, which allowed the synthesis of diverse peptide sequences with simple chemistry. It was reasoned that the main interaction in the self-assembling system is the π–π stacking of the azobenzene's phenyl rings, and the peptide backbone provides hydrogen bonding sites for hydrophilic interactions, improving the immobilization of water in the three-dimensional fibrous network (Figure 7). The photoisomerization of azobenzene disturbs the self-assembled system by decreasing the amount of π–π interactions, inducing the gel-to-sol transition of the hydrogel. Several azobenzene-substituted short dipeptides were found to form hydrogels. It was

also demonstrated that aromatic amino acids, such as Phe and Tyr, promote hydrogelation, whilst cationic amino acids, such as Arg, are unfavorable to forming hydrogels. Photoresponsivity experiments revealed that the hydrogels formed by azo-tripeptides responded to light irradiation differently depending on the peptide sequence. For example, the gel-to-sol transition was very fast for some azo-tripeptides, such as for azo-Gln-Phe-Ala (3 minutes) and azo-D-Lys-Phe-Ala (4 minutes). However, some showed only partial phase transition, or no photoinduced phase transition, indicating that the trans-to-cis isomerization of azobenzene was restricted in some gel matrices.[21]

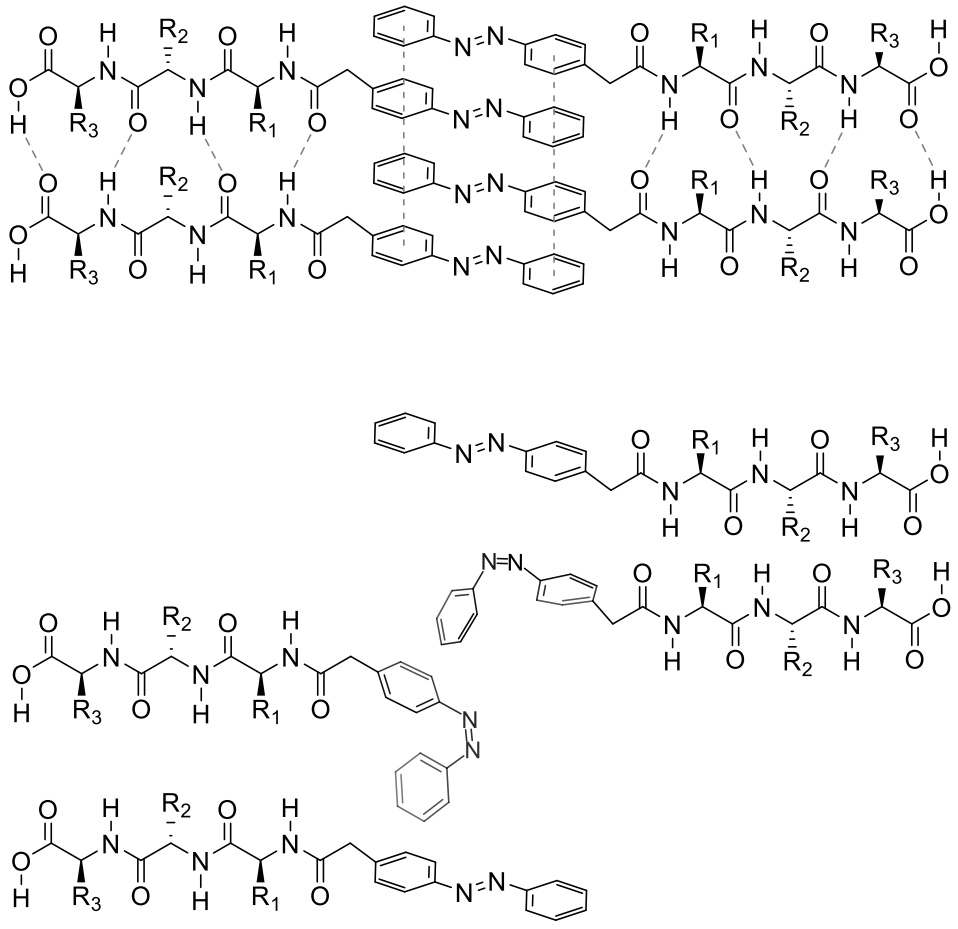

Figure 7. Schematic representation of the short peptides functionalized with photoisomerizable azobenzene unit.[21] Top: Balanced intermolecular interactions between hydrogen bonding and π–π stacking. Bottom: Disturbed balance of intermolecular interactions due to partial cis-trans isomerization of azobenzene.

3.2 Stilbenes

Stilbenes (Scheme 1) are the simplest examples of chemical compounds that belong to a class of diarylethenes. They have a similar structure to azobenzenes, but instead of a N=N bond, they have a C=C double bond that connects the two phenyl rings. Like azobenzenes, stilbenes can undergo a photoisomerization process upon irradiation of UV light.[4] The *cis*-stilbene can be converted back to *trans*-stilbene thermally or by irradiation of visible light. The main difference between the properties of azobenzenes and stilbenes is that the *trans*-to-*cis* isomerization of stilbene requires a shorter wavelength.[11] In addition, the *cis*-stilbene is more stable than *cis*-azobenzene. Although azobenzenes seem to be a much more popular choice in the design of photoisomerizable LMWGs, there are several studies involving a photoresponsive stilbene unit. For example, Geiger and colleagues studied cholesterol-stilbene organogels and their photophysical properties.[22] Eastoe and his group made a photoresponsive organogel from stilbene-containing gemini photo-surfactant that could be spatially controlled by UV light to trigger gel-to-sol transition.[23]

Milandnić and her group have studied photoisomerizable LMWGs based on oxamide derivatives and stilbene.[24,25] In their research, a variety of oxamide-based derivatives bearing one (**4a-f**) or two oxamide moieties (**5a-e**) coupled with *trans*-stilbene were synthesized (Figure 8), and their gelation abilities were examined. Out of the *trans*-stilbene mono- and dioxamide derivatives, only the ones bearing a leucine side chain (*trans*-**4e** and *trans*-**5e**) could form gels. *trans*-**4e** could gelate methanol, toluene and tetralin, while *trans*-**5e** could gelate only in tetralin. However, the introduction of an alkyloxy substituent (**6a-f**) to the stilbene part resulted in an increased gelation ability of some molecules. The gelation abilities of the corresponding *cis* isomers (**6a-d**) were then investigated. Interestingly, there was one *cis*-compound incorporated with oxalamide and alkyloxy substituent (*cis*-**6d**) that could form gels in toluene and tetralin. Another *cis*-compound that could gelate was the one incorporated with ethyl ester and alkyloxy substituent (*cis*-**6a**), which formed gels in ethanol. These findings are interesting, since the gelation of *cis* compounds is quite rare. Light responsiveness of an oxamide-based derivative with ethyl ester and alkyloxy substituent (*trans*-**6a**) was studied with Raman spectroscopy. Photoinduced gelation was achieved upon UV irradiation ($\lambda > 250$) nm at room temperature within an hour, as confirmed by the shifts of the vibrational bands in the Raman spectra.

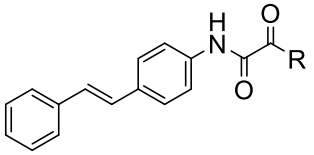

trans-**4a** R= OCH_2CH_3
trans-**4b** R= OH
trans-**4c** R= O^-Na^+
trans-**4d** R= $NH(CH_2)_{11}CH_3$
trans-**4e** R= $NHCHCOOCH_3$
$CH_2CH(CH_3)_2$
trans-**4f** R= $NHC_6H_4CHCHC_6H_5$

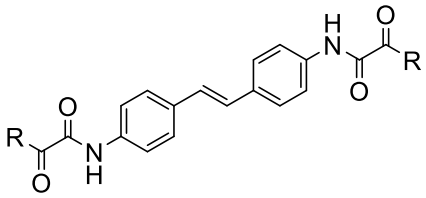

trans-**5a** R= OCH_2CH_3
trans-**5b** R= OH
trans-**5c** R= O^-Na^+
trans-**5d** R= $NH(CH_2)_{11}CH_3$
trans-**5e** R= $NHCHCOOCH_3CH_2CH(CH_3)_2$

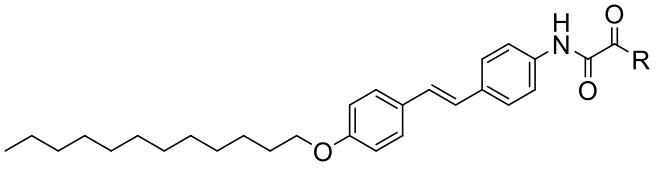

trans-**6a** R= OCH_2CH_3
trans-**6b** R= OH
trans-**6c** R= O^-Na^+
trans-**6d** R = NH_2
trans-**6e** R= $NHCHCOOCH_3$
$CH_2CH(CH_3)_2$
trans-**6f** R= NHCHCOOH
$CH_2CH(CH_3)_2$

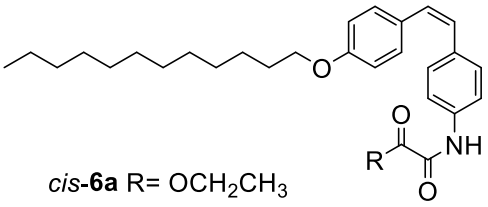

cis-**6a** R= OCH_2CH_3
cis-**6b** R= OH
cis-**6c** R= O^-Na^+
cis-**6d** R = NH_2

Figure 8. Molecular structures of the stilbene-functionalized mono-and dioxamide derivatives studied by Milandnić *et al*.[25]

4 Ring-closing and opening

Photoinduced ring-closing and opening is another example of a response that can be used in dynamic photoresponsive LMWGs. Molecules undergoing these kinds of photoreactions can be reversibly switched between the open and closed forms upon light irradiation. Because the open and closed forms differ in conjugation, the molecules can be photochromatic, meaning they can change their colour in the photoreactions. The ring-closing and opening can also affect the electronic properties of the molecules. Due to these characteristics, photoresponsive LMWGs based on ring opening/closing reactions can be used in applications such as optical switches and displays, to name a few. Examples of compounds that can be used as photoresponsive units in this category include spiropyrans and dithienylethenes (Scheme 2).[3,4]

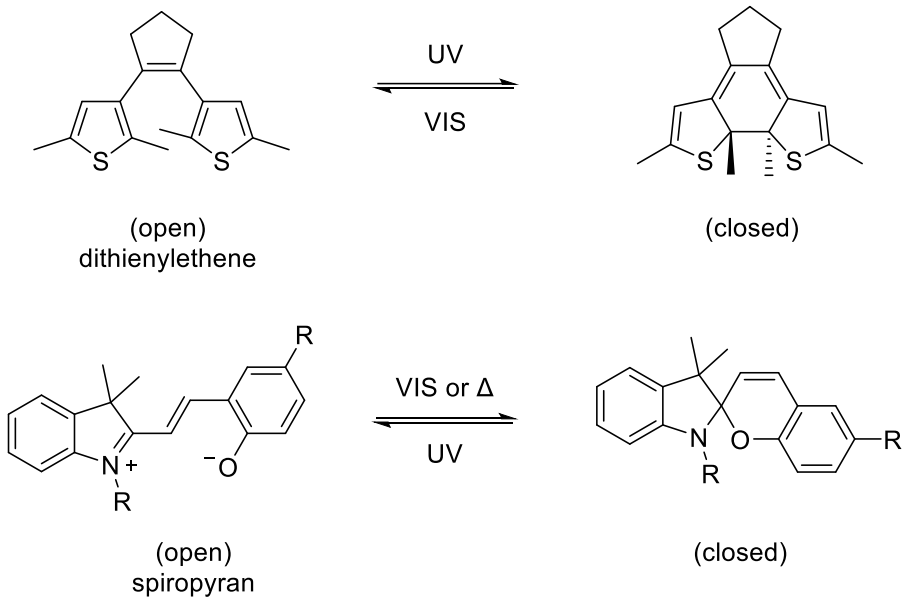

Scheme 2. Photoinduced ring opening and closing of dithienylethene and spiropyran.

4.1 Dithienylethenes

Dithienylethenes (Scheme 2) are photoswitchable diarylethenes that consist of an alkene with two thiophene rings. The open form of dithienylethene can be converted to the closed form upon UV light irradiation and reversed back to the open form with visible light.[4] Compared to photoisomerizing groups, the molecular geometry of dithienylethenes does not change significantly upon exposure to light. Because of this, dithienylethene-based gels are able to maintain their rheological properties during irradiation with light.[4] However, the conjugation of the open and closed forms differ, resulting in them becoming photochromic switches. Due to the photochromic response to light and the thermal stability of both the open and closed forms in the dark, diarylethenes have been applied to optical memories and switches.[3,4]

There are many studies of dithienylethene-based LMWGs. For example, Jiang *et al*.[26] reported a multi-stimuli responsive organogel incorporating a tetrapeptide-based dithienylcyclopentene conjugate (**7**) (Figure 9). Stable organogels were formed in various solvents, such as THF, acetonitrile and acetone. The tetrapeptides self-assembled into anti-parallel β-sheets; therefore, hydrogen bonding was thought to be a key factor in the gelation process. The organogel exhibited multi-stimuli responsivity for temperature, light, chemicals, and mechanical force. Ring-opening and closing of the photoresponsive dithienylcyclopentene group were studied spectroscopically. Upon UV light irradiation at λ=365 nm, the pale-yellow gel changed into deep brown within 8 minutes (Figure 9). The colour could be reversed by irradiation with visible light at λ=670 nm, and the cycle could be repeated reversibly. The prominent color change is caused by the extended π-conjugation of the closed ring form. The photoinduced conformational change of the dithienylcyclopentene was confirmed by the UV/VIS spectra of the gel during UV light irradiation (Figure 9). The ring-closing reaction could be observed by the appearance of a new absorption band at $\lambda\approx$510 nm.

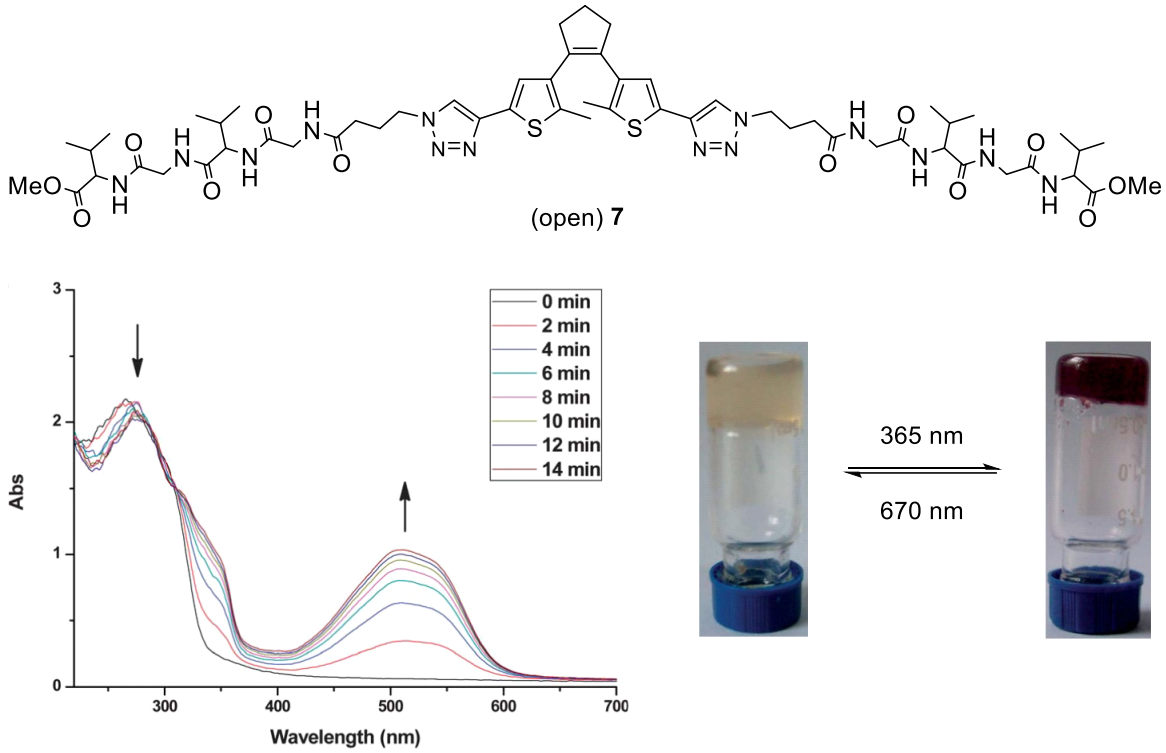

Figure 9. Top: Molecular structure of the organogel **7**. Left: Compound **7** in THF (9 mg/ml) absorption spectra measured within different time intervals under 365 nm irradiation. Right: Photochromic behavior of the organogel. Reproduced from ref. 26 with permission from the Royal Society of Chemistry.

Aryal *et al.*[27] prepared LMWGs based on dithienylethene moiety linked with two carbohydrates. Compound **8** and its hexafluorinated derivative **9** (Scheme 3) formed gels in various solvents in their open forms. Compound **8** was an efficient gelator in nine different solvents, especially in DMSO/water mixtures. On the other hand, the fluorinated derivative **9** was more soluble in organic solvents but formed gels in only several alcohols at higher concentrations. Most of the gels were either opaque or translucent. The photochromatic properties of the compounds were studied both in solution and gel phase. After UV light irradiation (λ=302 nm) of the solutions, compound **8** changed colour from colourless to pink-purple, whereas compound **9** turned from colourless to dark blue. Moreover, the gels formed by the compounds exhibited reversible photochromism during ring-closing and opening while maintaining the gelatinous state.

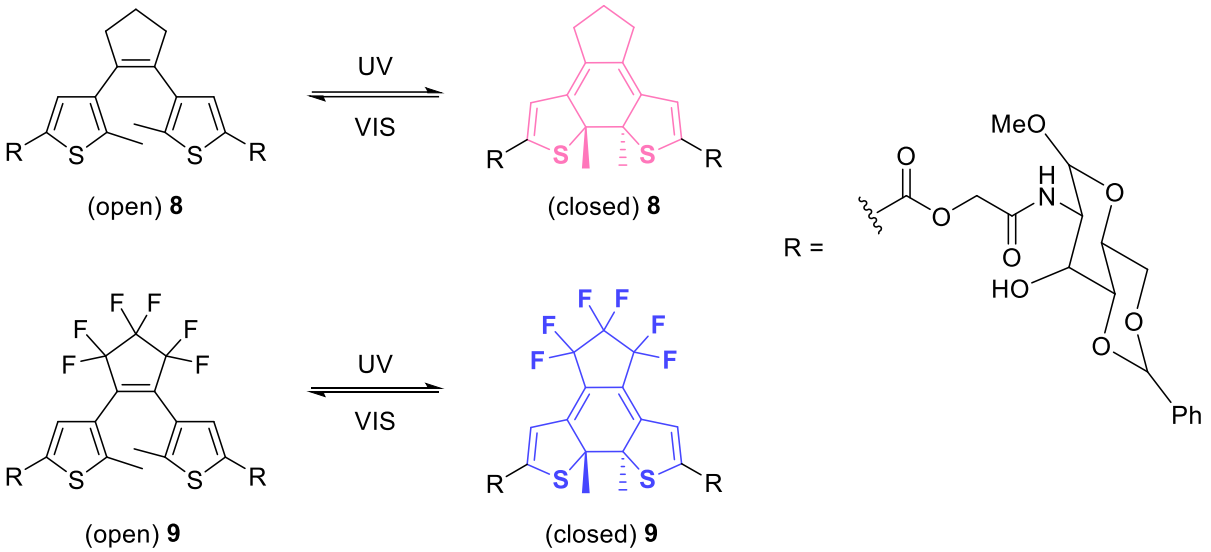

Scheme 3. Photoinduced ring-closing and opening of compound **8** and its hexafluorinated derivative **9** studied by Aryal *et al.*[27]

In both examples above, the gels exhibited photochromic shifting caused by photoinduced ring-closing and opening, but the gels remained indestructible throughout the process. This is typical for dithienylethene-based LMWGs, since they can usually respond to light irradiation while maintaining their rheological properties. However, Akazawa *et al.*[28] described a novel photoresponsive dithienylcyclopentene-based LMWGs with bisurea moieties (Scheme 4) that underwent gel-to-sol phase transitions upon UV light irradiation. The gelation and photo responsiveness of two series of derivatives were studied, with (**10a-c**) and without (**11a-c**) alkyl spacers between the dithienylcyclopentene and urea moieties. Of the three derivatives that incorporated propylene spacers, only one compound (**10a**) showed gelation behavior, while the others formed precipitates in the same solvents. The derivatives without the propylene spacers formed gels in several solvents, except compound **11b** that formed precipitates. The gelation ability of the derivatives without the spacers (**11a** and **11c**) showed an increased gelation ability compared to compound **10a**, as their MGCs were almost half of that of compound **10a**. The photoresponsive studies were performed for gels formed by compounds **10a**, **11a** and **11c** in THF. The photoinduced gel-to-sol transition was achieved even at very low conversion (up to 1.4 %) of the dithienylethene unit. The photoinduced phase transitions were rationalized with the weak hydrogen bonding between the molecules in their open form, which are further destabilized by the conversion of the molecules into their closed form.

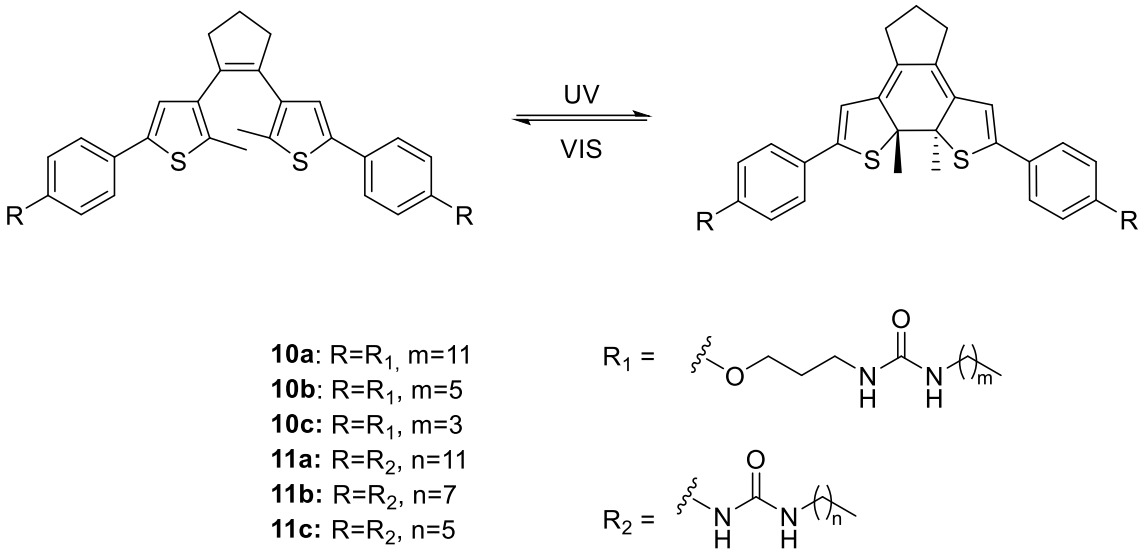

Scheme 4. Molecular structures of the dithienylethene derivatives with propylene spacers (compounds **10a-c**) and without spacers (compounds **11a-c**) studied by Akazawa *et al*.[28]

Dithienylethene-based photoswitches are among the most hydrophobic photoswitchable moieties.[27,29] Therefore, there are not many examples of their incorporation in hydrogels. However, van Herpt *et al*.[29] have proven that incorporating dithienylethenes into hydrogelator systems is possible. The group synthesized eight different dithienylethene-based derivatives including dipeptides with different polarities. The polarity of the molecules could be tuned by altering the use of apolar (Phe), neutral (Gly) and polar (Lys) amino acids. The dithienylethene moiety was thought to play a key role in gelation, while the dipeptide moiety provides solubility. Five of the eight derivatives formed hydrogels with MGC in the 20-40 mg/ml range. A gel formed by a dithienylethene-based derivative with Lys-Gly dipeptide was irradiated with UV light at λ=312 nm, upon which the photoinduced ring-closing reaction resulted in a colour change from bright yellow to red. The process could be reversed by irradiation of visible light at $\lambda > 500$ nm, upon which the colour of the gel returned to the original yellow. The cycle could be repeated multiple times while the rheologic properties remained unchanged.

4.2 Spiropyrans

Spiropyrans are organic compounds that can undergo a reversible ring-closing and opening through their C-O bond (Scheme 5). The closed form of spiropyran (SP) is the more stable one, and the geometry of the molecule is non-planar. The ring-opening reaction can be induced by UV light and reversed with visible light, forming a planar molecule called merocyanine (MC). The planar merocyanine form has more favorable π-stacking, and therefore, a stronger tendency to form gels. The photochromic properties of spiropyrans were first discovered in the early 1950s, giving the basis for extensive research on applications in materials and nanoscience. There are many studies about photoresponsive polymeric gels based on spiropyran, but relatively few studies have been conducted on LMWGs.[30]

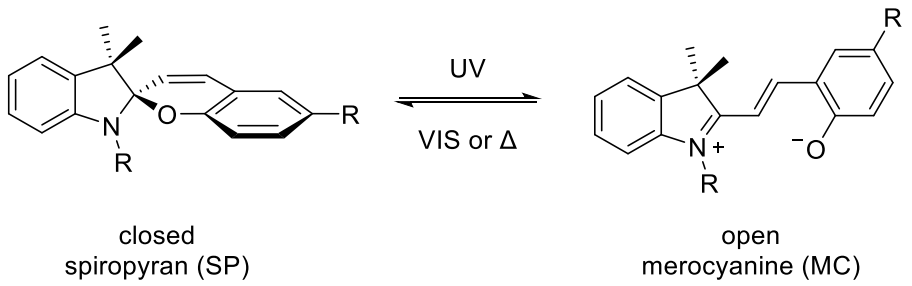

Scheme 5. Photoinduced ring-closing and opening between spiropyran (SP) and merocyanine (MC) forms.

Qiu *et al*.[30] designed and synthesized a hydrogel consisting of a dipeptide D-Ala-D-Ala and a spiropyran unit (**12**) (Figure 10). The hydrogel was responsive to light and ligand-receptor interaction with antibiotic vancomycin. The dark red coloured hydrogel was irradiated with light at $\lambda > 400$ nm, triggering a rapid (5 minutes) gel-to-sol transition into a yellow slurry. The reversed photo response was also investigated by irradiating the yellow slurry with UV light, upon which it turned into a red slurry instead of the original red hydrogel. However, the UV light triggered the sol-to-gel transition, which was made possible by adjusting the pH of the red slurry to acidic. This indicates that the photo response is not fully reversible, and the process needs further improvement.

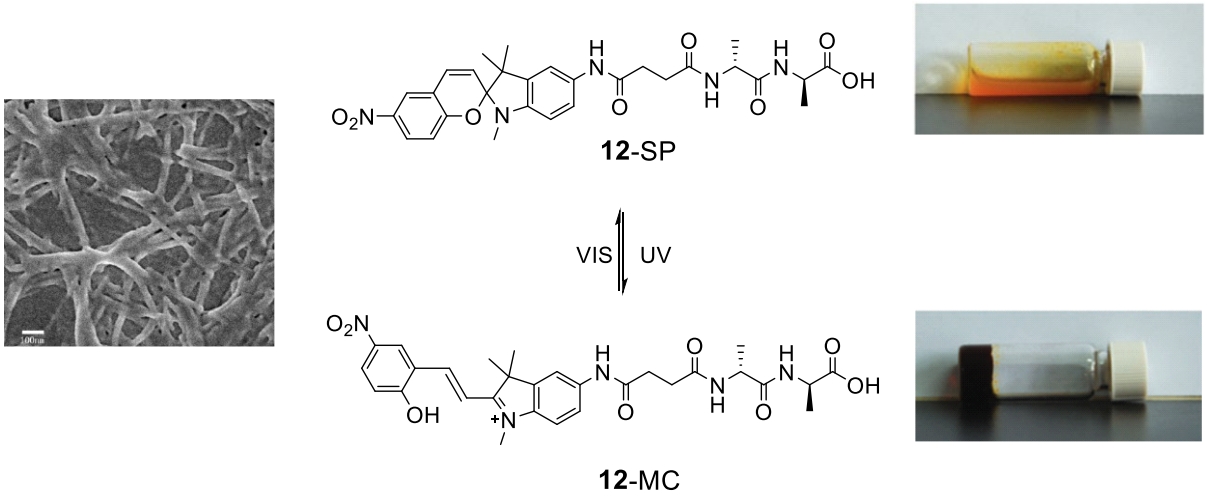

Figure 10. Left: SEM image of the fibrous network of the gel formed by **12**-MC (11 mM in water at pH 3.0). Right: Molecular structure of **12** in its SP and MC forms and their photoinduced phase transition. Reproduced from ref. 30 with permission from the Royal Society of Chemistry.

In another study, the self-assembly and spectroscopic properties of a dendritic organogel based on spiropyran (**13**) (Scheme 6) were investigated.[31] The compound **13** formed yellow gel in SP form in toluene and benzene upon cooling. The transformation from SP to the MC form was achieved by UV light irradiation, upon which a photochromic gel-gel transition changed the colour of the gel from yellow to dark purple. The MC form could then be converted back to the SP form with visible light irradiation. Since both forms of compound **13** formed gels, it was thought that the π–π interactions between the dendrons would be responsible for forming such stable aggregates. Moreover, it was found that the dark purple gel formed by **13**-MC has a relatively strong red fluorescence. Therefore, the fluorescence could be reversibly switched by altering the irradiation of the organogel between UV and visible light. These findings could provide insights into potential applications in fluorescence imaging.

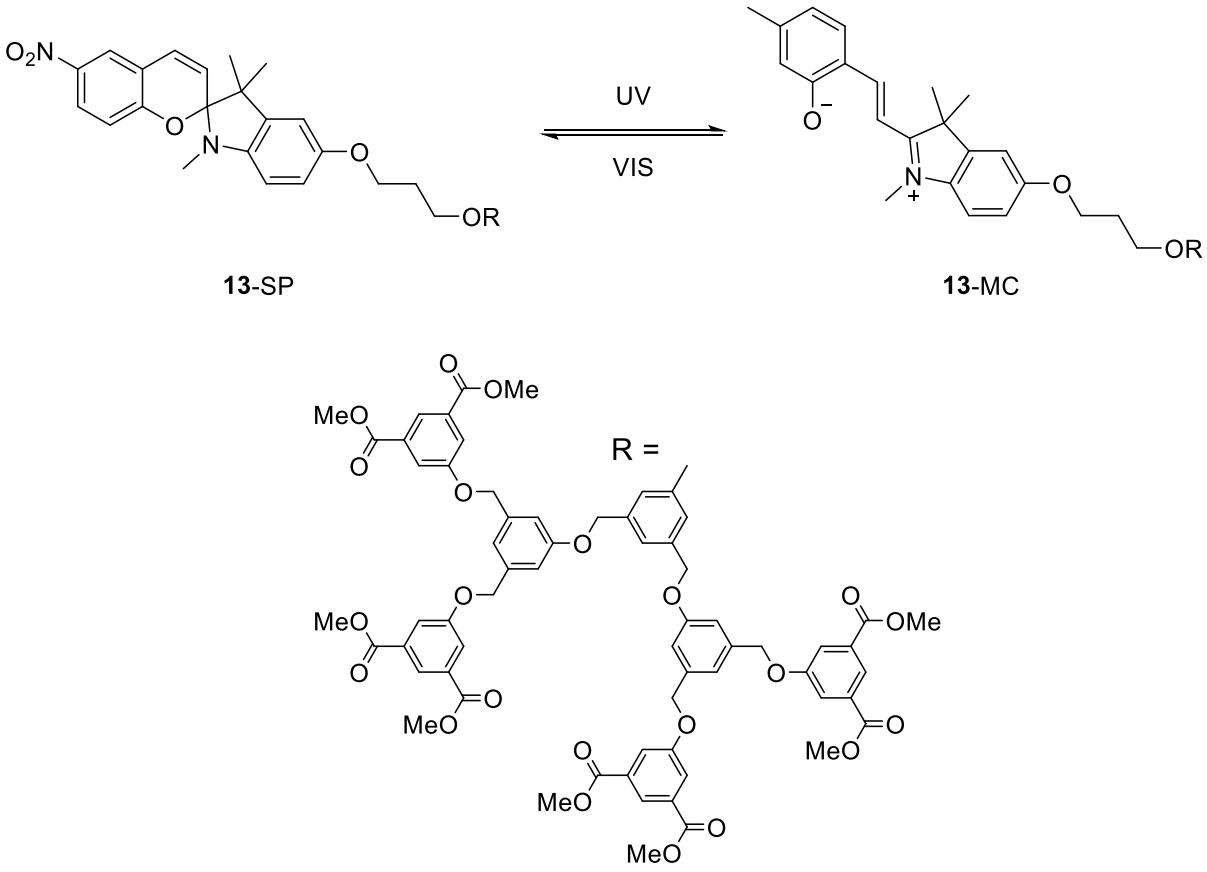

Scheme 6. Molecular structure of **13** in its SP and MC forms.[31]

5 Photodimerization and photopolymerization

5.1 Photodimerization

Photodimerization occurs when two molecules are oriented so that they can form a covalent bond upon exposure to light. Photodimerization typically proceeds through pericyclic cycloaddition reactions. In solution, the probability of photodimerization is lower than in the gel phase because the molecules can move more freely and are, therefore, less likely to be in a suitable position for dimerization. Photodimerization often causes the molecules to become less soluble and more hydrophobic due to the doubled size of the molecules.[4] Reduced solubility of the gelator molecules may cause gel-to-sol phase transition or a decrease in the rheological properties of the gel.[4] In some cases, photodimerization causes a gel reinforcement upon light irradiation.[32,33] Therefore, photodimerizable LMWGs may be suitable for applications requiring responsive and more robust properties. Photodimerization typically happens with conjugated molecules, such as coumarins and anthracenes (Scheme 7).

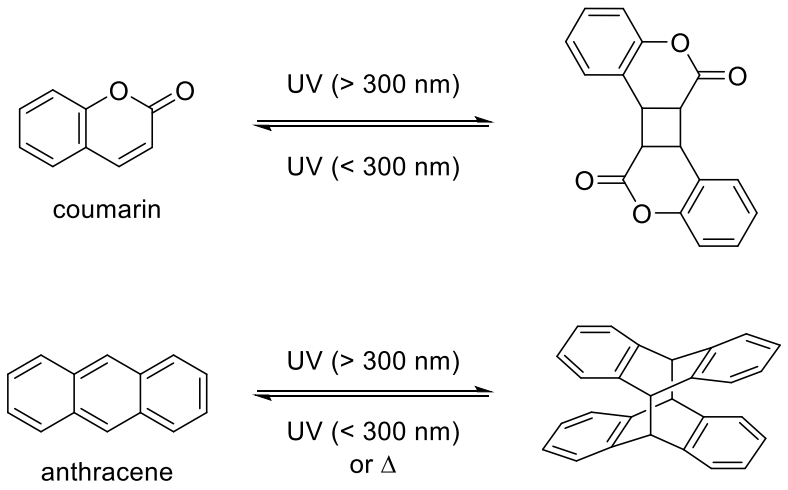

Scheme 7. Photodimerization of coumarin and anthracene.

5.1.1 Coumarins

Coumarins (Scheme 7) are aromatic organic compounds with fused benzene and α-pyrone rings. The photochemical properties of coumarins and their derivatives have been extensively investigated. Coumarins are known to exhibit reversible photodimerization upon light irradiation. Photodimerization proceeds by the [2+2] cycloaddition of the ethylenic groups of coumarin molecules that can be triggered by UV light irradiation at $\lambda > 300$ nm, resulting in cyclobutane-type dimers.[32,34] The photodimerization of coumarins typically gives a mixture of *syn*-head-head, *anti*-head-head, *syn*-head-tail and *anti*-head-tail diastereomers (Scheme 8) depending on the orientation of the molecules to each other.[35] The dimers can be reverted into the monomers by photocleavage of the cyclobutane ring upon irradiation with light at $\lambda < 300$ nm.[32] Another noteworthy feature is that the photodimerization of coumarin causes changes in its emission intensity. That is, while coumarin exhibits fluorescence upon excitation at λ=320 nm, its dimers do not.[34]

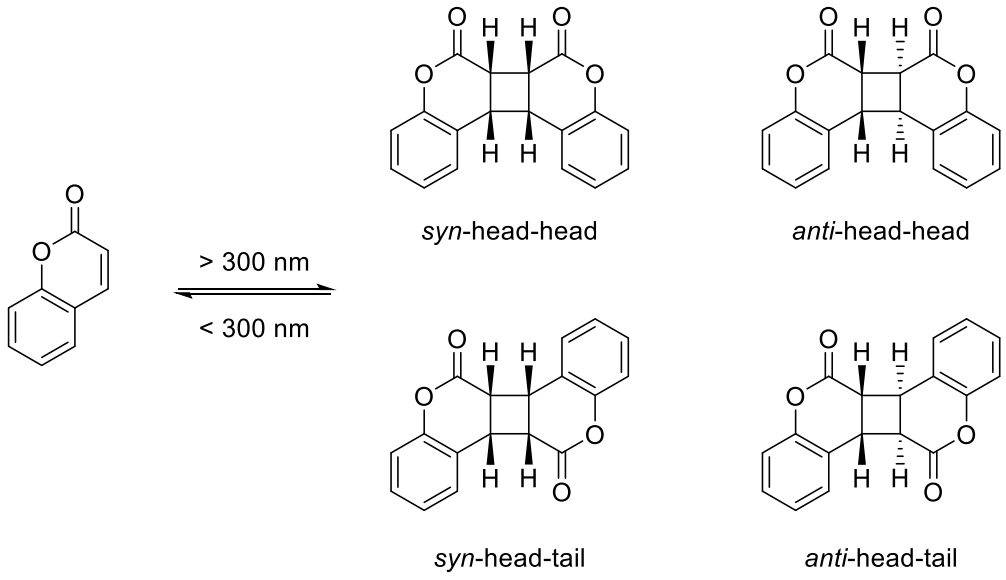

Scheme 8. [2+2] Photodimerization of coumarin.

There are a great number of studies dealing with the photodimerization of coumarin incorporated in LMWGs. One of the first studies was by Yu *et al*.,[34] who designed and synthesized a series of coumarin derivatives with amide and alkyl chain spacers of different lengths (**14$_n$**, n=2, 4, 5, 7, 9, 11, 13, 15 or 17) (Figure 11). All the coumarin derivatives formed gels in various apolar and polar organic solvents. The derivatives with longer alkyl chains were found to be better gelators than the ones with shorter alkyl chains, suggesting that the gelation ability is affected by the enhanced π–π interactions and hydrogen bonding in nonpolar and polar solvents, respectively. The contribution of hydrogen bonding of the amide groups was also studied by replacing the amide group with alkyl chains. The absence of the amide group significantly impacted gelation ability, since the coumarin derivatives without the amide group were more soluble and did not form gels at all. The photoresponse of a gel formed by **14$_{17}$** in cyclohexane was studied by fluorescence spectroscopy. Before irradiation, the gel showed strong fluorescence emission at λ=390 nm. After irradiation with light at λ > 300 nm for 24 hours, the emission intensity decreased, and continued decreasing significantly after prolonged irradiation for 48 hours. The emission intensity increased again upon irradiation with light at λ < 280 nm for 24 hours, but the peak height was not fully recovered to the initial peak height. These results indicate that the gel undergoes photodimerization and that the reaction is reversed by photocleavage. Moreover, the results suggest that the photocleavage might be slower in the gel phase than in the solution and that the photodimerization reaction in the gel phase is not fully reversible.

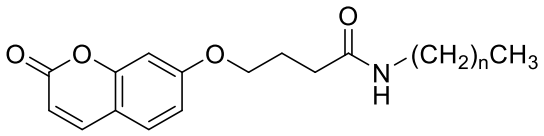

14$_n$ (n=2, 3, 5, 7, 9, 11, 13, 15 or 17)

Figure 11. Molecular structures of the coumarin derivatives with amide and alkyl chain spacers.[34]

Yabuuchi *et al*.[32] studied the photoresponsivity of a coumarin-based organogel **15** with *trans*-(1*R*,2*R*)-1,2-cyclohexanediamine moiety **16** (Figure 12). Compound **15** was able to gelate a wide range of organic solvents, and the addition of **16** to **15** has a positive effect on the transparency of the gels. Transparent gels were more desired because they were believed to

scatter light less efficiently and thus promote photodimerization. Spectroscopic experiments showed that 92 % of the photodimerizing coumarin units in a THF solution of **15** dimerize upon irradiation at λ > 300 nm, and 67 % of dimers revert to the corresponding monomers upon irradiation at λ=254 nm. However, in a gel formed by **15/16** (1:10) in toluene, the dimerization of the coumarin units upon UV irradiation at λ > 300 nm was only 69 %, indicating that the photodimerization may be disturbed by scattering of the irradiated light by self-assembled fibres that form the gel. The rate for the conversion of the dimers into the corresponding monomers upon UV light irradiation at λ=254 nm was only 13 %, which was affected significantly by the absorption by the solvent. This is unfortunate because obtaining transparent gels with less light scattering was restricted to aromatic solvents, such as benzene and toluene, with absorption bands overlapping with the irradiated light. Moreover, it was thought that longer exposure to UV light does not increase the conversion further and may cause the decomposition of the coumarin units. Based on the previous examples it can be stated that the reversibility of photodimerizing LMWGs still needs improvement.

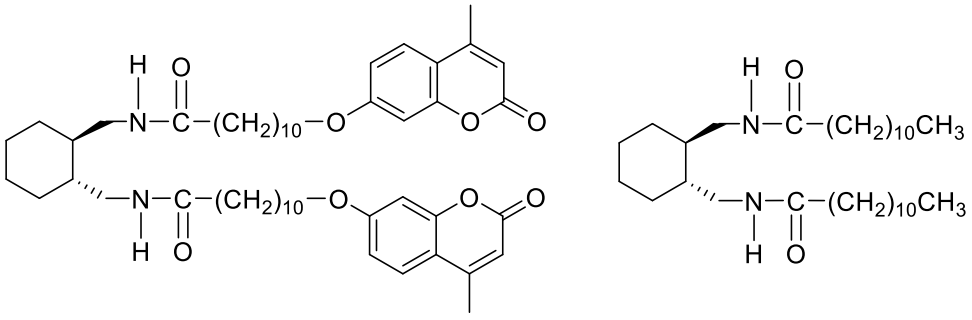

15 **16**

Figure 12. Molecular structures of compounds **15** and **16**.[32]

The same study investigated the effects of UV light irradiation at λ > 300 nm on the gel properties. The photodimerization of the coumarin units in gels formed by **15/16** in toluene improved the thermal and mechanical stabilities of the gels. Thermal stabilities of the gels were studied by following the gel-sol transition temperatures ($T_{gel\text{-}sol}$) of gels with different molar ratios (Figure 13a). The $T_{gel\text{-}sol}$ values increased with UV light irradiation, and the increase in $T_{gel\text{-}sol}$ over time was larger as the proportion of **16** was increased, except for a 1:1 mixture. Rheological experiments were performed to investigate the changes before and after light exposure. Frequency sweep measurements showed that the storage modulus G' of the gel was higher than the loss modulus G" up to approximately 0.1 % strain limit, over which both the G'

and G" started to decrease, indicating collapsing of the gels. Frequency sweeps at a strain of 0.05 % show the enhancement of mechanical stability upon light irradiation (Figure 13b).

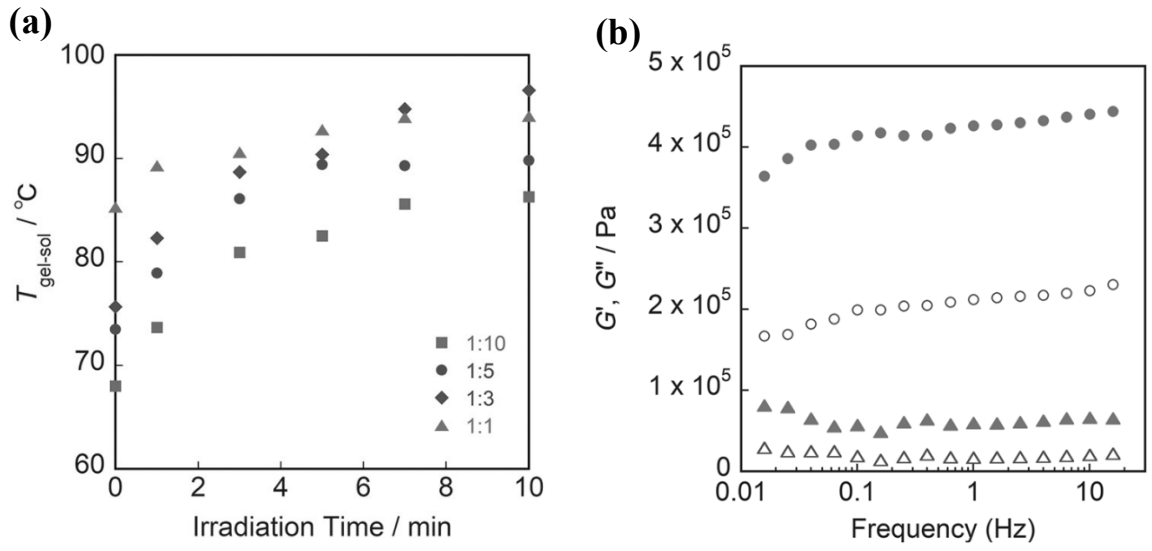

Figure 13. Effects of UV irradiation (λ > 300 nm) on the gel formed by **15/16** in toluene (0.078 M). (a) $T_{gel-sol}$ values as a function of irradiation time for different ratios of **15/16**; (b) Frequency sweeps of **15/16** (1:10) at a strain of 0.05 % before (G':○, G":△) and after (G':●, G":▲) UV irradiation. Reproduced from ref. 32 with permission from Springer Nature.

Another example of coumarin-based LMWGs that can undergo photoinduced reinforcement is a study by Draper and Adams.[33] They reported a photodimerizing diphenylalanine gelator with a coumarin unit attached to the N-terminus (Figure 14). The gels were prepared by dissolving the compound **17** at a high pH and lowering the pH by adding glucono-δ-lactone (GdL). The compound **17** formed transparent, self-supporting gels with MGC of 5 mg/ml (Figure 14). Upon UV light irradiation by a 365 nm LED, the gel became more turbid, especially in areas directly exposed to light. The inhomogeneous change in the gel network can be observed in the SEM images of the irradiated sample (Figure 14). To study the effect of light irradiation on the rheological properties of the gels, thin hydrogel films were prepared to eliminate the difficulty of studying an inhomogeneous sample. Irradiation with UV light increased the rheological properties of the gels, which is believed to be caused by the dimerization within the fibres rather than the cross-linking between the fibres. These types of gels that can be modified post-gelation with UV light may be useful in photopatterning applications.

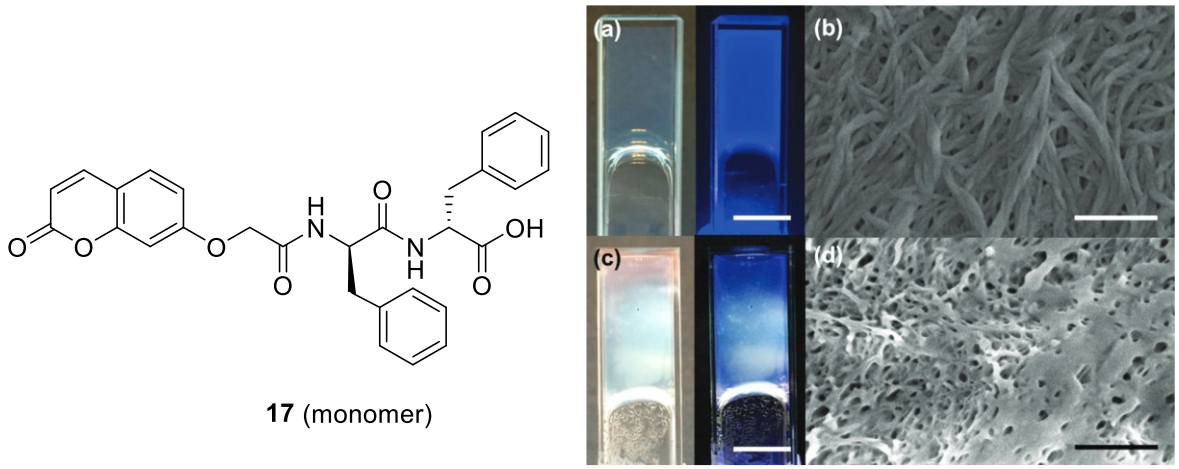

Figure 14. Left: Molecular structure of **17**. Right: Gel formed using GdL before irradiation (a) photographed in natural and UV light (scale bar = 1 cm); (b) SEM image of the gel (scale bar = 500 nm). Gel after irradiation (λ=365 nm) for 2 hours (c) photographed in natural and UV light (scale bar = 1 cm); (d) SEM image of the gel (scale bar = 500 nm). Reproduced from ref. xx with permission from the Royal Society of Chemistry.

Kim *et al.*[36] reported a hydrogel consisting of dilysine peptide functionalized with two coumarin moieties. Upon irradiation with UV light at λ=365 nm, the coumarin moieties could form cross-links across the self-assembled β-sheet structures of the hydrogel (Figure 15). Partial cross-linking enhanced the mechanical stability of the hydrogel, but prolonged irradiation caused a disruption of the gel phase and led to the formation of water-insoluble precipitates. However, the solid-state network remained intact when dissolved in TFE, a potentially denaturing solvent that dissolves the non-crosslinked material.

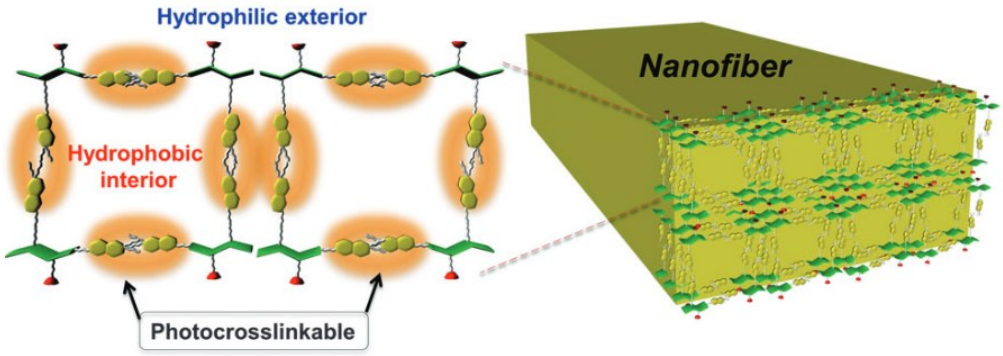

Figure 15. Schematic representation of crosslinked β-sheet nanostructure of the hydrogel reported by Kim *et al.*[36] Reproduced from ref. 36 with permission from The Royal Society of Chemistry.

5.1.2 Anthracenes

Anthracenes (Scheme 7) are polyaromatic hydrocarbons that consist of three fused benzene rings. Photodimerization of anthracene is one of the oldest known photoreactions. The photodimerization of anthracenes proceeds by the [4+4] cycloaddition when irradiated with UV light at $\lambda > 300$ nm, forming an eight-membered ring that connects the molecules. The reversed reaction occurs when the dimer is irradiated with light at $\lambda < 300$ nm or with heat. As in the case of coumarins, the photodimerization usually gives a mixture of *syn*-head-head, *anti*-head-head, *syn*-head-tail and *anti*-head-tail diastereomers (Scheme 9). The stereoselectivity of the photodimerization can be controlled by varying the substituents in the anthracene ring.[37,38]

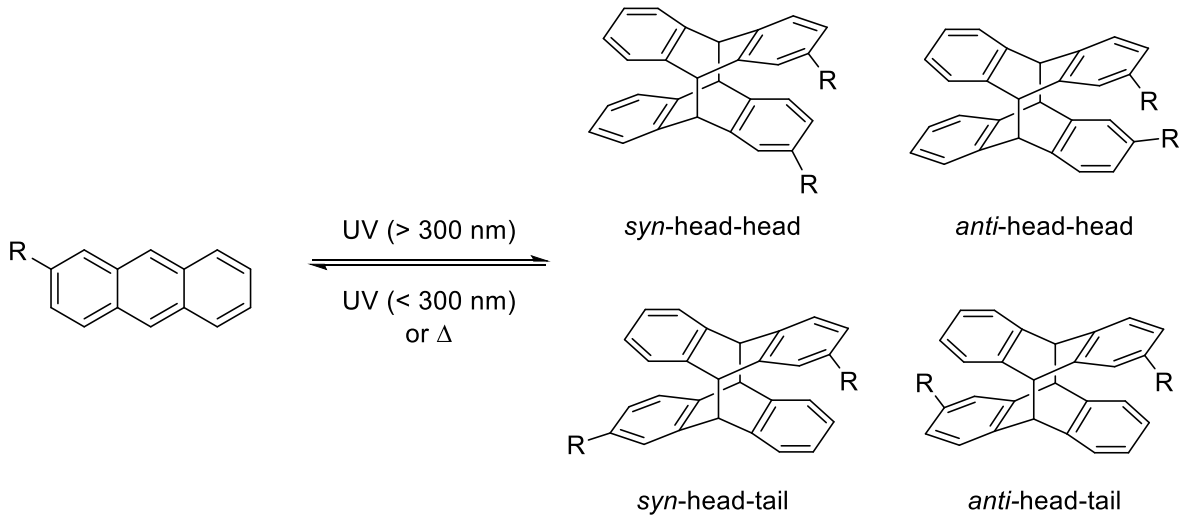

Scheme 9. Photodimerization of anthracene.

Ayabe *et al.*[39] studied the gelation and photoresponsive behavior of ten alkylammonium anthracene-9-carboxylate derivatives (Figure 16). The gelation was studied by dissolving **18**$_n$ (n=4-12 and 16) into boiling cyclohexane and cooling to 20 °C. Compounds **18**$_4$, **18**$_5$, **18**$_6$ and **18**$_7$ formed precipitates whereas compounds **18**$_{11}$, **18**$_{12}$ and **18**$_{16}$ formed viscous solutions. Compounds **18**$_8$, **18**$_9$ and **18**$_{10}$ gave a partial gel, a turbid gel, and a translucent gel, respectively. These results imply that the intermolecular forces between the anthracene moieties and the solubilization forces arising from the alkylammonium moieties in **18**$_8$, **18**$_9$ and **18**$_{10}$ are well balanced to promote gelation. The photoresponsive behavior of a gel formed by **18**$_{10}$ in cyclohexane upon UV light irradiation at $\lambda > 300$ nm was examined spectroscopically. Photodimerization was demonstrated by the decay in absorption intensity typical to anthracene-

9-carboxylate, upon which the photoinduced gel-to-sol transition took place after 2 minutes of irradiation. The monomeric form could be regenerated thermally by heating at boiling point and cooling to 15°C.

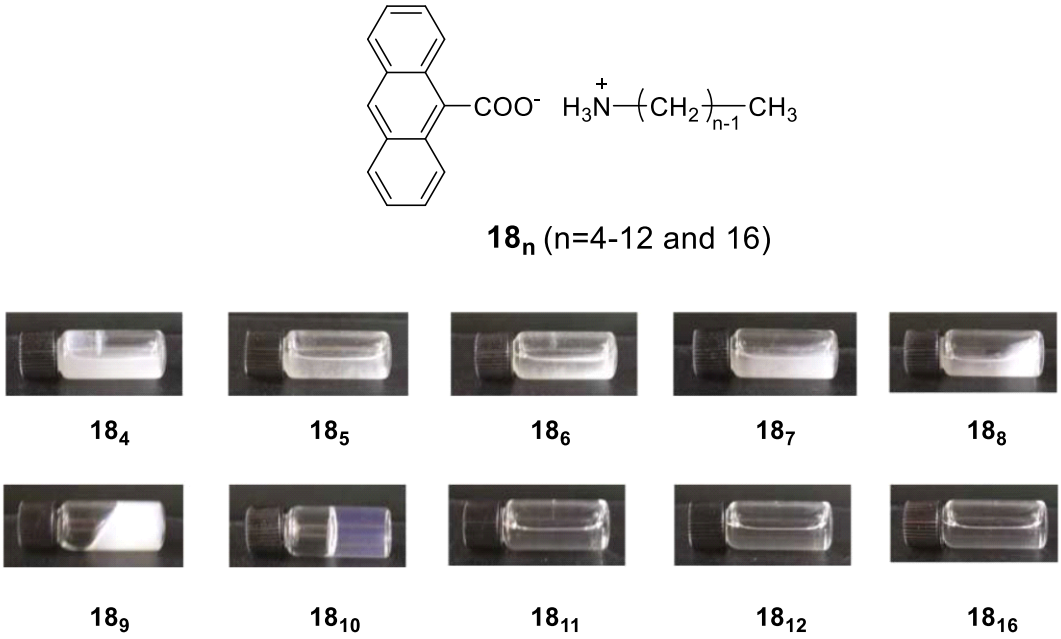

Figure 16. Top: Molecular structures of the alkylammonium anthracene-9-carboxylate derivatives **18**$_n$. Bottom: Pictures of **18**$_n$ (0.005 M) after dissolving in boiling cyclohexane and cooling to 20 °C. Reproduced from ref. 39 with permission from the Royal Society of Chemistry.

Wang *et al.*[40] designed and synthesized a photoresponsive LMWG based on anthracene and urea moieties (**19**). Compound **19** could form opaque gels in 1,2-dichloroethane with an MGC of 16 mg/ml. The gels were prepared by slowly cooling a hot solution of **19** at room temperature. The gelation was thermoreversible, but UV light irradiation could not induce the gel-to-sol transition. Gelation-induced enhanced fluorescence was observed by measuring the fluorescence of compound **19** before and after gelation. The fluorescence intensity in the gel phase was about 10 times higher than in solution, and the fluorescence intensity maximum was red-shifted by about 60 nm after gel formation. Based on these insights, the organogel system could be a potential thermal sensor and a thermally driven fluorescence molecular switch. Photodimerization of compound **19** was studied in THF solution. Exposure to UV light for 160 minutes led to a formation of white suspension, of which the pure photodimer of compound **19** was isolated. NMR spectroscopic studies indicated that only a head-tail dimer is formed in the photodimerization reaction (Scheme 10). This was believed to be affected by

steric hindrance and electronic repulsion between the oxygen atoms linked to the anthracene rings. The gelation ability of the photodimer was also investigated. The photodimer formed organogels in several solvents, including cyclohexane, *n*-hexane, and *n*-heptane. These gels were very stable; only a small proportion of the gel phase was transformed into solution upon either heating or visible light irradiation.

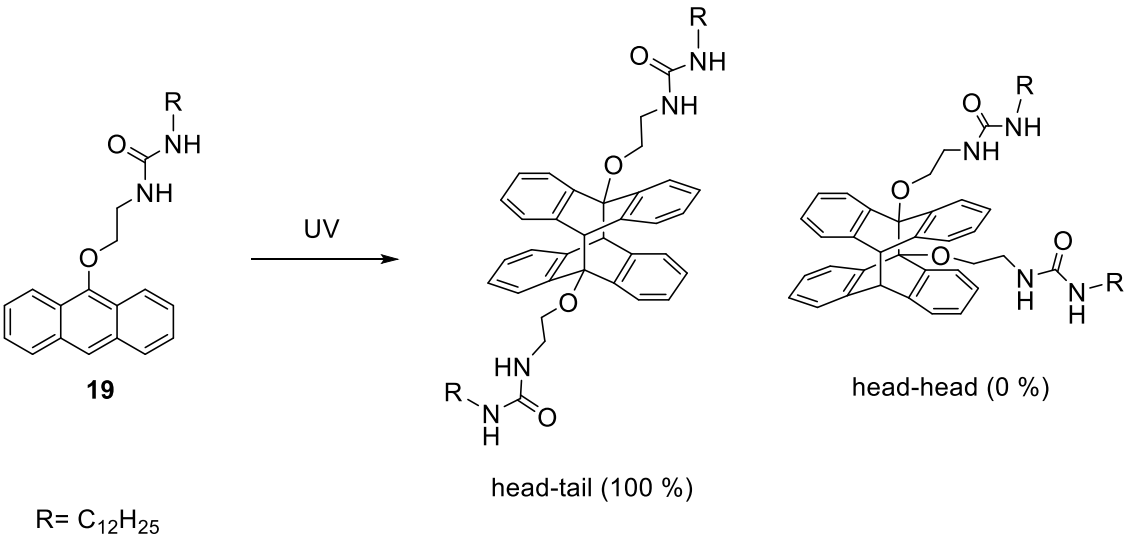

Scheme 10. Photodimerization of compound **19**. Photodimerization gives only a head-tail dimer.[40]

The first anthracene-based hydrogelator was reported by Sako and Takaguchi[41]. They designed and synthesized a hydrogel with a photoresponsive anthracene unit consisting of an anthryl dendron having gluconamides at its peripheral branches (**20**) (Figure 17). The gel was prepared using the heating and cooling method, with an MGC of 0.035 mol/l. The photoresponsivity of the gel was studied spectroscopically by UV-VIS, fluorescence, and ^{1}H NMR spectroscopy. Photodimerization was observed upon UV light irradiation at $\lambda > 300$ nm with up to > 99 % conversion, leading to a gel-to-sol transition. Photodimerization was evidenced by the UV-VIS spectrum showing the disappearance of an absorption band characteristic of anthracene and by the fluorescence spectrum showing the decay of the fluorescence emission band corresponding to anthracene. The formation of the photodimer was also demonstrated by the proton spectrum as the disappearance of the signals corresponding to protons at the 9- and 10-positions in the anthracene moiety. Further studies revealed that the photodimerization reaction produces only head-tail dimers, indicating that the fibrous network consists of anthryl dendrons arranged in an anti-parallel orientation.

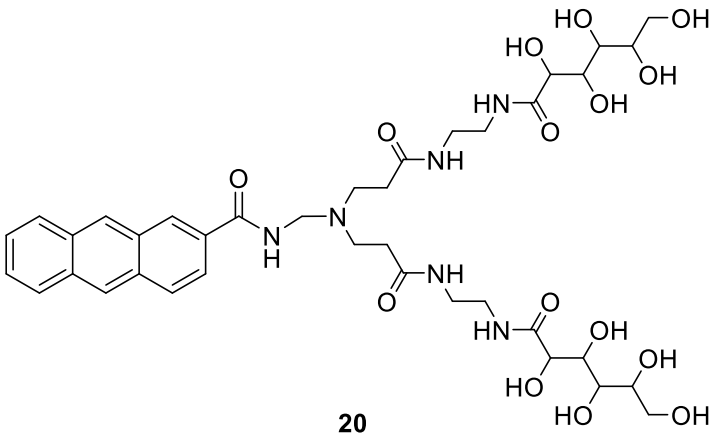

20

Figure 17. Molecular structure of a hydrogelator **20**.[41]

5.2 Photopolymerization

LMWGs based on photopolymerization have been studied quite extensively. One of the most interesting properties of photopolymerizable gels is that light irradiation often strengthens the gels. Photopolymerization can also result in remarkable increases in the thermal stabilities of the gels. Many photopolymerizable LMWGs are based on diacetylene, a hydrocarbon compound which contains two triple bonds. Diacetylenes are known to undergo solid-state polymerization through 1,4-addition reactions when the monomers are in such a position that favors polymerization (Scheme 11).

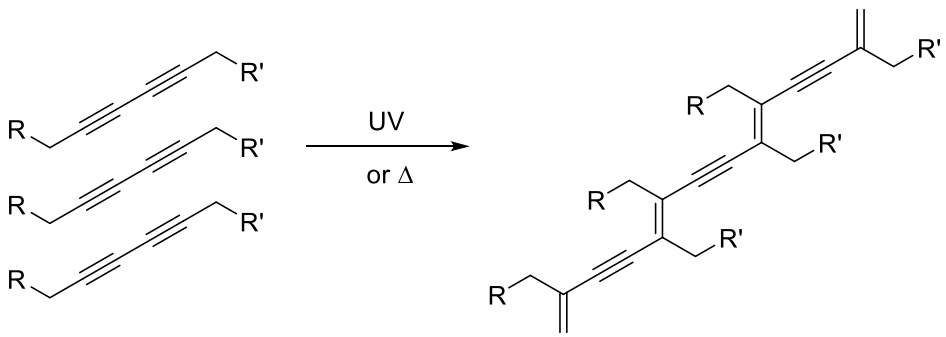

Scheme 11. Photopolymerization of diacetylene.

For example, George and Weiss[42] studied the properties of organogels based on 10,12-pentacosadiynoic acid. Upon UV light irradiation, the gels became intensely coloured, which was expected due to the formation of a highly conjugated network of polydiacetylenes. Before photopolymerization, the gels were thermally reversible, but almost all polymerized gels were stable upon heating up to temperatures that exceeded those where the monomeric gels undergo gel-to-sol transitions. In another example, gels based on urethane-amide dendrons and polymerizable diacetylene peripheral units were investigated.[43] The dendritic compounds formed gels in several organic media and water. Interestingly, the self-assembled aggregates showed different morphologies depending on the solvent. In organic media, the compounds self-assembled into lamella and columnar hexagonal structures, whereas in water, the compounds self-assembled into vesicular structures. Furthermore, the gels underwent photopolymerization upon light irradiation, as implied by severe colorimetric transitions, and stabilization of the solid-state nanostructures.

6 Photocleavage

Another photoreaction that can be exploited in photoresponsive LMWGs is photocleavage. Photocleavable compounds incorporate photoremovable protecting groups (PPGs) that absorb light and convert the energy to trigger certain bond cleavage. As a result, light irradiation causes a permanent bond breaking. Photoinduced bond cleavage typically occurs via intermolecular rearrangement or the formation of a positive charge at the bond break site, leading to a heterolytic dissociation of the leaving groups. Typically, photocleavage can be induced with light at shorter wavelengths, such as UV light. Examples of PPGs utilized in photocleavable LMWGs are 2-nitrobenzyl and coumarin derivatives.[44]

The photocleavage of the 2-nitrobenzyl group has been used to trigger self-assembly and gel formation. In a study by Haines *et al*.,[45] a photocleavable α-carboxy-2-nitrobenzyl group was incorporated into a peptide consisting of a 20 amino acid sequence. An aqueous solution of the peptide was prepared. In its initial form, the peptide remained unfolded due to the presence of the 2-nitrobenzyl group that inhibits the folding of the peptide through electrostatic repulsion. Irradiation of the solution with UV light at $\lambda > 300$ nm induced bond cleavage of the 2-nitrobenzyl group, triggering the peptide folding into amphiphilic β-hairpins, that underwent facial and lateral self-assembly to form a hydrogel (Figure 18). Rheological studies showed that the resulting hydrogel was mechanically rigid, with a storage modulus G' being approximately 1000 Pa and loss modulus G" being considerably smaller in magnitude than the storage modulus. Moreover, laser scanning confocal microscopy imaging of NIH/3T3 mouse embryonic fibroblasts seeded onto the hydrogel was exploited to study its compatibility for future applications in tissue engineering or fabrication of high-density cell arrays. The hydrogel was noncytotoxic, conducive to cell adhesion and suitable for cell migration, proving its potential in biomedical applications.

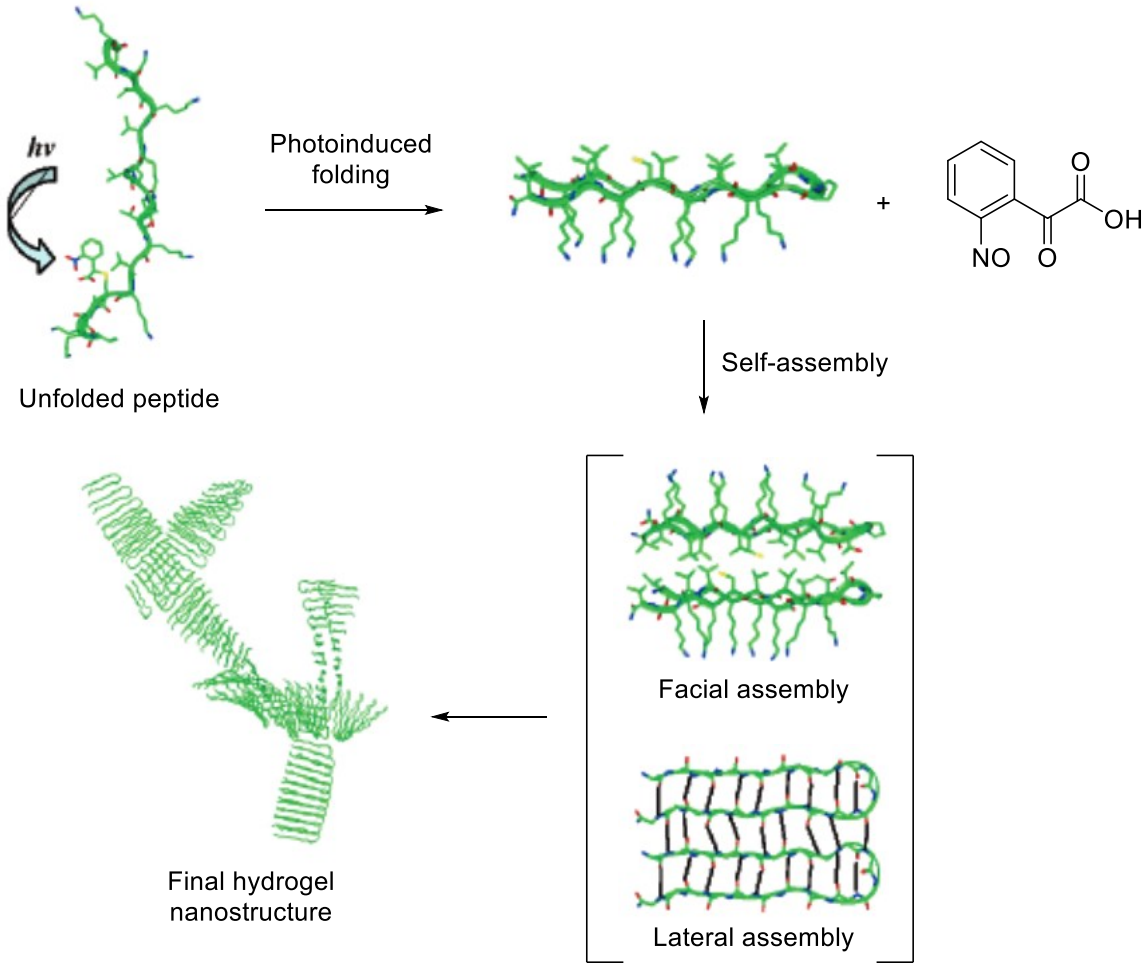

Figure 18. Schematic representation of photoinduced folding of the dipeptide into β-hairpin structure through photocleavage of α-carboxy-2-nitrobenzyl and subsequent formation of a hydrogel *via* facial and lateral self-assembly. Reprinted with permission from ref. 45. Copyright 2005, American Chemical Society.

Another example is a peptide amphiphile molecule **21** with a photocleavable 2-nitrobenzyl group and a bioactive fibronectin epitope Arg-Gly-Asp-Ser (RGDS) reported by Muraoka *et al.*[46] Upon light irradiation at λ=350 nm, the 2-nitrobenzyl group was cleaved to afford compound **22** (Scheme 12), which exhibited light-induced sol-to-gel transition in the presence of charge-screening salt $CaCl_2$ used to trigger the self-assembly of the β-sheet peptide domains. TEM images of compounds **21** and **22** in solution under self-assembling conditions revealed the formation of nanospheres in **21** and nanofibres in **22**. Given this observation, the potential effect of light irradiation on bioactivity was investigated. It was shown that the light-induced gelation of compound **21** significantly improved its bioactivity. Moreover, the compound **21** and the by-products of the photoreaction were found to be noncytotoxic, and that

cell proliferation was normal after light irradiation. These findings provide a framework for creating biomaterials that exhibit light-induced bioactivity.

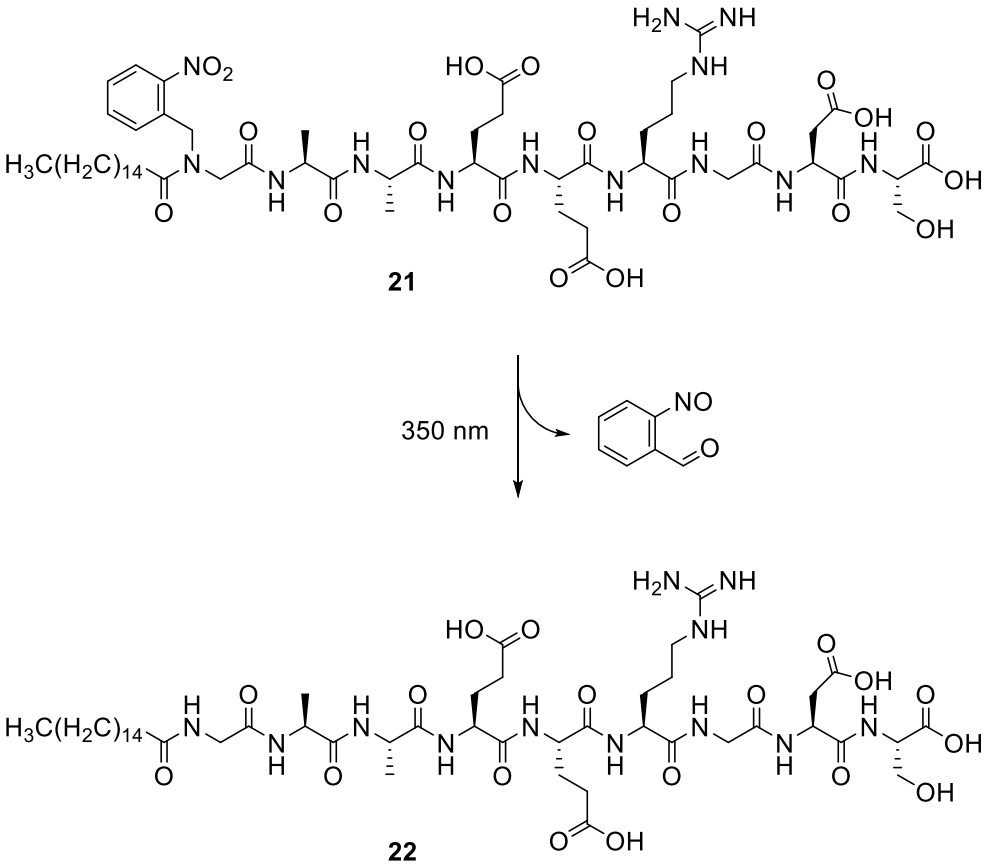

Scheme 12. Molecular structure of the peptide amphiphile compound **21**. Photocleavage of the 2-nitrobenzyl group from compound **21** upon light irradiation at λ=350 nm affords compound **22**.[46]

Photocleavable compounds have been utilized in light-responsive drug delivery systems due to their spatio-temporal resolution and high controllability.[44] As for the gels, drug-loaded hydrogels are currently being studied in research focusing on tumor treatment. Recently, Liu *et al*.[47] reported a photocleavable LMWG for light-triggered drug delivery. The coumarin-based gelator molecule (**23**) (Figure 19) had a good gelation ability, and the MGC in 1:2 PEG200:H_2O solution was 2.7 mg/ml. The SEM image of the gel indicated a formation of spiral-shaped fibres that further assembled to form a three-dimensional solid-state network. Self-assembly of gelator molecules was thought to be driven by intermolecular hydrogen bonding and π–π interactions. Studies regarding the photoresponsivity showed that the gelator molecule underwent a C-N bond photocleavage in 7-amino coumarin upon UV light irradiation

at λ=365 nm, inducing gel-to-sol transition. As discussed in the previous chapter, LMWGs based on coumarin derivatives typically respond to light by photodimerization. However, the light response of the hydrogel formed by **23** was mainly achieved by photocleavage. The utilization of photocleavage for controlled drug release was investigated in more detail. Drug-loaded hydrogels with cytarabine hydrochloride, a chemotherapy medication used to treat leukemia, were prepared and the release of cytarabine was carried out *in vitro*. The hydrogel demonstrated promising controlled release behavior with light irradiation by cleavage of the C-N bond and destruction of the gel phase, upon which the accelerated cytarabine release occurred. In the future, these types of drug-loaded hydrogels could be used in intratumoral injection with light-triggered drug release.

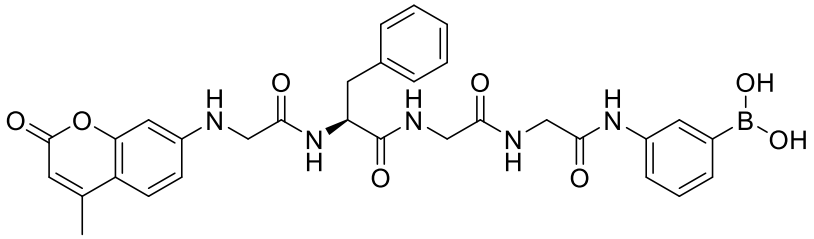

23

Figure 19. Molecular structure of compound **23**.[47]

7 Applications

In the previous chapters, examples of potential applications for photoresponsive LMWGs have been mentioned. These gels can be utilized in applications that take advantage of their different light-induced responses, such as phase transitions (gel-to-sol or sol-to-gel), photochromic switching, fluorescence switching, gel reinforcement and changes in electronic properties. Many possible uses have been suggested, but only a few concrete examples can be yet found. Although the applications of other types of supramolecular gels have been more widely reported, the application of photoresponsive LMWGs will likely become more common in the near future. Possible applications in optoelectronics, environmental remediation, photopatterning and sensing have been envisioned.[48–50] The following sub-chapter will focus on the biomedical applications of photoresponsive LMWGs.

7.1 Biomedical applications

The structural similarity between gels and body tissues has led to their widespread use as biomaterials in various applications. Photoresponsive supramolecular gels have been utilized, for example, in controlled drug delivery and cell culturing.[51] For biomedical applications, hydrogels are preferred due to their polarity and better biocompatibility. This makes an additional challenge to the design of photoresponsive hydrogels since many photoresponsive units are highly non-polar. Moreover, the majority of these systems require activation with UV light. Since tissue penetration is more efficient at longer wavelengths and shorter wavelengths may cause phototoxic damage, visible light-activated materials that work in an aqueous environment are in high demand. To fulfil these demands, researchers have aimed to develop photoresponsive hydrogel materials that operate within the so-called “therapeutic window”, a term used for the 650-1100 nm wavelength range.[52]

7.1.1 Drug delivery

Proteins and other macromolecules can be physically entrapped in the gel networks, and the change in the mesh size of the network can regulate the release of the entrapped molecules.[51] Another option is the release of drug molecules with a gel-to-sol transition. Light-induced drug release from the gel network enables targeted delivery, extension of circulation time, and reduced toxicity and side effects.

In the previous example by Liu *et al.*[47], photocleavable LMWGs can be used in light-controlled drug delivery. The coumarin-based hydrogels were loaded with a chemotherapy medication, and the light-induced release from the gel matrix was obtained by gel-to-sol transition. In some examples, the drug release is achieved by photoisomerization of azobenzene. For example, in the previously discussed study by Huang *et al.*[21], a hydrogel formed by azo-Gln-Phe-Ala demonstrated a controlled release of vitamin B_{12}. Without light irradiation, the release from the gel matrix to the upper water phase occurred by diffusion, which took more than two days to complete. The release ratio increased significantly under exposure to UV light (Figure 20). After 4 hours, the release ratio of the irradiated sample was 97 %, while the ratio for the non-irradiated sample was only around 30 %.

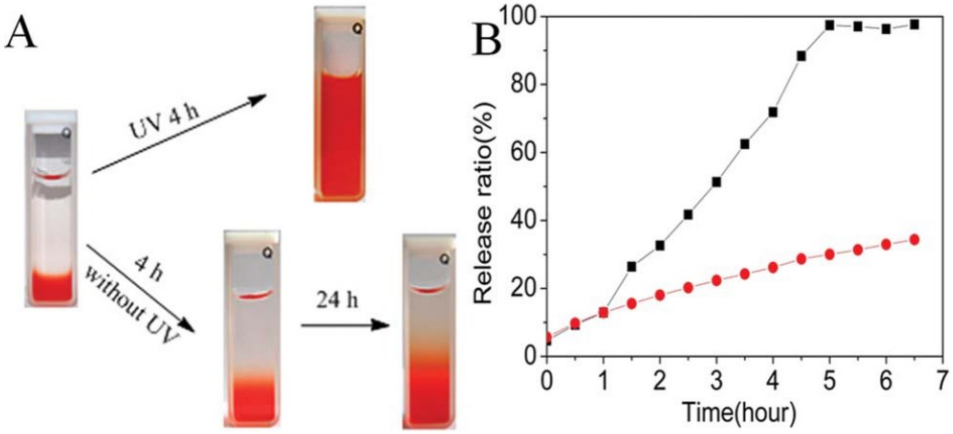

Figure 20. A) Images of the controlled drug release of vitamin B_{12} upon UV light irradiation (top) and spontaneous diffusion (bottom). B) Release ratio of vitamin B_{12} with (black square) and without (red dot) UV light irradiation. Reproduced from ref. 21 with permission.

A hydrogel formed by azobenzene-functionalized cyclic dipeptide PAP-DKP-Lys (**24**) was used for light-induced release of dsDNA oligomers and an anticancer drug doxorubin.[53] Compound **24** could form very fragile hydrogels that were delicate to mechanical stress. However, the addition of dopants like NaCl, acids or DNA improved the rigidity of the gels. Light-induced gel-to-sol transition was observed upon irradiation with UV light at λ=365 nm (Figure 21).

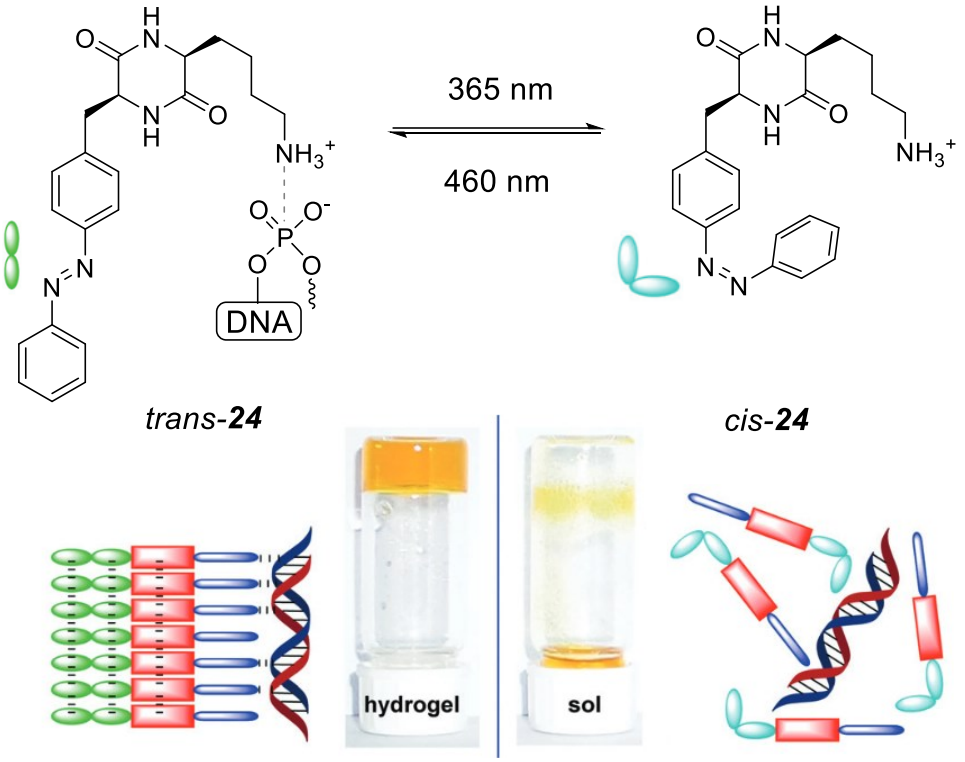

Figure 21. Photoisomerization of compound **24**. UV-light irradiation induces gel-to-sol transition, releasing DNA. Reproduced from ref. 53 with permission from the Royal Society of Chemistry.

In a recent study, Leistner *et al.*[54] developed a "molecular syringe" based on azobenzene and cyclic peptide moieties (**25**) (Figure 22) that releases previously encapsulated cargo in response to red light. A fluorescent dye 5(6)-carboxyfluorescein was mixed with a hydrogel formed by **25**. Upon irradiation with light at λ=660 nm, the gel underwent a light-induced shrinking by reducing to 25-50 % of its initial size, releasing the fluorescent dye in liquid form (Figure 22). Quantitatively pre-loaded hydrogels released up to 66 % of the cargo upon red light irradiation, whereas the hydrogels stored in the dark firmly held the cargo inside the network. Inspired by these findings, the work will continue with the use of bioactive cargo such as anticancer and antimicrobial substances.

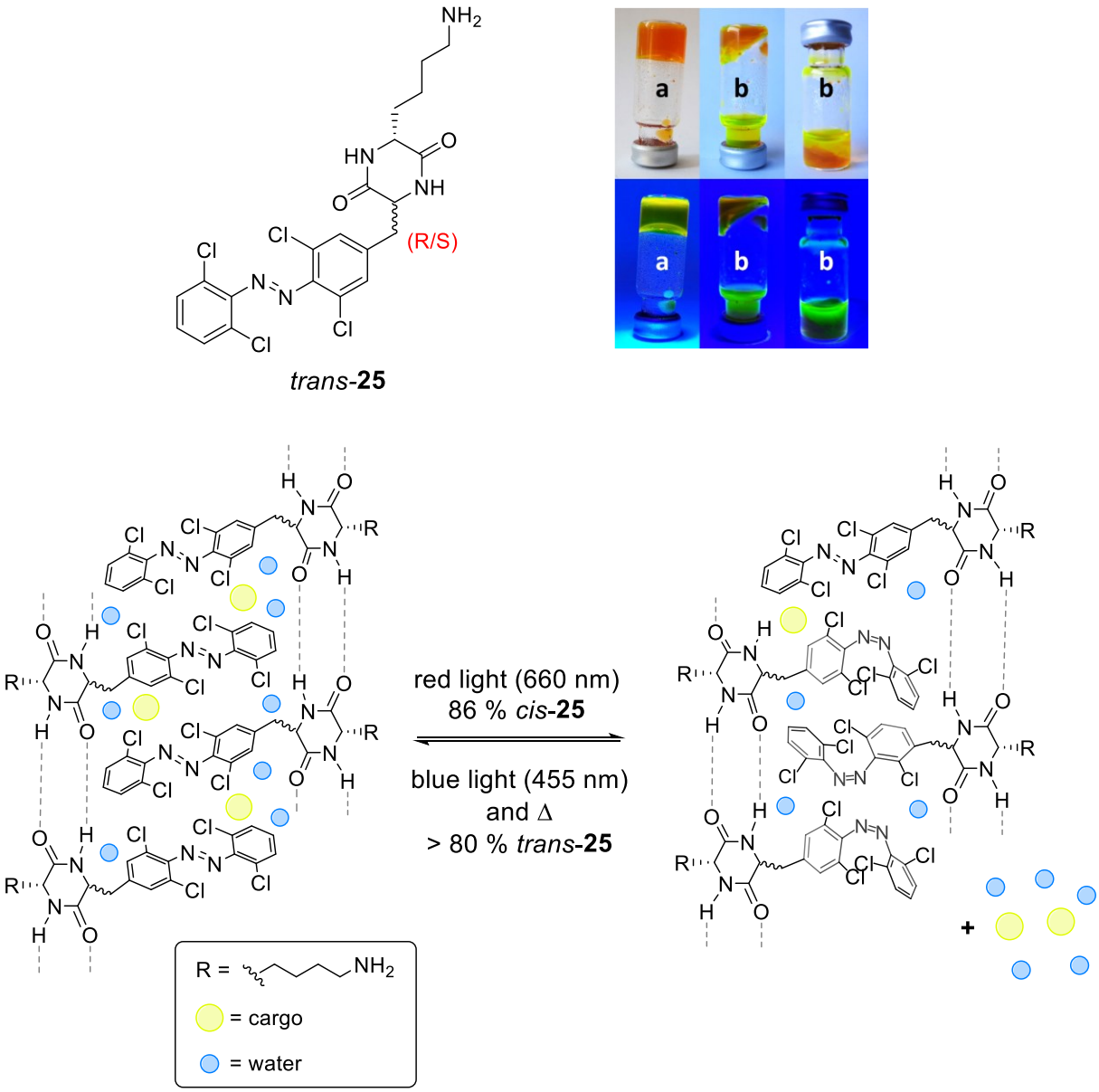

Figure 22. Top left: Molecular structure of *trans*-**25**. Top right: Photos of hydrogels (0.2 wt% of **25** in PBS at pH 7.4) loaded with fluorescent dye in normal light or under UV irradiation. Sample a was equilibrated in the dark and sample b was irradiated with red light (660 nm), during which the fluorescent cargo was released from the gel. Bottom: Schematic representation of the hydrogel loaded with cargo before and after irradiated with red light (660 nm). Reproduced from ref. 54, Copyright 2023, with permission from Wiley-VCH GmbH. https://doi.org/10.1002/chem.202302295

7.1.2 Cell culturing

Another example of biomedical applications utilizing photoresponsivity is cell culturing. Hydrogel matrices are a suitable growth media for cells due to their structural similarities to hydrated living tissues. The hydrogels can be used to support, guide, and stimulate cell development, while photoresponsivity enables the altering of bioactivity and manipulation of the environment surrounding the cells. In this field, the incorporation of 2-nitrobenzyl moieties has been used for selective bioactivity and guidance of cell growth, as shown in the previous example by Muraoka *et al*.[46] In the study, NIH/3T3 mouse embryonic fibroblasts were cultured in a medium incorporated with an RGDS-containing peptide amphiphile bearing a photoresponsive 2-nitrobenzyl group (**21**) seeded into tissue-culture-treated plates. One plate was irradiated for 90 minutes to induce sol-to-gel transition through photocleavage, while the other one was kept in the dark to avoid gelation. The focal adhesions formed by the cells in the different plates were investigated by monitoring vinculin, a cytoskeletal protein found in focal adhesion plaques. The vinculin expression was 1.9 times more efficient in the plate exposed to light, indicating that the light-induced gelation significantly increased the bioactivity.

8 Summary

This literature part was about photoresponsive low molecular weight gels (LMWGs). These gels have photoresponsive functional groups that can be categorized based on the different types of photoreactions (Scheme 13). Light irradiation can cause a wide range of responses, enabling their utilization for many kinds of applications. Given their structural resemblance to body tissues and their remotely controllable nature, photoresponsive LMWGs are suitable for biomedical applications, such as drug delivery and cell culturing. Of all reported photoresponsive LMWGs, the ones based on the photoisomerization of azobenzene are the most common, while only a few examples of photocleavable LMWGs have been reported.

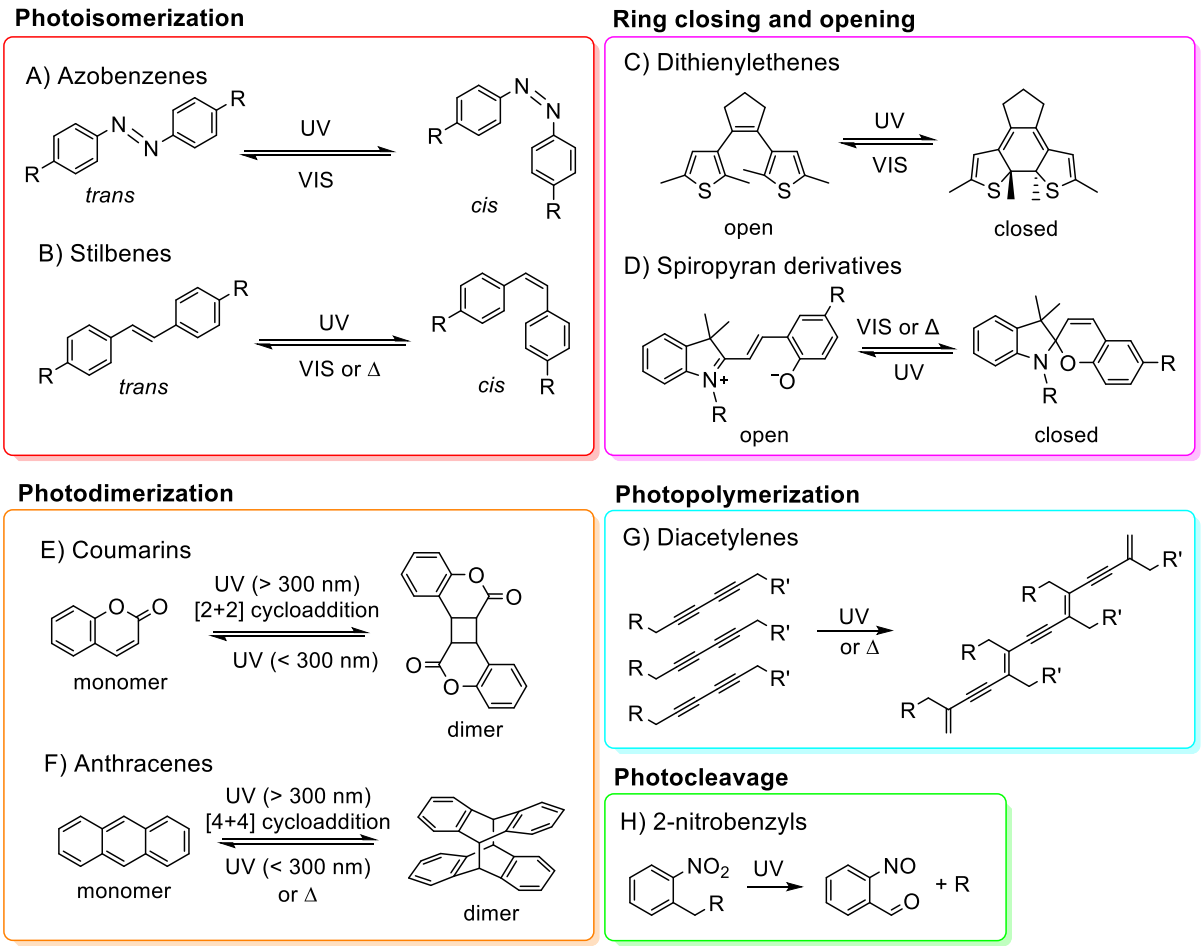

Scheme 13. Summary of different photoreactions used in photoresponsive LMWGs.

Photoresponsive LMWGs have been studied quite extensively in the last decades, and the ongoing work will most probably continue in the near future. Despite being extensively studied, there are still significant gaps in understanding their self-assembly process. Among the already discovered photoresponsive LMWGs, there is room for improvement in their robustness. The reversibility of these gels should also be further developed, especially if they are intended for applications that require such behavior.

The study of multiresponsive LMWGs is expected to intensify in the future since the use of multiple stimulants enables more diverse applications. Currently, most of the reported photoresponsive LMWG systems function with UV light. This is expected to change, since biological applications require activation with visible light to have better tissue penetration and cause less photodamage. For biomedical applications, the research will presumably shift from organogels towards hydrogels.

EXPERIMENTAL PART

9 Motivation

Boron dipyrromethene (BODIPY) and its derivatives have been the subject of extensive research over the past decades. Due to their excellent photophysical properties, such as long wavelength emission, high molar absorption coefficients and high fluorescence quantum yields, BODIPY-based supramolecules have been widely used in applications related to responsive materials, gels, and liquid crystals, to name a few.[55] One example related to supramolecular gels is the study by Sun *et al.*[56], where a BODIPY-based rotaxane host-guest supramolecule system was investigated. The gel showed reversible gel-to-sol phase transition upon multiple external stimuli, such as temperature, mechanical stress, and the addition of different anions. Another example is the study by Camerel *et al.*[57], which studied the properties of a polymeric BODIPY-based organogel. However, there are no examples of photoresponsive LMWGs based on BODIPY compounds.

Previous studies have shown that certain types of (*meso*-methylhydroxy)-BODIPY compounds enable the photocleavage *via* carbamate bond upon irradiation of green light (Scheme 14).[58] Based on this insight, it was thought that this type of BODIPY compound could be used to synthesize a potential photocleavable LMWGs. Therefore, the BODIPY moiety was designed to be linked with a gelator molecule. The incorporation of mono- and dipeptides was chosen due to their efficient gelation and dynamic self-assembling properties.[7,59] The potential LMWGs could be controlled *in situ* by visible light[58], and they could be developed further for the applications in controlled drug delivery, for example.

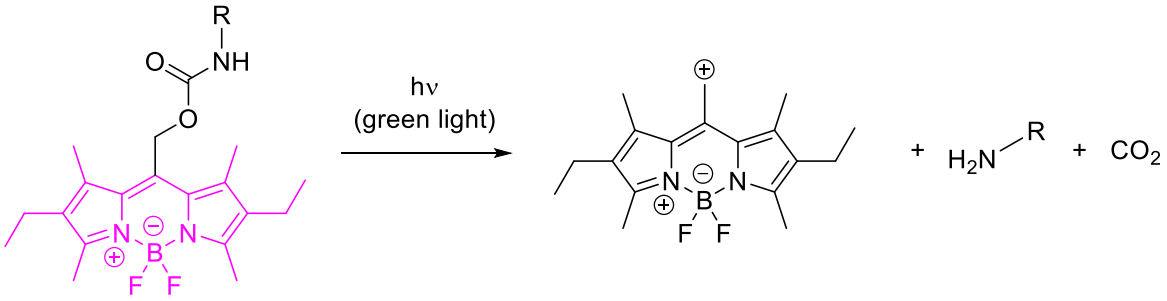

Scheme 14. Schematic representation of a photocleavable (*meso*-methylhydroxy)-BODIPY compound under irradiation of green light.[58] The final decomposition products of the BODIPY core are still unknown.

The aim of the experimental part was to design and synthesize potential photocleavable peptide-based LMWGs integrated into a BODIPY moiety (**33-34**) (Figure 23). The BODIPY compounds **26-28**, the Boc-protected dipeptides **29-30** and their corresponding unprotected dipeptides **31-32** were synthesized. To enable photocleavage, the BODIPY moiety was tried to be linked to a peptide-based gelator *via* a carbamate bond. Two approaches were used to introduce the carbamate bond between the BODIPY and the peptide part. The first one was to make the compound **28** react with the mono- and dipeptides via nucleophilic substitution in basic conditions, and the second one was to use the compound **27** and the mono-and dipeptides together with a commonly used coupling reagent, N-N'-carbonyldiimidazole (CDI).

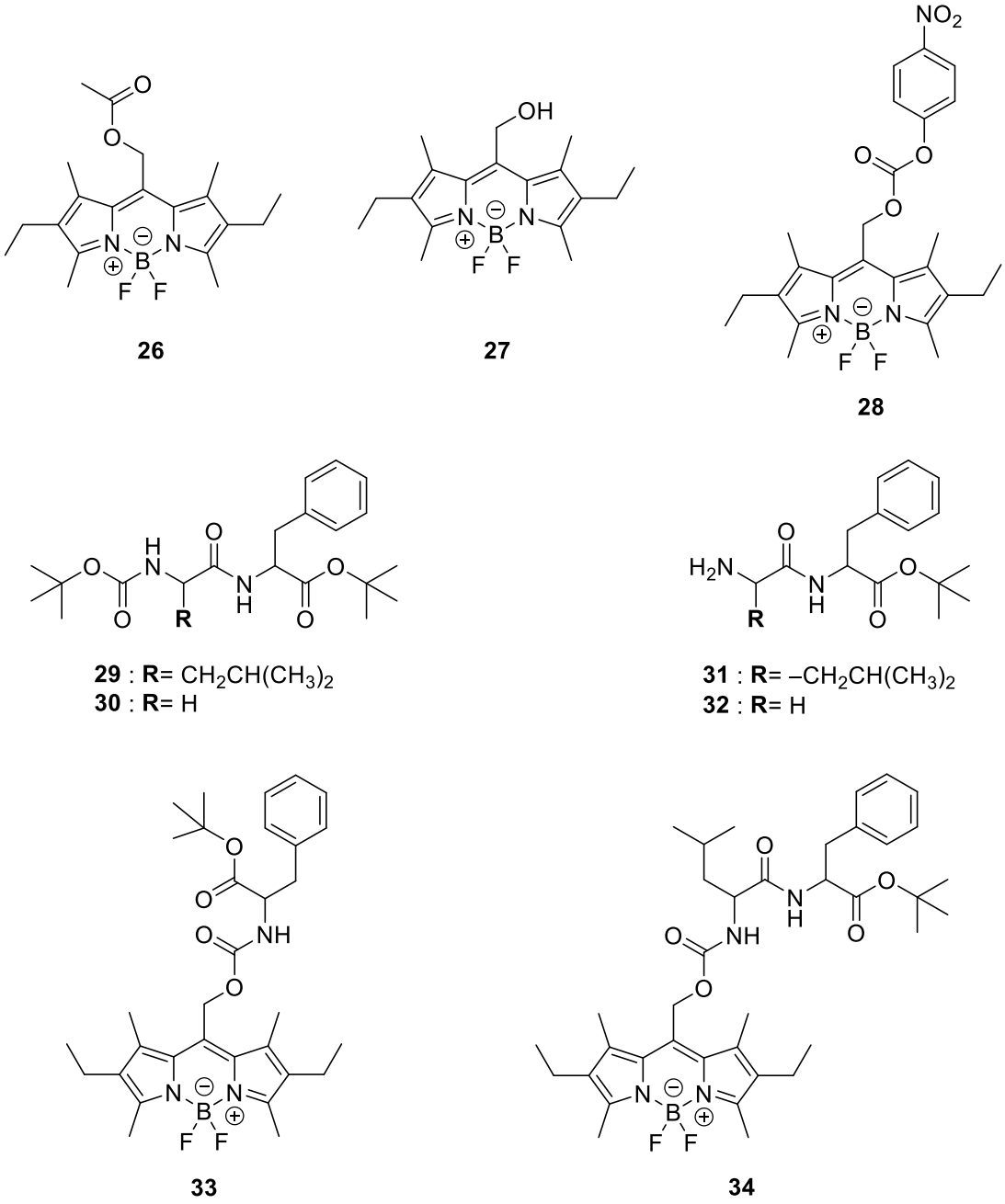

Figure 23. Molecular structures of the synthesized BODIPY compounds **26-28**, Boc-protected dipeptides **29-30,** their corresponding unprotected dipeptides **31-32**, and the potential LMWGs **33-34**.

10 Materials and methods

All the reactions were performed in an inert atmosphere using nitrogen gas, dry solvents, and oven-dried glassware, excluding the deprotection reactions of the dipeptides.

Dry dichloromethane and tetrahydrofuran were obtained with MBraun SPS-800 series solvent purification system. Pyridine was distilled before use. Other chemicals (Table 1) were used without further purification.

Mettler Toledo XP205 scale was used to weigh reagents and VWR LAG 214i scale was used to weigh glassware. Heidolph Laborota 4000 rotary evaporator was utilized to evaporate solvents. Hermle Z206A centrifuge was used to separate precipitates and Elmasonic S ultrasonic bath was used to dissolve some compounds.

The reactions were monitored by TLC with Merck silica gel 60 F_{254} plates and visualized with UV lamp. Hanessian's stain was used with the dipeptides. Hanessian's stain was prepared by dissolving $(NH_4)_6Mo_7O_{24}\cdot H_2O$ (5 g) and $Ce(SO_4)_2$ (1 g) into deionized water (90 ml) in an ice bath, adding H_2SO_4 (10 ml) and stirring at RT until the color turned bright yellow.

CombiFlash Nextgen 300 chromatography system with RediSep columns and silica gel packing of manual columns were used for chromatographic purifications.

^{1}H NMR spectra were recorded with Bruker Avance III HD 300 MHz and Bruker Avance III 500 MHz spectrometers. The ppm scale was calibrated by using the chemical shift of the residual protons (for $CDCl_3$ δ_H=7.26 ppm and for DMSO-*d*$_6$ δ_H=2.50 ppm) or carbons (for $CDCl_3$ δ_C=77.16 ppm) of the solvent.

Mass spectra were recorded with Agilent Technologies' 6560 Ion Mobility Q-TOF mass spectrometer.

Table 1. List of chemicals and their purities.

Chemical	**Manufacturer**	**Purity (%)**
Ammonium chloride	J. T. Baker	≥ 99.5
Boc-Gly-OH	Sigma Aldrich	≥ 99.0
Boc-Leu-OH	Sigma Aldrich	≥ 99.0
Boron trifluoride diethyl etherate	Thermo Scientific	> 98
Chloroform D	Eurisotop	99.80 D
Dichloromethane	Honeywell	> 99.8
Dichloromethane	VWR	> 99.5
Diethyl ether	VWR	> 99.7
Dimethylformamide	VWR	> 99.8
N, N-Dimethylformamide (Extra dry over Molecular Sieve)	Thermo Scientific	99.8
2,4-Dimethyl-3-ethylpyrrole	Acros Organics	96
Dimethyl sulfoxide D6	Eurisotop	99.80 D
Ethyl acetate	VWR	> 99.5
n-Hexane	Honeywell	≥ 97.0
Hydrochloric acid	Honeywell	≥ 37
Lithium hydroxide monohydrate	Honeywell Fluka	≥ 98.5
Magnesium sulfate hydrate	Honeywell	> 99.0
Methanol	Honeywell	≥ 99.8
N, N′-Carbonyldiimidazole	Fluorochem	98.0
N, N-diisopropylethylamine	Sigma Aldrich	99
4-Nitrophenyl chloroformate	TCI	> 98.0
Petroleum ether (bp. 40-60 °C)	Honeywell	≥ 90
(*S*)-3-Phenylalanine *t*-butyl ester HCl	Biosynth	≥ 95
Pyridine	VWR Chemicals	≥ 99.7
Silica gel (0.040-0.063 mm)	Merck Millipore	
Sodium chloride	VWR	100
Sodium hydrogen carbonate	Fisher Scientific	≥ 99.7
Sodium sulfate anhydrous	Fisher Scientific	≥ 99
Sulfuric acid	Fluka	95-97
TBTU	Biosynth	> 98
tert-Butyl Methyl Ether	TCI Chemicals	> 99.0
Toluene	VWR	≥ 99.5
Triethylamine	Sigma Aldrich	≥ 99.5

10.1 Syntheses

10.1.1 EtBODIPYOAc (26)

EtBODIPYOAc (**26**) was synthesized following a procedure developed by Korhonen *et al*.[60] (Scheme 15). In the synthesis of compound **26**, a 3-substituted pyrrole is acylated using an acid chloride, that further reacts to form a dipyrrinium intermediate via condensation reaction. The final product is obtained by fluoroboration of the dipyrromethene intermediate in the presence of TEA.

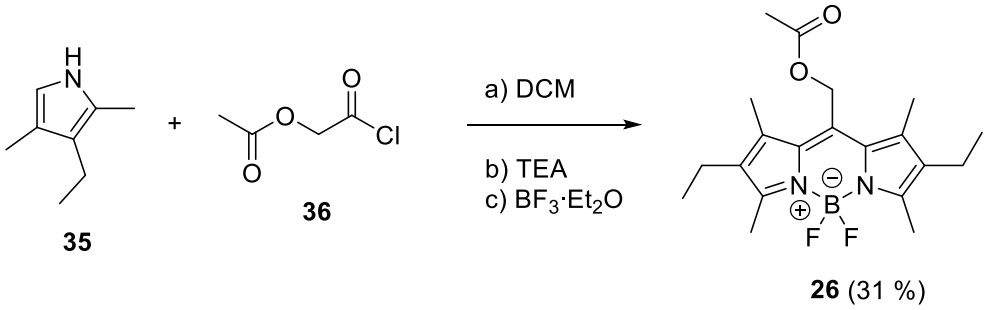

Scheme 15. The synthesis of BODIPYOAc (**26**).

2,4-dimethyl-3-ethyl-pyrrole (**35**) (4.3 ml, 32.0 mmol, 2.0 eq) was dissolved in dry DCM (180 ml) at RT under N_2 atmosphere. Acetoxyacetyl chloride (**36**) (1.7 ml, 16.0 mmol, 1.0 eq) was added to the solution dropwise within 10 minutes, after which the colour of the solution turned from light brown to red. The reaction mixture was stirred at 50 °C under N_2 in the dark for 2 hours, while monitored by TLC (eluent: DCM). TEA (11 ml, 76.0 mmol, 4.8 eq) was added at 0 °C and the reaction mixture was stirred for 40 minutes at RT in the dark. $BF_3 \cdot Et_2O$ (13.6 ml, 110.0 mmol, 6.9 eq) was added, and the reaction mixture was stirred for 1 hour at 50 °C in the dark.

The reaction mixture was extracted with deionized water (180 ml). The water phase was extracted with DCM (90 ml) and the combined organic phases were washed with saturated $NaHCO_3$ (180 ml) and brine (200 ml). The water phases were extracted with DCM (50 ml) between each washing, and the combined organic phases were dried with $MgSO_4$ and the solvent was evaporated under reduced pressure.

The crude was purified by flash chromatography with silver silica gel column (220g, 40-60 µm) (eluent: 40-95 % DCM in petroleum ether (bp. 40-60 °C) as gradient). The residue was recrystallized from MeOH at -20 °C overnight. The crystals were filtered and dried overnight under vacuum, yielding product **26** as a dark purple-green powder (1.87 g, 31 %).

10.1.2 EtBODIPYOH (27)

EtBODIPYOH (**27**) was synthesized following a procedure developed by Korhonen *et al.*[60] (Scheme 16). In the reaction, the BODIPY compound **26** reacts through basic hydrolysis to form the BODIPY compound **27**.

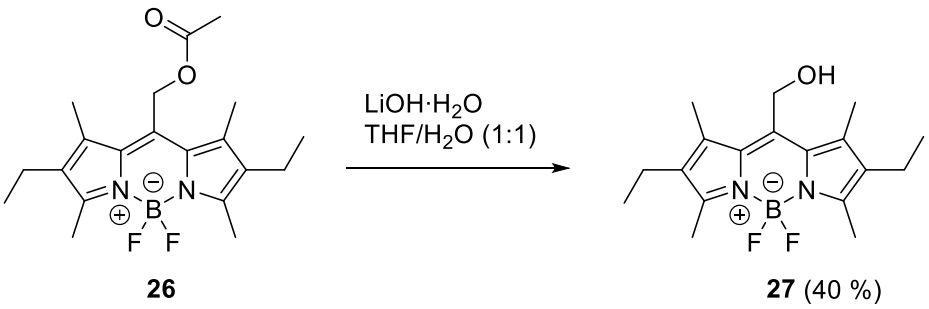

26 **27** (40 %)

Scheme 16. The synthesis of EtBODIPYOH (**27**).

EtBODIPYOAc (**26**) (1.59 g, 4.22 mmol, 1.0 eq) was dissolved in THF (84 ml) under N_2 atmosphere. $LiOH \cdot H_2O$ (885.89 mg, 21.1 mmol, 5.0 eq) in deionized water (84 ml) was added, and the reaction mixture was stirred for 2 hours at RT in the dark while monitored by TLC (eluent: 20 % EtOAc in *n*-hex).

The reaction mixture was dissolved in EtOAc (84 ml) and the organic phase was separated. The water phase was extracted with EtOAc. The combined organic phases were washed with saturated $NHCl_4$ solution and brine, dried with $MgSO_4$, and evaporated under reduced pressure.

The crude was purified by flash chromatography with silver silica gel column (80 g, 40-60 µm) (eluent: 5-20 % EtOAc in *n*-hex as gradient), yielding product **27** as a red solid (574 mg, 40 %).

10.1.3 EtBODIPYPNP (28)

EtBODIPYPNP (**28**) was synthesized following a procedure developed by Korhonen *et al.*[60] (Scheme 17). The BODIPY compound **28** is obtained by the nucleophilic substitution reaction of the compound **27** and *p*-nitrophenol chloroformate (**37**). A significant amount of *p*-nitrophenol is formed in a side reaction of compound **37** and water, but it can be removed by thorough extraction.

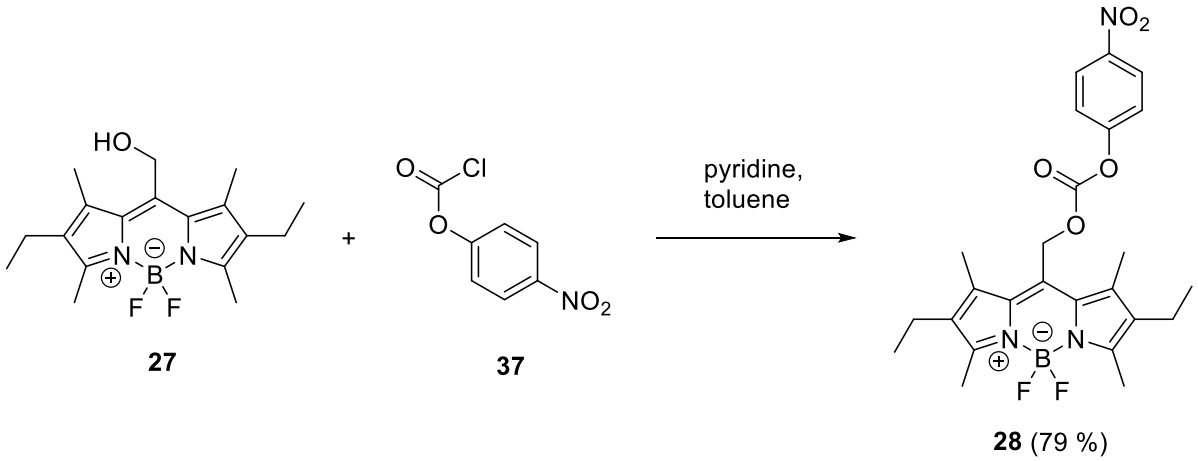

Scheme 17. The synthesis of EtBODIPYPNP (**28**).

EtBODIPYOH (**27**) (200.91 mg, 0.60 mmol, 1.0 eq) was dissolved in toluene (20 ml) under N_2 atmosphere. *p*-Nitrophenyl chloroformate (**37**) (485.36 mg, 2.40 mmol, 4.0 eq) was added, followed by the addition of pyridine (24 µl). The reaction mixture was stirred for 2.5 hours in the dark at RT while monitored by TLC (eluent: 20 % EtOAc in *n*-hexane).

The reaction mixture was diluted with EtOAc, and the separated organic phase was washed with saturated $NHCl_4$ solution (2x40 ml) and brine (1x100 ml). The organic phase was dried with $MgSO_4$ and evaporated under reduced pressure.

The crude was purified by flash chromatography with a gold silica gel column (40 g, 20-40 µm) (eluent: 0-20 % EtOAc in *n*-hexane as gradient). The residue was dissolved in EtOAc (30 ml) and washed with 5 % NaOH solution (12x20 ml) and deionized water (1x20 ml). The organic phase was dried with $NaSO_4$ and evaporated under reduced pressure. The residue was dissolved in MeOH (50 ml) with slight heating and sonication and recrystallized at -20 °C overnight.

The precipitate was separated by centrifugation (6000 rpm, 20 minutes) and the obtained pellet was transferred to a flask with DCM. The solvent was evaporated under reduced pressure, and the product was dried in a vacuum overnight, yielding product **28** as a dark pink solid (237 mg, 79 %).

10.1.4 Boc-protected dipeptides

BocLeuPheO*t*Bu (**29**) was synthesized according to a procedure developed by Chevigny *et al*.[61] (Scheme 18). The same procedure was applied for BocGlyPheO*t*Bu (**30**). The reagent amounts and yields are presented in Table 2.

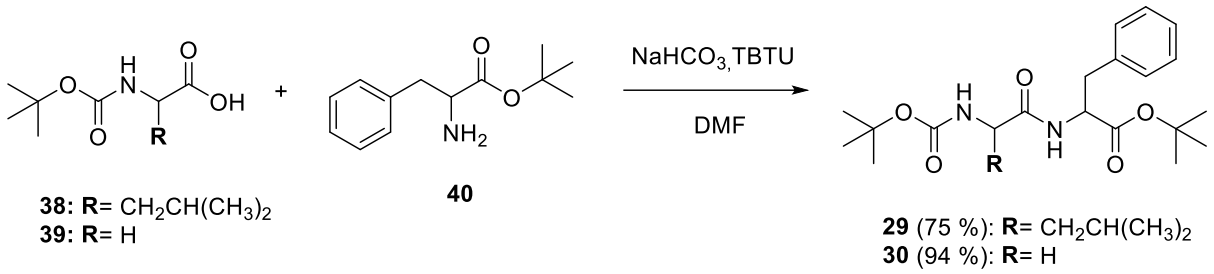

Scheme 18. Syntheses of the dipeptides **29-30**.

Table 2. Yields and reagent amounts for the syntheses of Boc-protected dipeptides **29-30**.

Product	Yield (g, %)	m[Boc-amino acid **38-39**] (mg)	m[$NaHCO_3$] (mg)	m[TBTU] (mg)	m[**40**] (mg)	m[$NaHCO_3$] (mg)
BocLeuPheO*t*Bu (**29**)	0.75, 75	534.41	194.59	741.54	656.01	213.83
BocGlyPheO*t*Bu (**30**)	1.02, 94	500.34	240.41	916.03	809.89	264.15

General procedure: Boc-protected amino acids **38-39** (1.0 eq) and TBTU (1.0 eq) were added to a solution of $NaHCO_3$ (1.0 eq) in dry DMF (7 ml or 8 ml, respectively) under N_2 atmosphere. The solution was stirred for 1 hour at RT. PheO*t*Bu (**40**) (1.1 eq) and $NaHCO_3$ (1.1 eq) were dissolved in dry DMF (7 ml or 8 ml, respectively) in a separate flask and added to the reaction mixture. The reaction mixture was stirred overnight at RT under an N_2 atmosphere. Completion

of the reactions was confirmed by TLC (eluent: EtOAc:MeOH:H_2O 7:2:1, Hanessian's stain). The solvent was co-evaporated with toluene (x2) under reduced pressure.

The residue was dissolved in DCM and the organic phase was extracted with water (2x), 1 M HCl (1x), deionized water (2x) and saturated $NaHCO_3$ solution (1x). The water phase was washed with DCM. The combined organic phases were dried with $MgSO_4$, evaporated under reduced pressure, and dried under vacuum, yielding product **29** as a yellowish powder and product **30** as a yellow oil.

10.1.5 Deprotection of the dipeptides

The dipeptides **31-32** were synthesized according to a procedure developed by Chevigny *et al.*[61] (Scheme 19). Previously, the deprotection reaction had been done with BocLeuPheO*t*Bu (**31**) but not with BocGlyPheO*t*Bu (**32**). The reagent amounts and yields are presented in Table 3.

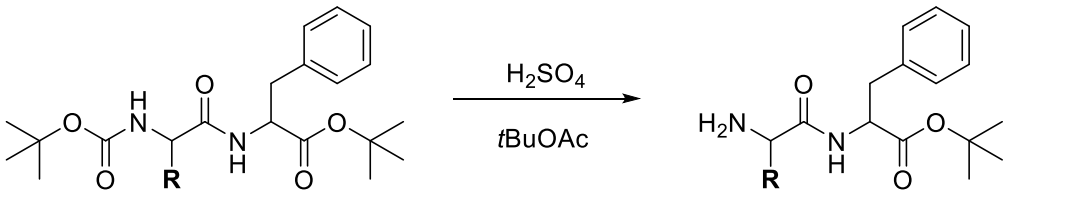

29: **R**= $-CH_2CH(CH_3)_2$
30: **R**= H

31 (44 %): **R**= $-CH_2CH(CH_3)_2$
32 (65 %): **R**= H

Scheme 19. Deprotection of the dipeptides.

Table 3. Yields and reagent amounts for the syntheses of the dipeptides **31-32**.

Product	Yield (g, %)	m[Boc-dipeptide **29-30**] (mg)	V[H_2SO_4] (µl)
LeuPheO*t*Bu (**31**)	0.25, 44	744.60	442
GlyPheO*t*Bu (**32**)	0.24, 65	502.09	354

General procedure: The dipeptides **29-30** (1.0 eq) were dissolved in *t*BuOAc (9 ml or 7 ml, respectively) to form a 0.2 M solution. Concentrated H_2SO_4 (5.0 eq) was added dropwise, and the reaction mixture was stirred for 1 hour at RT, while monitored by TLC (eluent: EtOAc:MeOH:H_2O 7:2:1, Hanessian's stain). The reaction mixture was neutralized with saturated $NaHCO_3$ and extracted with ethyl acetate (10 ml). The organic phase was separated, and the water phase was washed with ethyl acetate. The combined organic phases were dried with $MgSO_4$ and evaporated. The products were dried under a vacuum overnight, yielding product **31** as a pale-yellow powder and product **32** as a yellow oil.

10.1.6 Linkage of EtBODIPYPNP (28) with mono- and dipeptides

EtBODIPYPheO*t*Bu (**33A**) and EtBODIPYLeuPheO*t*Bu (**34A**) were aimed to synthesize by using EtBODIPYPNP (**28**) as starting material (Scheme 20). The reagent amounts are listed in Table 4. The reaction conditions for both reactions were the same, except for the solvents. DMF was used in the reaction of **33A** and THF in the reaction of **34A**.

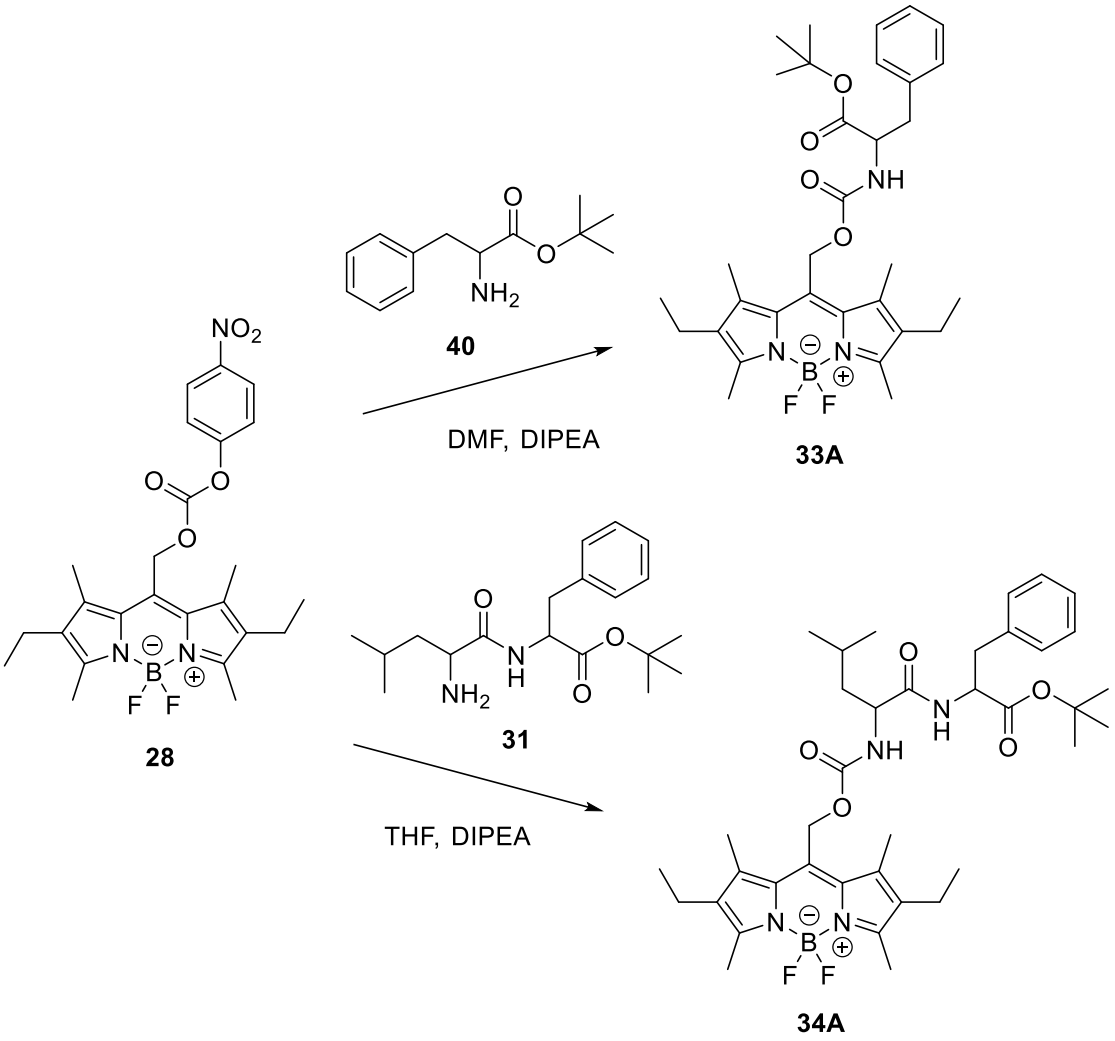

Scheme 20. Syntheses of EtBODIPYPheO*t*Bu (**33A**) and EtBODIPYLeuPheO*t*Bu (**34A**).

General procedure: EtBODIPYPNP (**28**) (1.0 eq) was dissolved in dry DMF/THF (24 ml) under a N_2 atmosphere. PheO*t*Bu (**40**) or LeuPheO*t*Bu (**31**) and DIPEA (1.0 eq) were dissolved in dry DMF/THF (1.5 ml) under N_2 and the solution was transferred to the reaction mixture. The reaction mixture was stirred at RT in the dark under N_2. The reaction was monitored with TLC (eluents: 20 % EtOAc in *n*-hex for **33A** and 80 % DCM in *n*-hex for **34A**). The reaction was carried on for 4 h, after which the solvent was evaporated, and the crude product was dried under vacuum overnight. In the case of the synthesis of **33A**, the presence of the product could not be concluded based on TLC. Therefore, the crude was purified by column chromatography (eluent: 80-90 % DCM in *n*-hex). The separation was unsuccessful, so the purification was repeated using a different eluent (30-40 % ether in petroleum ether). The ^{1}H NMR spectrum was recorded after the second purification. Based on the spectrum, it was concluded that the reaction did not produce the desired product.

In the case of **34A**, the TLC looked like the one of **33A**. Since the reaction of **33A** had previously been found to be unsuccessful, the purification of **34A** was not done.

Table 4. Reagent amounts for syntheses of **33A-34A**.

Product	m[EtBODIPYPNP] (mg)	m[**40, 31**] (mg)	V[DIPEA] (µl)
EtBODIPYPheO*t*Bu (**33A**)	25.24	12.99	8.8
EtBODIPYLeuPheO*t*Bu (**34A**)	25.43	17.19	8.9

10.1.7 Coupling EtBODIPYOH (27) with mono- and dipeptides

EtBODIPYPheO*t*Bu (**33B**) and EtBODIPYLeuPheO*t*Bu (**34B**) were aimed to synthesize by using EtBODIPYOH (**27**) as a starting material (Scheme 21). The reaction of **33B** was repeated twice with different reaction times. Reagent amounts and different reaction times are presented in Table 5.

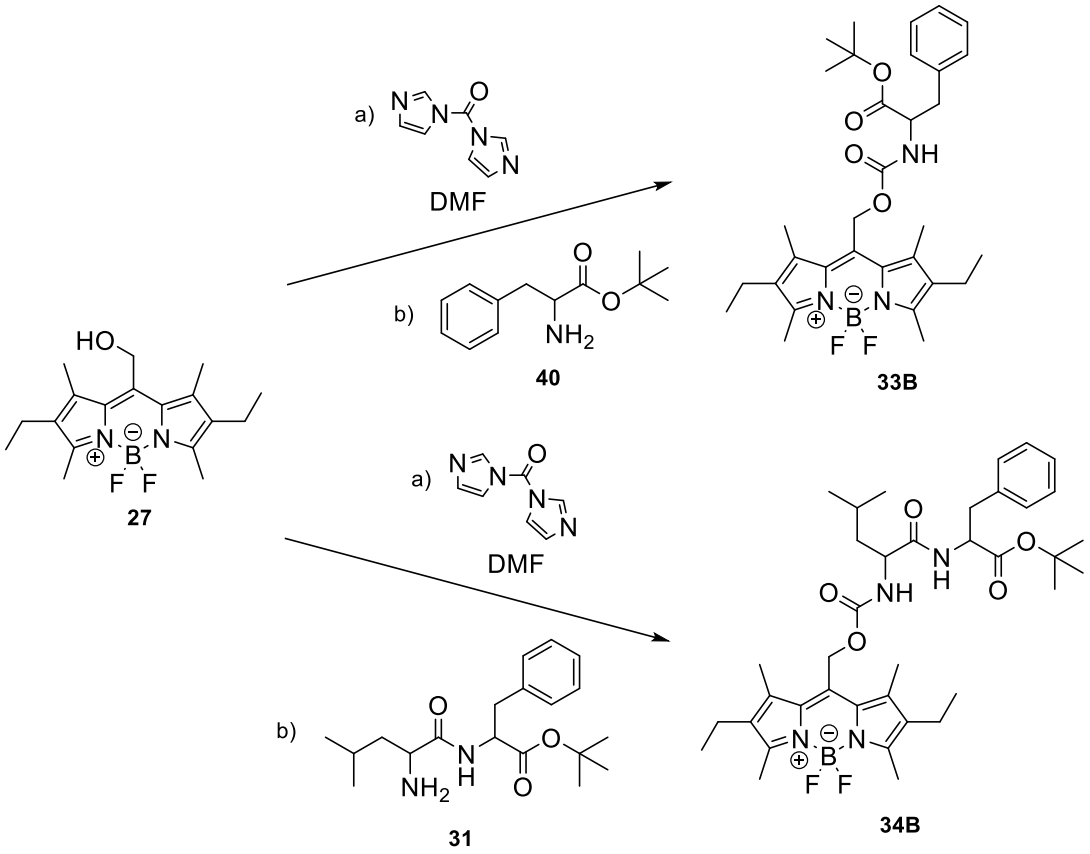

Scheme 21. Syntheses of EtBODIPYPheO*t*Bu (**33B**) and EtBODIPYLeuPheO*t*Bu (**34B**).

CDI was dissolved in dry DMF (1 ml) under a N_2 atmosphere. EtBODIPYOH (**27**) in DMF was added, and the reaction mixture was stirred at RT under N_2 in the dark. PheO*t*Bu (**40**) or LeuPheO*t*Bu (**31**) in DMF was added to the reaction mixture, and the reaction mixture was stirred at RT under N_2 in the dark while monitored with TLC (eluent: 2:3 EtOAc in *n*-hex or 7:2:1 EtOAc/MeOH/H_2O). The reaction mixture was then evaporated and dried under a vacuum overnight.

In case of **33B**, the reaction mixture was extracted with EtOAc and washed with 10 % HCl (4x) and brine (1x). The organic phase was dried with $MgSO_4$, evaporated, and dried under a vacuum.

Table 5. Reagent amounts and reaction times for syntheses of **33B-34B**.

Product	m[EtBODIPYOH] (mg)	m[CDI] (mg)	a) Reaction time (h)	m[**40, 31**] (mg)	b) Reaction time (h)
EtBODIPYPheO*t*Bu (**33B**)	30.86	14.96	1	23.64	5
EtBODIPYPheO*t*Bu (**33B**)	30.85	15.26	3	23.82	overnight
EtBODIPYLeuPheO*t*Bu (**34B**)	16.84	8.72	1	16.84	5

To further investigate the first step a) of the reaction, EtBODIPYOH (**27**) and CDI were used to prepare the assumed alkoxycarbonylimidazole intermediate **41** (Scheme 22). EtBODIPYOH (**27**) (30.64 mg, 0.092 mmol, 1.0 eq) and CDI (17.90 mg, 0.11 mmol, 1.2 eq) were dissolved in dry THF (2 ml) under N_2 atmosphere. The reaction mixture was stirred at RT under N_2 in the dark while monitored with TLC (eluent: 7:2:1 EtOAc/MeOH/H_2O). After 24 hours, deionized water (10 ml) was added to the reaction mixture and the mixture was extracted with diethyl ether (3x). The combined organic phases were washed with deionized water, dried with $MgSO_4$, evaporated, and dried under a vacuum.

The crude was purified by column chromatography (eluent: 5 % MeOH in EtOAc). The fractions were further investigated with NMR spectroscopy.

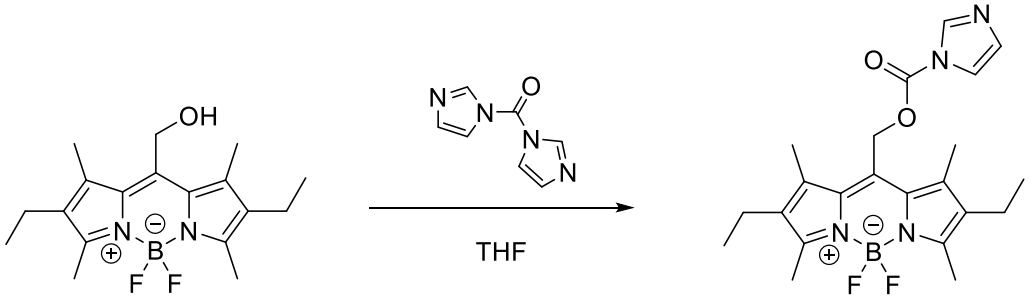

27 **41**

Scheme 22. Formation of the expected alkoxycarbonylimidazole intermediate **41**.

11 Results and discussion

11.1 BODIPY compounds

The BODIPY compounds **26-28** were successfully synthesized and the yields (31 %, 40 % and 79 %, respectively) were similar to those in previously reported.[60] Suggested reaction mechanisms for the syntheses of **26-28** are presented in Schemes A1-3, respectively.

^{1}H NMR spectrum of EtBODIPYOAc (**26**) (Figure 24) agrees with the previously published spectrum.[60] The signals at 7.26 ppm and 1.53 ppm correspond to $CHCl_3$ and water, respectively.

^{1}H NMR δ_H (300 MHz; $CDCl_3$): 1.05 (t, 6H, J=7.56 Hz, **CH_3**), 2.14 (s, 3H, **CH_3**), 2.26 (s, 6H, **CH_3**), 2.40 (q, 4H, J=7.59 Hz, **CH_2**), 2.51 (s, 6H, **CH_3**), 5.32 (s, 2H, **CH_2**).

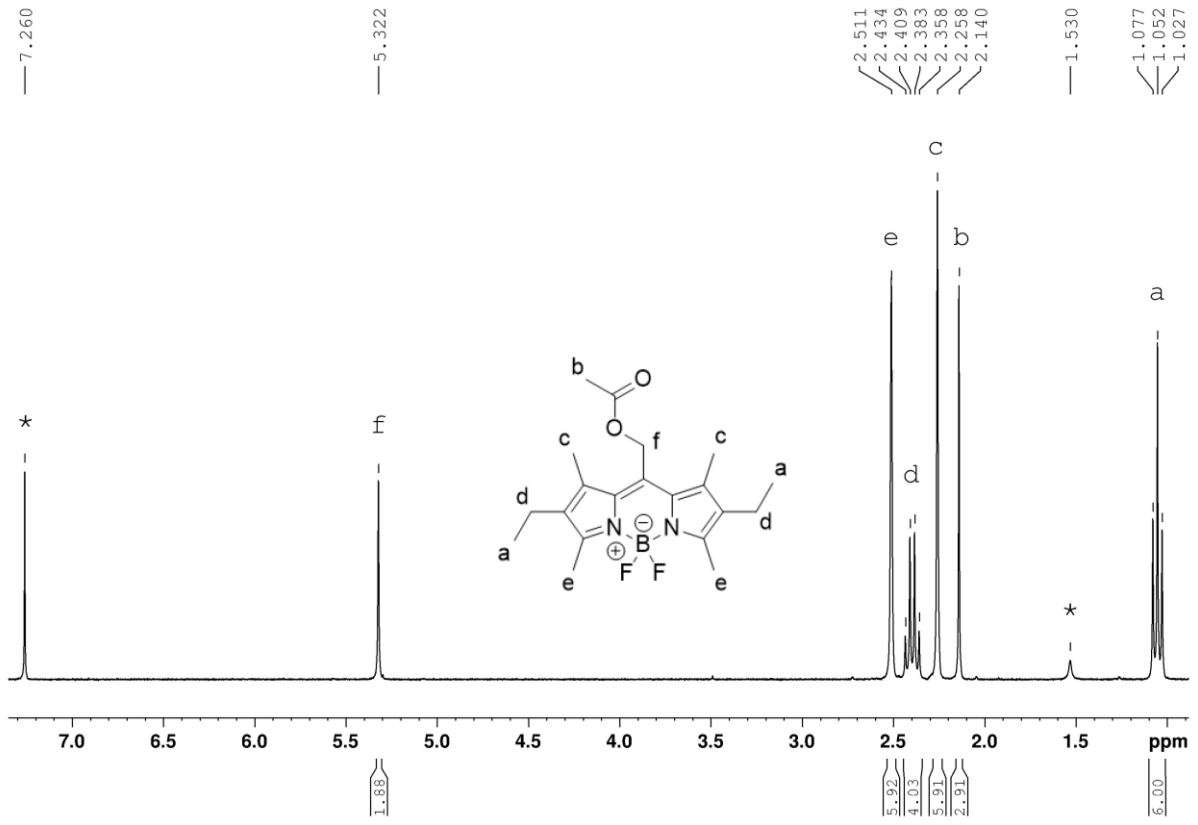

Figure 24. EtBODIPYOAc (**26**) ^{1}H NMR spectrum at 300 MHz in $CDCl_3$. Water and solvent peaks are denoted with *.

^{1}H NMR spectrum of EtBODIPYOH (**27**) (Figure 25) agrees with the previously published spectrum.[60] The signals at 7.26 ppm and 1.53 ppm correspond to $CHCl_3$ and water, respectively.

^{1}H NMR δ_H (300 MHz; $CDCl_3$): 1.06 (t, 6H, J=7.56 Hz, **CH_3**), 1.53 (s, 1H, **OH**), 2.40 (q, 4H, J=7.56 Hz, **CH_2**), 2.42 (s, 6H, J=7.56 Hz, **CH_3**), 2.50 (s, 6H, **CH_3**), 4.93 (s, 2H, **CH_2**).

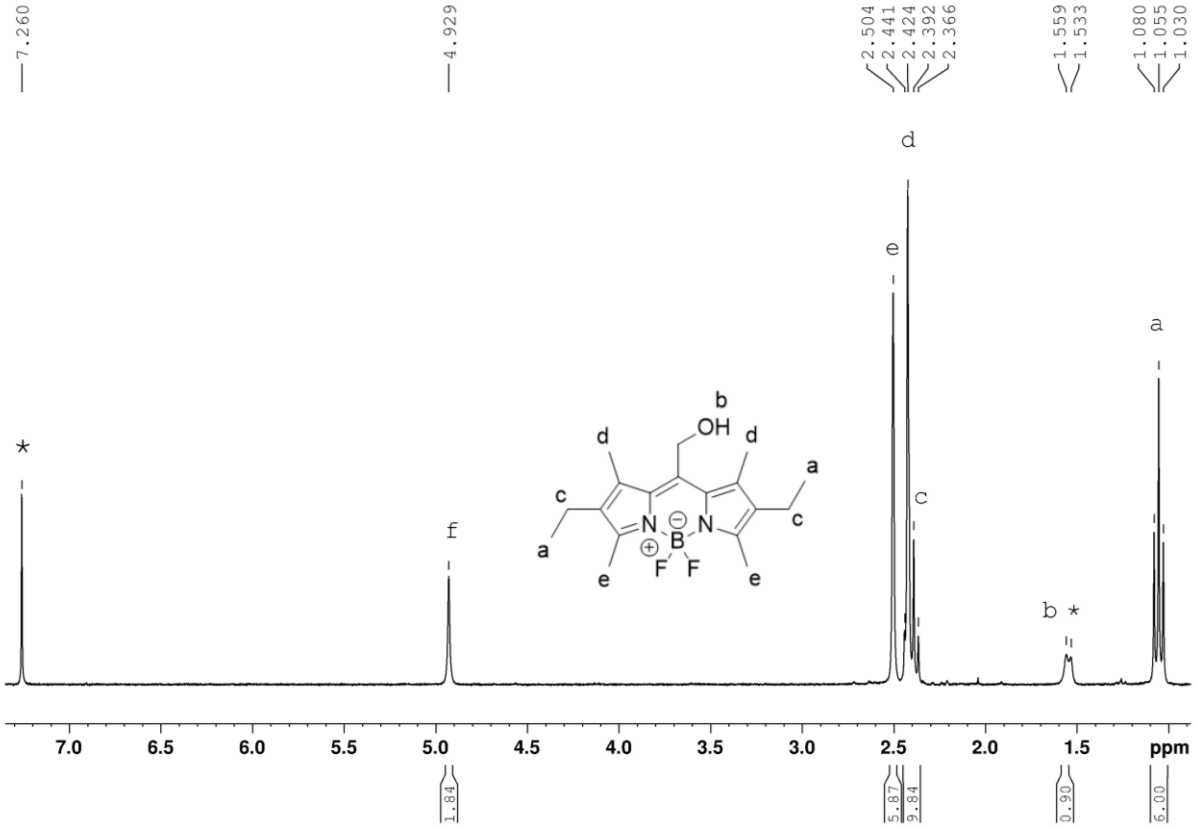

Figure 25. EtBODIPYOH (**27**) ^{1}H NMR spectrum at 300 MHz in $CDCl_3$. Solvent residuals, water and NMR solvent peaks are denoted with *.

^{1}H NMR spectrum of EtBODIPYPNP (**28**) (Figure 26) agrees with the previously published spectrum.[60] The signals at 7.26 ppm, 5.30 ppm, 2.17 ppm and 1.52 ppm correspond to $CHCl_3$, residual DCM solvent, acetone, and water, respectively.

^{1}H NMR δ_H (300 MHz; $CDCl_3$): 1.07 (t, 6H, J=7.53 Hz, **CH_3**), 2.36 (s, 6H, **CH_3**), 2.41 (q, 4H, J=7.62 Hz, **CH_2**), 2.53 (s, 6H, **CH_3**), 5.60 (s, 2H, **CH_2**), 7.41 (d, 2H, J=9.12 Hz, **Ar-H**), 8.29 (d, 2H, J=9.15 Hz, **Ar-H**).

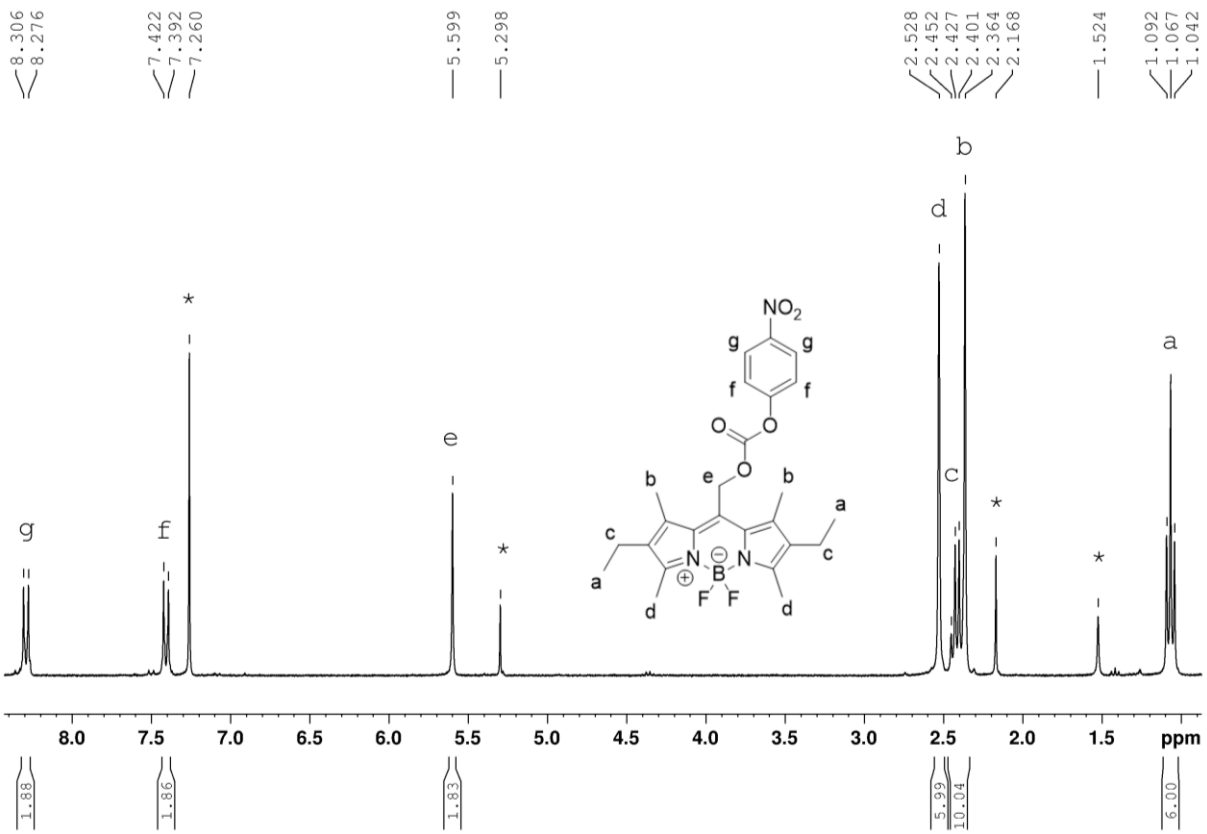

Figure 26. EtBODIPYPNP (**28**) ^{1}H NMR spectrum at 300 MHz in $CDCl_3$. Solvent residuals, water and NMR solvent peaks are denoted with *.

11.2 Dipeptides

The Boc-protected dipeptides **29-30** were synthesized by coupling the corresponding Boc-amino acid and PheO*t*Bu (**40**) with TBTU. The yield for product **29** was 75 % and for product **30** it was 94 %. The yield of **29** was similar to that reported in the literature.[61] Applying the literature procedure[61] for the synthesis of **30** was successful, although a greater amount of impurities remained in the product.

^{1}H NMR spectrum of BocLeuPheO*t*Bu (**29**) (Figure 27) agrees with the previously published spectrum.[61] The peaks at 2.50 ppm and 3.29 ppm correspond to DMSO and water, respectively. The peak at 2.69 ppm may correspond to tetramethylurea byproduct formed in the coupling reaction. The signal of the CH_2 in the Leu side chain (1.34 ppm) is overlapping with the signals of Boc (1.31 ppm) and *t*Bu (1.37 ppm) groups.

^{1}H NMR δ_H (300 MHz; DMSO-d$_6$): 0.84 (dd, 6H, J=8.07 Hz, 6.75 Hz, **CH$_3$**), 1.31 (s, 9H, **Boc**), 1.34 (s, 2H, **CH$_2$-Leu**) 1.37 (s, 9H, ***t*Bu**), 1.55-1.59 (m, 1H, **CH-Leu**), 2.91-2.98 (m, 2H, **PhCH$_2$**), 3.97 (q, 1H, J=7.08 Hz, **CH*-Leu**), 4.35 (q, 1H, J=6.87 Hz, **CH*-Phe**), 6.79 (d, 1H, J=8.61 Hz, **NH-Leu**), 7.17-7.30 (m, 5H, **Ar-H**), 7.98 (d, 1H, J=7.83 Hz, **NH-Phe**).

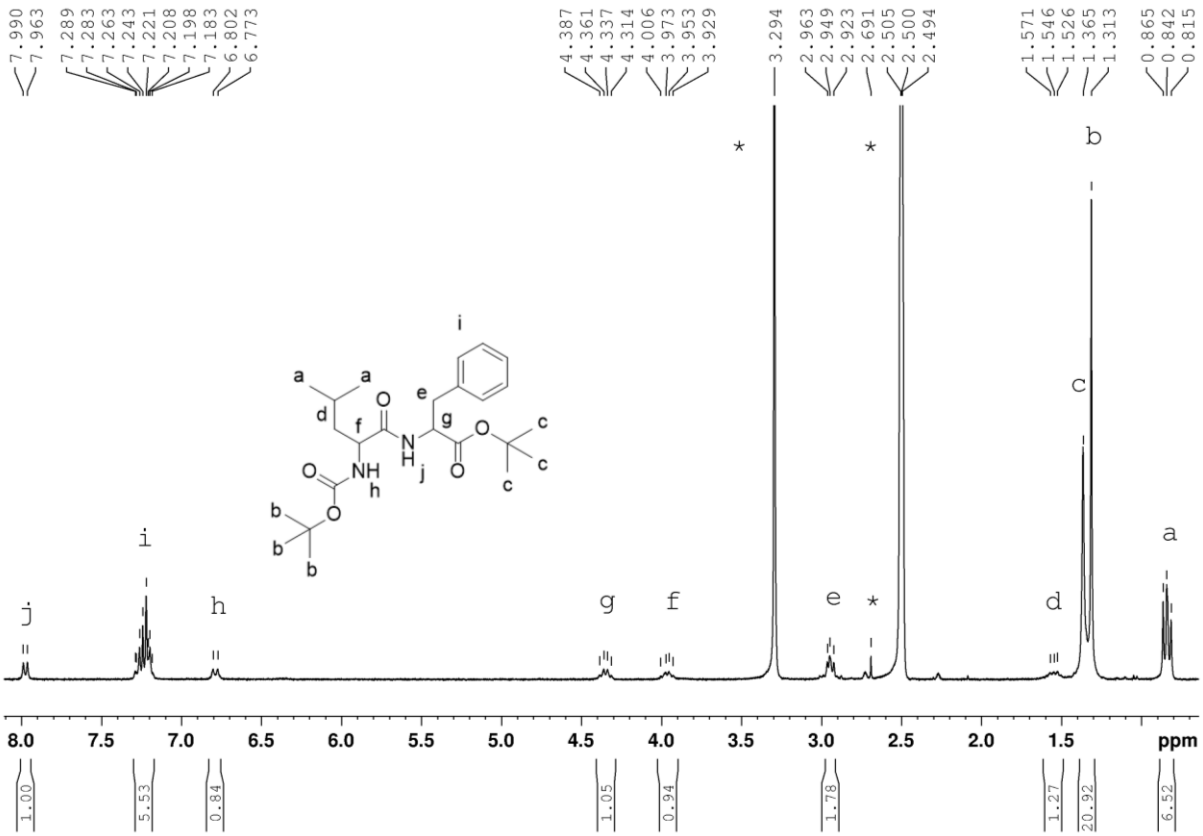

Figure 27. BocLeuPheO*t*Bu (**29**) ^{1}H NMR spectrum at 300 MHz in DMSO-d$_6$. Solvent residuals, impurities and NMR solvent peaks are denoted with *.

^{1}H NMR spectrum of BocGlyPheO*t*Bu (**30**) (Figure 28) is consistent with previously published spectrum.[62] The peaks at 2.50 ppm, 2.08 ppm, 3.30 ppm and 5.74 ppm correspond to DMSO, acetone, water, and residual DCM solvent, respectively. Peaks at 2.73 ppm, 2.89 ppm and 7.95 ppm correspond to DMF. The peak at 2.69 ppm may correspond to tetramethylurea byproduct.

^{1}H NMR δ_H (300 MHz; DMSO-d$_6$): 1.28 (s, 9H, **Boc**), 1.34 (s, 9H, ***t*Bu**), 2.90-2.97 (m, 2H, **PhCH$_2$**), 3.54 (d, 2H, J=5.76 Hz, **NHCH$_2$**), 4.38 (q, 1H, J=7.02 Hz, **CH*-Phe**), 6.90 (t, 1H, J=5.16 Hz, **NH-Gly**), 7.17-7.32 (m, 5H, **Ar-H**), 8.01 (d, 1H, J=7.59 Hz, **NH-Phe**).

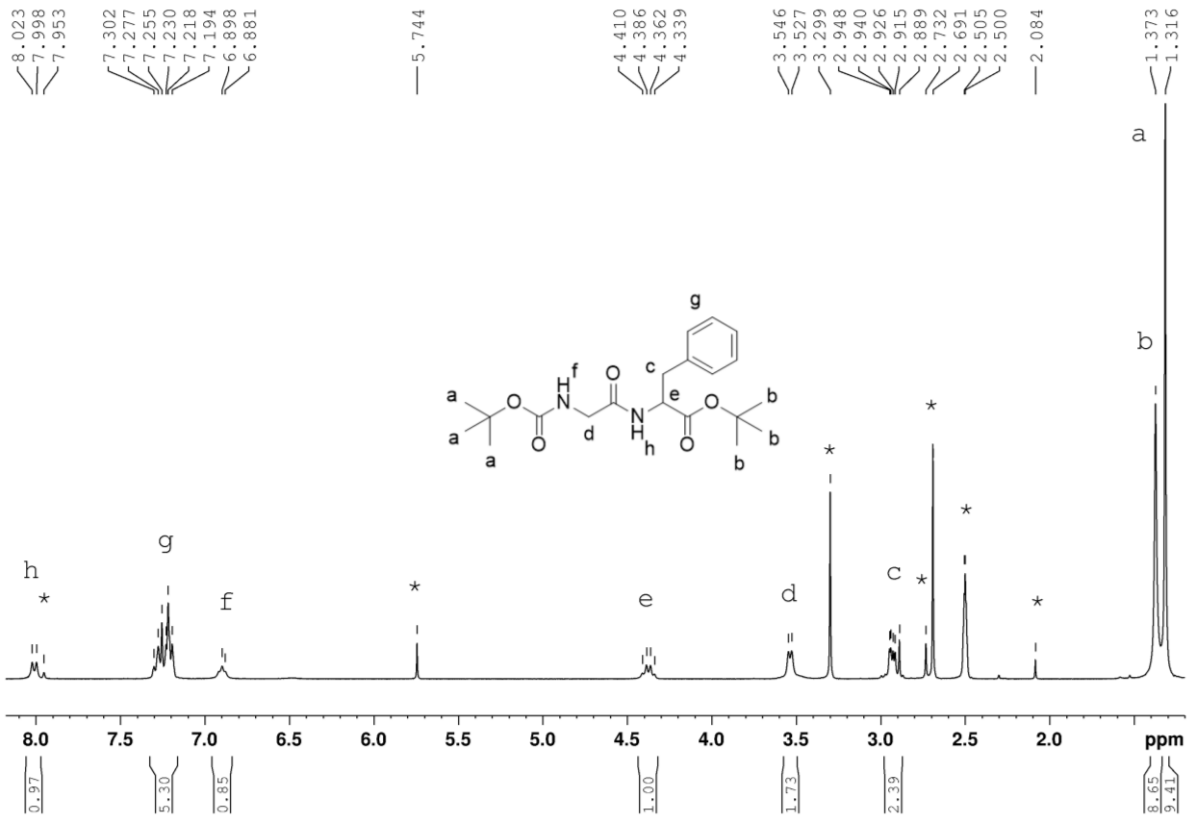

Figure 28. BocGlyPheO*t*Bu (**30**) ^{1}H NMR spectrum at 300 MHz in DMSO-d_6. Solvent residuals, impurities and NMR solvent peaks are denoted with *.

The deprotected dipeptides **31-32** were obtained by removing the Boc-protecting group in acidic conditions. The yields for the dipeptides **31-32** were 44 % and 65 %, respectively.

The ^{1}H NMR spectra of LeuPheO*t*Bu (**31**) (Figure 29) is similar to the previously published spectrum.[61] Although there would have been room for improvement of spectrum quality, the presence of the product was confirmed. A C-H correlation NMR spectrum would have provided additional information about the signals. The peaks at 2.50 ppm and 2.69 ppm correspond DMSO and possible tetramethylurea byproduct, respectively. There is also a significant amount of impurities coming from *t*BuOAc (1.11 ppm, 1.39 ppm and 1.90 ppm). The CH_2 of the Leu side chain is not visible in the spectrum, most probably because it is overlapping with the *t*Bu signal (1.32 ppm).

^{1}H NMR δ_H (300 MHz; DMSO-d_6): 0.86 (dd, 6H, J=8.22 Hz, 6.60 Hz, **CH_3**), 1.32 (s, 9H, ***t*Bu**), 1.60-1.73 (m, 1H, **CH-Leu**), 2.89-3.05 (m, 2H, **CH_2Ph**), 3.39 (dd, 1H, J=8.70 Hz, 5,49 Hz, **CH*-Leu**), 4.42 (q, 1H, J=7.44 Hz, **CH*-Phe**), 7.18-7.30 (m, 5H, **Ar-H**), 8.40 (d, 1H, J=7.89 Hz, **NH**).

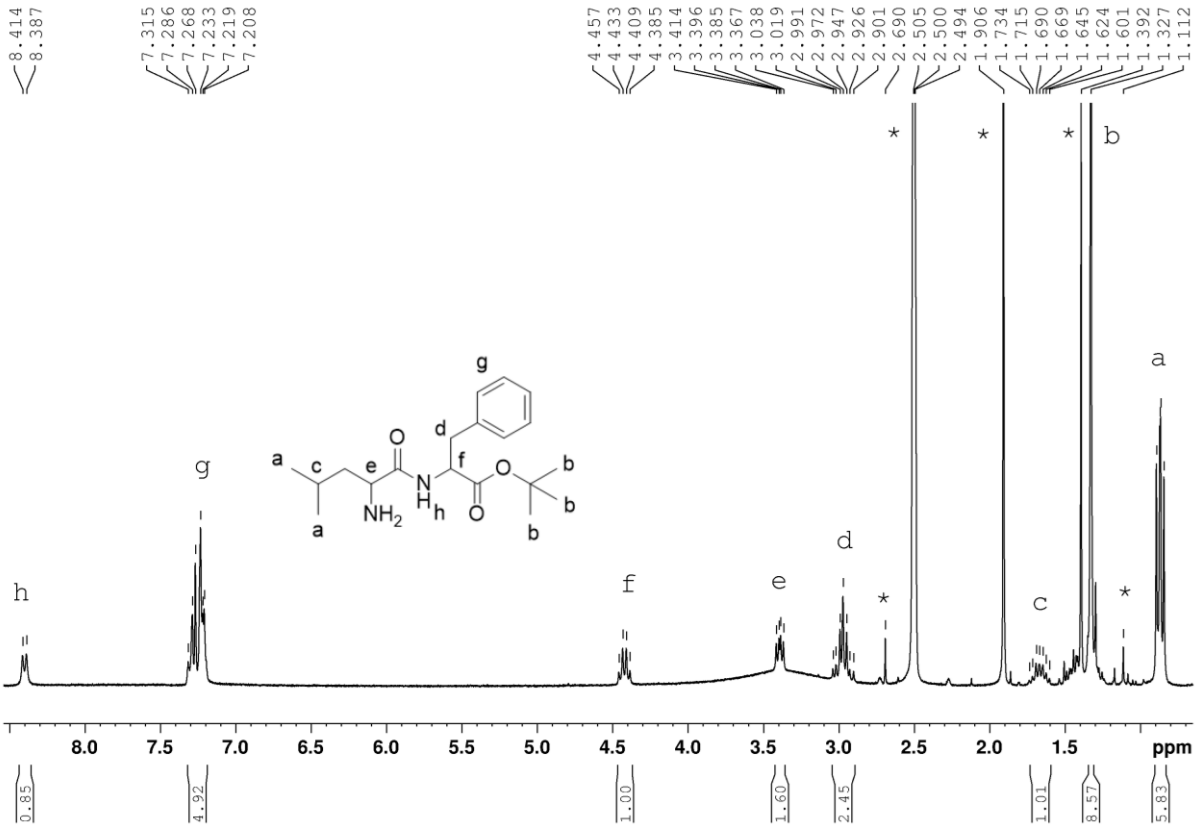

Figure 29. LeuPheO*t*Bu (**31**) ^{1}H NMR spectrum at 300 MHz in DMSO-d_6. Solvent residuals, impurities from *t*BuOAc and NMR solvent peaks are denoted with *.

^{1}H NMR spectrum of GlyPheO*t*Bu (**32**) (Figure 30) is consistent with the structure of the molecule and a previously published spectrum measured in $CDCl_3$.[29] The peak at 2.50 ppm corresponds to DMSO solvent and the peak at 2.69 ppm may correspond to tetramethylurea byproduct. The major impurities are from *t*BuOAc (1.51 ppm, 1.90 ppm and 3.02 ppm), EtOAc (1.17 ppm, 1.99 ppm and 4.03 ppm) and DMF (2.73 ppm, 2.89 ppm and 7.95 ppm).

^{1}H NMR δ_H (300 MHz; DMSO-d_6): 1.33 (s, 9H, ***t*Bu**), 2.91-3.00 (m, 2H, **PhCH_2**), 3.16 (s, 2H, **CH_2**), 4.44 (q, 1H, J=6.9 Hz, **CH*-Phe**), 7.17-7.33 (m, 5H, **Ar-H**), 8.19 (d, 1H, J=7.98 Hz, **NH-Phe**).

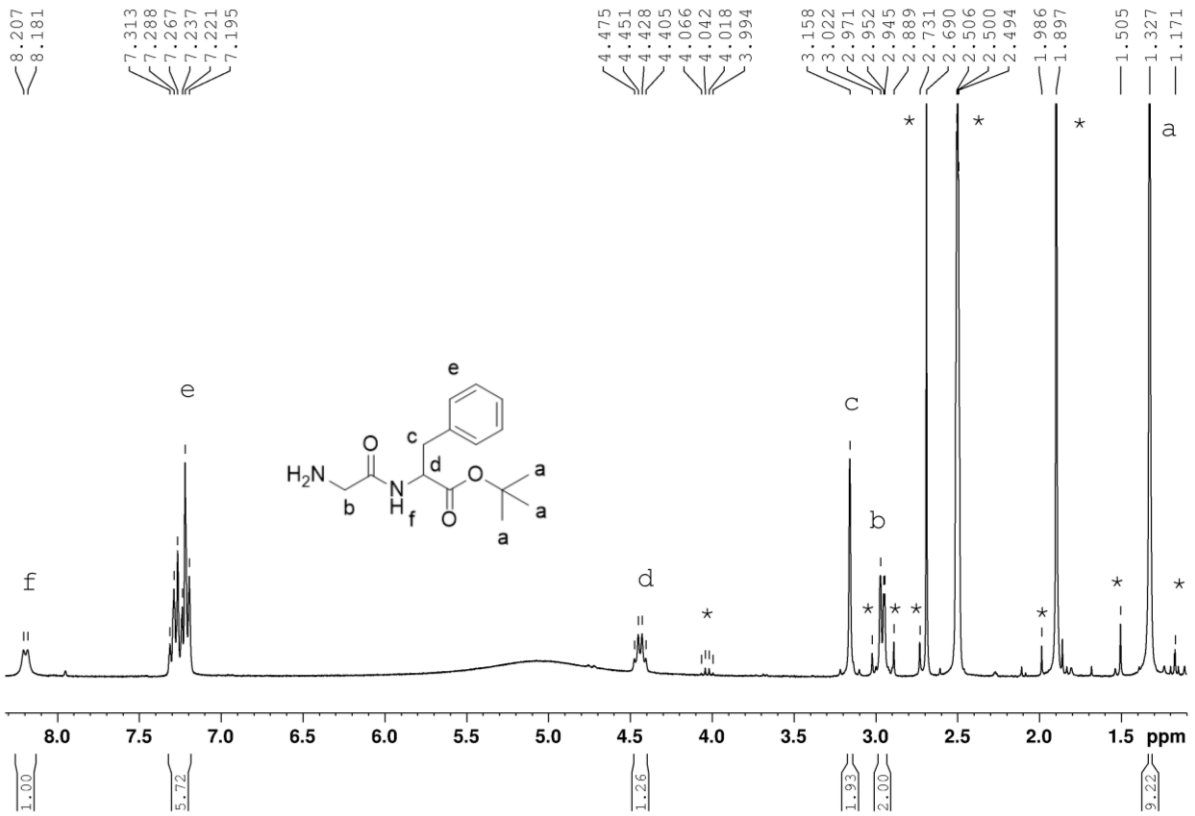

Figure 30. GlyPheO*t*Bu (**32**) ^{1}H NMR spectrum at 300 MHz in DMSO-d_6. Solvent residuals, impurities from *t*BuOAc and NMR solvent peaks are denoted with *.

There were some problems during the extraction of **32** that could have affected the yield. During the extraction, some of the product seemed to remain in the water phase instead of the organic phase. Therefore, it could be better to use another solvent in the extraction, for example DCM, and see if the separation would be more efficient. The product also contained a large amount of solvent residues, indicating that drying and solvent evaporation were inefficient. Because the time to complete the experiment was running short, the original plan to use GlyPheO*t*Bu (**32**) with the BODIPY starting compounds **27-28** as for LeuPheO*t*Bu (**31**) was discarded.

11.3 Linkage of EtBODIPYPNP (28) with mono- and dipeptides

Previously, a similar reaction with BODIPYPNP (**28**) had been carried out with a primary amine attached to a long hydrocarbon chain. With that, the carbamate bond was successfully introduced between the amine and the BODIPY compound **28**.[60] However, these types of reactions with amino acids as nucleophiles were not found in the literature.

11.3.1 EtBODIPYPheOtBu (33A)

The compound **33A** was aimed to synthesize by nucleophilic substitution including EtBODIPYPNP (**28**) and PheO*t*Bu (**40**) (Scheme 20). The TLC implied that something formed in the reaction, but after chromatographic purifications and further investigation with NMR spectroscopy (Figure A1), it was discovered that the new spot on the TLC plate was not from the product. For example, for product **33A**, the peaks from the BODIPY core and the peak corresponding to the protons in *t*Bu (around 1.28 ppm) should be visible. Based on the NMR spectra, the crude mixture mostly consists of the BODIPY starting compound **28**, its decomposition products and other impurities.

11.3.2 EtBODIPYLeuPheOtBu (34A)

Since the reaction with phenylalanine (**40**) did not work, it was decided to be replaced by phenylalanine-containing dipeptides **31-32**. Leucine and glycine were chosen as other amino acids because they were available in the laboratory, and it was reasoned that they would better work as nucleophiles and have less steric hindrance in the N-terminus. As mentioned before, the reaction was not tested with the dipeptide **32** due to a lack of time scheduled for the experiment.

The compound **34A** was tried to synthesize similarly, but with EtBODIPYPNP (**28**) and LeuPheO*t*Bu (**31**) as starting materials (Scheme 20). Unfortunately, the synthesis of **34A** was not more successful than the one of **33A**, as stated by NMR spectroscopy (Figure A2). The recorded ^{1}H NMR spectrum looked like a mixture of the starting materials rather than the actual product.

11.4 Coupling EtBODIPYOH (27) with mono- and dipeptides

11.4.1 EtBODIPYPheO*t*Bu (33B)

The compound **33B** was also aimed to be synthesized by coupling EtBODIPYOH (**27**) and PheO*t*Bu (**40**) with CDI (Scheme 21). The first part of the reaction was carried out with the BODIPY compound **27** and CDI, and the second part was the addition of **40**. In the first part of the reaction, a new spot appeared on TLC, but there was still starting compound **27** left. Although the reaction was repeated with longer reaction times (Table 5), it seemed that the starting compound **27** was not fully consumed in the reaction. In the second part of the reaction, no changes were observed on TLC. It is possible that the spots were overlapping, and the product was not visible on the plate.

However, based on the ^{1}H NMR spectrum (Figure A3), the reaction with longer reaction times (Table 5) did not produce the product **33B**. Comparison with the starting compound **27**, spectrum revealed almost the same spectrum. The reaction with shorter reaction times was more promising, as deduced by the ^{1}H NMR spectrum (Figure 31 and A4a). The signals in the proton and ^{13}C NMR spectra were consistent with the structure of the molecule (Figure 32). The peak interpretations for EtBODIPYPheO*t*Bu (**33B**) are as follows:

^{1}H NMR δ_H (500 MHz; $CDCl_3$): 1.07 (t, 6H, **CH_3**), 1.40 (s, 9H, ***t*Bu**), 2.40 (q, 4H, J=7.55 Hz, **CH_2**), 2.43 (s, 6H, **CH_3**), 2.51 (s, 6H, **CH_3**), 2.99-3.10 (m, 2H, **CH_2Ph**), 4.60 (q, 1H, **CH***), 4.81 (d, 1H, **NH**), 4.93 (s, 2H, **CH_2O**), 7.13-7.31 (m, 5H, **Ar-H**).

^{13}C NMR δ_C (75 MHz; $CDCl_3$): 12.61 (CH_3), 14.69 (**CH_3**), 17.15 (**CH_2**), 27.97 (**CH_3**), 38.71 (**CH_2**), 54,47 (**CH**), 56.19 (**CH_2**), 82.05 (**$C(CH_3)_3$**), 126.80 (**Ar-C**), 128.31 (**Ar-C**), 129.60 (**Ar-C**).

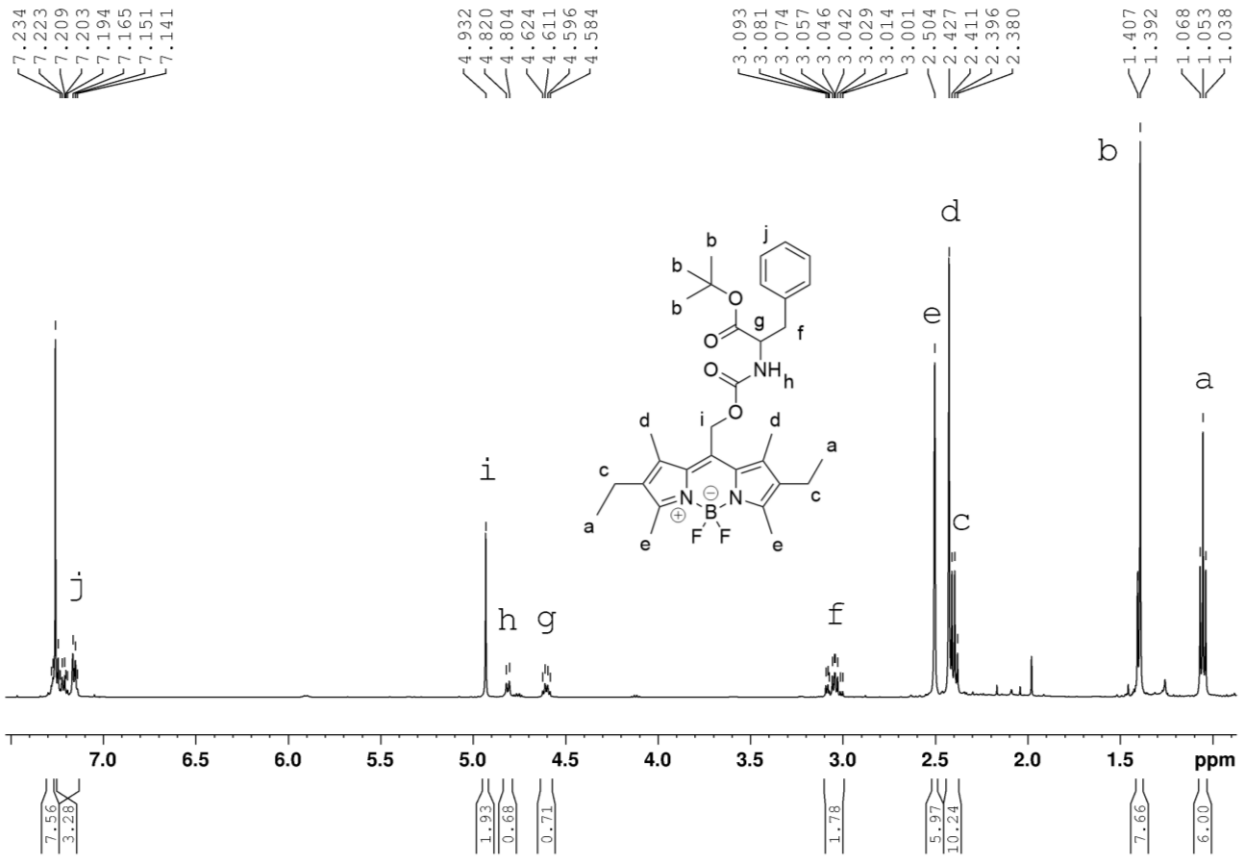

Figure 31. EtBODIPYPheO*t*Bu (**33B**) ^{1}H NMR spectrum at 500 MHz in $CDCl_3$.

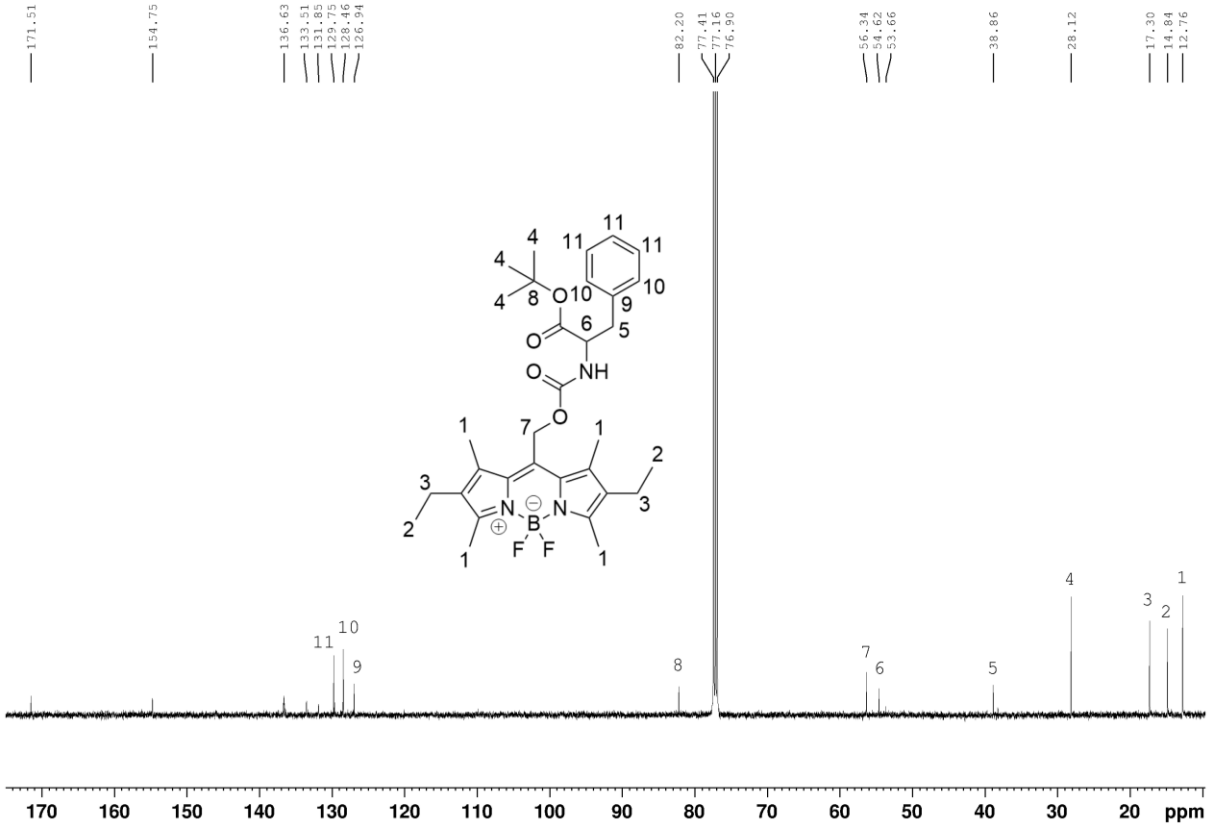

Figure 32. EtBODIPYPheO*t*Bu (**33B**) ^{13}C NMR spectrum at 500 MHz in $CDCl_3$.

In the carbon spectrum there is two peaks in the aromatic region that could originate from unreacted phenylalanine. The H-H COSY (Figure A4b), HSQC (Figure A4c), and HMBC (Figure A4d) NMR spectra also supported the structure of the molecule. However, the N-H correlation spectrum (Figure A4e) only reveals the nitrogen atoms of the BODIPY core. To have the product **33b**, the NH of the carbamate bond should be visible. It is also possible that the measure time was too short, and NH does not show due to a low concentration. Therefore, based on the recorded 2D NMR spectra, the presence of the product **33B** cannot be distinguished from a mixture of the starting materials **27** and **40**.

The crude mixture was also measured with ESI-MS using a positive ionization mode. The identified peaks are represented in Table A1. Unfortunately, there is no peak in the spectrum (Figure A5) that could correspond to the product **33B**, that should be observed for $[M+H]^+$ at *m/z* 581. The most abundant peak belongs to an unknown molecule with molecular weight of 469 u, for which the H^+, Na^+ and K^+ adducts are also observed, as well as the ones for the dimer. In addition, based on the MS spectrum, the presence of starting materials (**27** and **40**) is confirmed. The peaks with *m/z* 334 and 357 are from the BODIPY starting compound **27**. The peak with *m/z* 120 corresponds to a fragment formed by α-cleavage of **40** and the peak with *m/z* 166 corresponds to phenylalanine without the *tert*-butyl group. Besides them, there are no other recognizable peaks that could correspond to the other starting materials or expected intermediates. Since the NMR and MS spectra do not provide clear evidence about the presence of the desired product **33B**, the reaction did not work as desired.

11.4.2 EtBODIPYLeuPheO*t*Bu (34B)

Compound **34B** was tried to synthesize using the same procedure, but with EtBODIPYOH (**27**) and LeuPheO*t*Bu (**31**) (Scheme 21). On TLC, the first part of the reaction looked similar to the first part of the reaction of **33B.** No changes on TLC were visible after adding **31**, indicating no reaction to form the product **34B** occurred. The ^{1}H NMR spectrum (Figure A6) did not show any proof of the presence of the product.

11.4.3 Alkoxycarbonylimidazole intermediate (41)

CDI was used in the syntheses of **33B** and **34B** as a coupling agent to link the hydroxyl group of the BODIPY compound **27** with the amine group of **40** or **31** via a carbamate bond. In these reactions, CDI works as a double electrophile that links the two nucleophiles together (Scheme 23).

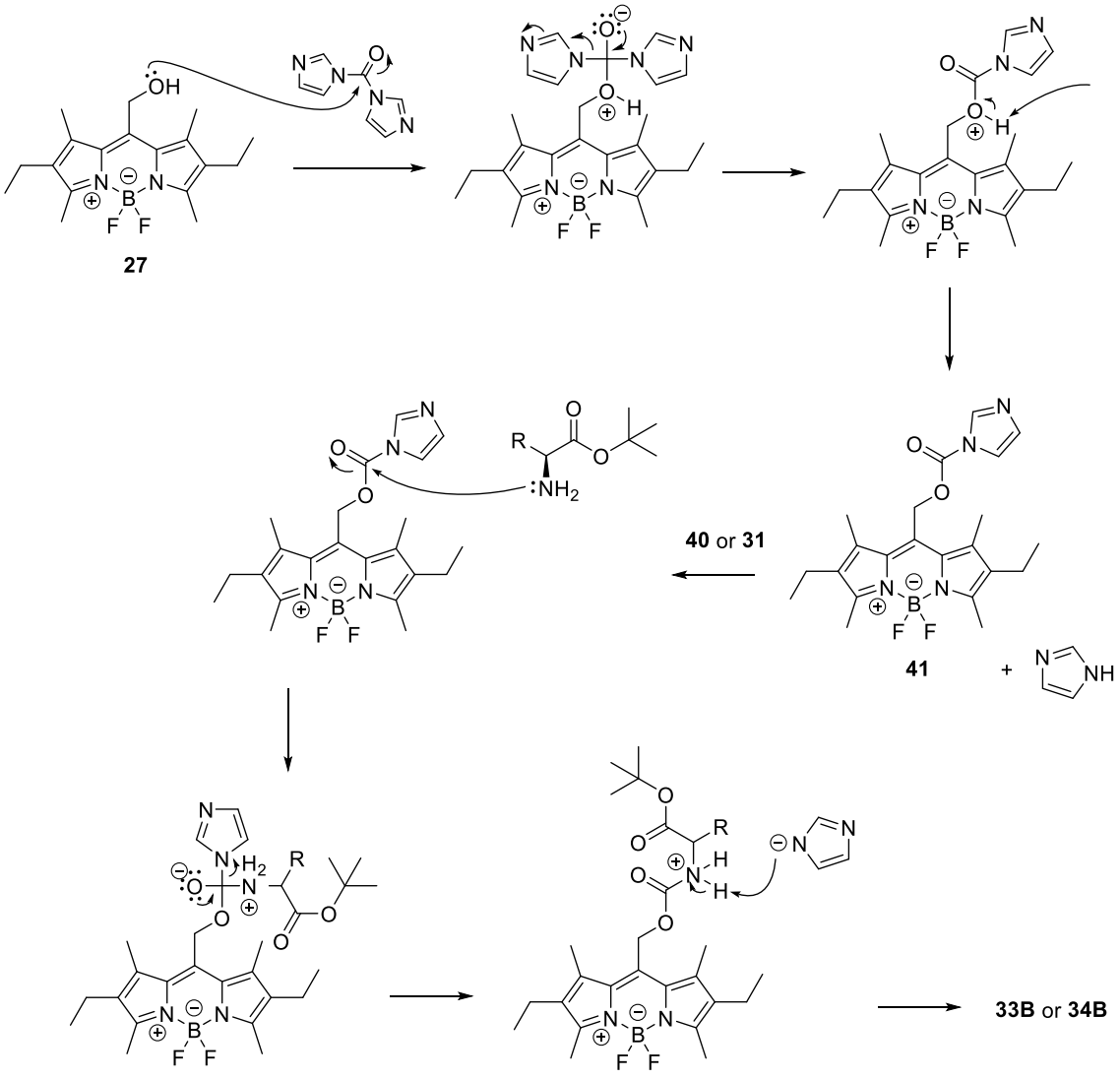

Scheme 23. A suggested mechanism for the reactions of **33B** and **34B**.

To further investigate the reaction between the hydroxyl group and CDI, EtBODIPYOH (**27**) and CDI were used to prepare the assumed alkoxycarbonylimidazole intermediate (**41**). There were two new spots on TLC, and the BODIPY starting compound was fully consumed in the reaction. Based on this, it could be said that the reaction produces more than one product. The crude mixture was purified chromatographically, and the collected fractions were investigated with ^{1}H NMR spectra (Figure A7). The spectrum of fraction c could belong to compound **41** since it has the peaks from the BODIPY core, a singlet peak at 5.35 ppm corresponding to -CH_2O, and two signals in the aromatic region corresponding to imidazole. However, other peaks imply that there is something else mixed with compound **41**.

Based on this information, it is likely that the BODIPY compound **27** reacts with CDI to form the alkoxycarbonylimidazole compound **41**. Therefore, the reason why the syntheses of **33B** and **34B** from the BODIPY compound **27** were unsuccessful may be because something disturbs the nucleophilic attack of the amine. The BODIPY itself may somehow affect the reaction in an undesired manner. In the future, this could be investigated by designing another molecule with the same side chain and testing the reaction with the same reaction conditions to see whether the reaction works without the BODIPY.

12 Conclusions

The aim of this experimental work was to synthesize a potential photocleavable peptide-based LMWGs with a photoresponsive BODIPY moiety (**33-34**). The BODIPY compounds **26-28** were synthesized according to procedures developed by Korhonen *et al*.[60] with yields of 31 %, 40 % and 79 %, respectively. Boc-protected dipeptides **29-30**, and their corresponding unprotected dipeptides **31-32** were synthesized following a previously reported procedure by Chevigny *et al*.[61] with yields of 75 %, 94 %, 44 % and 65 %, respectively. The ^{1}H NMR spectra of the synthesized precursors were consistent with the structures of the molecules. The dipeptide **32** contained a large amount of solvent residuals.

The syntheses of the potential LMWGs **33-34** were not successful. Compounds **33-34** were aimed to be synthesized by linking the BODIPY with mono- and dipeptides *via* carbamate bond with two different reaction types. The first one was the basic nucleophilic substitution reaction between the BODIPY compound **28** and the mono- and dipeptides, and the second one was the coupling of the BODIPY compound **27** with the mono- and dipeptides by using CDI. The NMR spectra of the crude compound **33B** synthesized from the BODIPY compound **27** and monopeptide **40** seemed promising, but the presence of the product could not be fully confirmed based on the information given by the recorded spectra. The HR-MS spectrum of the crude **33B** showed no peaks that could correspond to the desired product.

Since the syntheses of the compounds **33-34** were not successful, further studies related to gelation and photocleavage were not carried out. Therefore, the potential of the photocleavable peptide-based LMWGs with BODIPY moieties remains unresolved. In the future, it would be beneficial to focus on synthesis planning and learn more about the effect of the BODIPY core on the reactions. The unsuccessful reactions could also be tested with other dipeptides to see whether the reactions work better with different amino acids.

References

1. Sangeetha, N. M. and Maitra, U., Supramolecular gels: Functions and uses, *Chem. Soc. Rev.*, **2005**, *34*, 821–836.
2. Kuzina, M. A.; Kartsev, D. D.; Stratonovich, A. V. and Levkin, P. A., Organogels versus Hydrogels: Advantages, Challenges, and Applications, *Adv. Funct. Mater.*, **2023**, *33*, 2301421.
3. Chu, C.-W. and Schalley, C. A., Recent Advances on Supramolecular Gels: From Stimuli-Responsive Gels to Co-Assembled and Self-Sorted Systems, *Org. Mater.*, **2021**, *03*, 25–40.
4. Draper, E. R. and Adams, D. J., Photoresponsive gelators, *Chem. Commun.*, **2016**, *52*, 8196–8206.
5. Chalk, S. J., *Compendium of Chemical Terminology (the "Gold Book")*, 2nd edition, Blackwell Scientific Publications, Oxford, vol. 1997.
6. Du, X.; Zhou, J.; Shi, J. and Xu, B., Supramolecular Hydrogelators and Hydrogels: From Soft Matter to Molecular Biomaterials, *Chem. Rev.*, **2015**, *115*, 13165–13307.
7. Pramanik, B. and Ahmed, S., Peptide-Based Low Molecular Weight Photosensitive Supramolecular Gelators, *Gels*, **2022**, *8*, 533.
8. Draper, E. R. and Adams, D. J., Low-Molecular-Weight Gels: The State of the Art, *Chem*, **2017**, *3*, 390–410.
9. Draper, E. R.; Su, H.; Brasnett, C.; Poole, R. J.; Rogers, S.; Cui, H.; Seddon, A. and Adams, D. J., Opening a Can of Worm(-like Micelle)s: The Effect of Temperature of Solutions of Functionalized Dipeptides, *Angew. Chem. Int. Ed.*, **2017**, *56*, 10467–10470.
10. Dawn, A. and Kumari, H., Low Molecular Weight Supramolecular Gels Under Shear: Rheology as the Tool for Elucidating Structure–Function Correlation, *Chem. – Eur. J.*, **2018**, *24*, 762–776.
11. Dugave, C. and Demange, L., Cis−Trans Isomerization of Organic Molecules and Biomolecules: Implications and Applications, *Chem. Rev.*, **2003**, *103*, 2475–2532.
12. Cheng, H.-B.; Zhang, S.; Qi, J.; Liang, X.-J. and Yoon, J., Advances in Application of Azobenzene as a Trigger in Biomedicine: Molecular Design and Spontaneous Assembly, *Adv. Mater.*, **2021**, *33*, 2007290.
13. Murata, K.; Aoki, M.; Suzuki, T.; Harada, T.; Kawabata, H.; Komori, T.; Ohseto, F.; Ueda, K. and Shinkai, S., Thermal and Light Control of the Sol-Gel Phase Transition in Cholesterol-Based Organic Gels. Novel Helical Aggregation Modes As Detected by Circular

Dichroism and Electron Microscopic Observation, *J. Am. Chem. Soc.*, **1994**, *116*, 6664–6676.

14. Yang, R.; Peng, S. and Hughes, T. C., Multistimuli responsive organogels based on a reactive azobenzene gelator, *Soft Matter*, **2014**, *10*, 2188–2196.
15. Fatás, P.; Bachl, J.; Oehm, S.; Jiménez, A. I.; Cativiela, C. and Díaz Díaz, D., Multistimuli-Responsive Supramolecular Organogels Formed by Low-Molecular-Weight Peptides Bearing Side-Chain Azobenzene Moieties, *Chem. – Eur. J.*, **2013**, *19*, 8861–8874.
16. Yagai, S.; Nakajima, T.; Kishikawa, K.; Kohmoto, S.; Karatsu, T. and Kitamura, A., Hierarchical Organization of Photoresponsive Hydrogen-Bonded Rosettes, *J. Am. Chem. Soc.*, **2005**, *127*, 11134–11139.
17. Kim, J. H.; Seo, M.; Kim, Y. J. and Kim, S. Y., Rapid and Reversible Gel−Sol Transition of Self-Assembled Gels Induced by Photoisomerization of Dendritic Azobenzenes, *Langmuir*, **2009**, *25*, 1761–1766.
18. Ji, Y.; Kuang, G.-C.; Jia, X.-R.; Chen, E.-Q.; Wang, B.-B.; Li, W.-S.; Wei, Y. and Lei, J., Photoreversible dendritic organogel, *Chem. Commun.*, **2007**, 4233–4235.
19. A. Velema, W.; A. Stuart, M. C.; Szymanski, W. and L. Feringa, B., Light-triggered self-assembly of a dichromonyl compound in water, *Chem. Commun.*, **2013**, *49*, 5001–5003.
20. Salzano de Luna, M.; Marturano, V.; Manganelli, M.; Santillo, C.; Ambrogi, V.; Filippone, G. and Cerruti, P., Light-responsive and self-healing behavior of azobenzene-based supramolecular hydrogels, *J. Colloid Interface Sci.*, **2020**, *568*, 16–24.
21. Huang, Y.; Qiu, Z.; Xu, Y.; Shi, J.; Lin, H. and Zhang, Y., Supramolecular hydrogels based on short peptides linked with conformational switch, *Org. Biomol. Chem.*, **2011**, *9*, 2149–2155.
22. Geiger, C.; Stanescu, M.; Chen, L. and Whitten, D. G., Organogels Resulting from Competing Self-Assembly Units in the Gelator: Structure, Dynamics, and Photophysical Behavior of Gels Formed from Cholesterol−Stilbene and Cholesterol−Squaraine Gelators, *Langmuir*, **1999**, *15*, 2241–2245.
23. Eastoe, J.; Sánchez-Dominguez, M.; Wyatt, P. and Heenan, R. K., A photo-responsive organogel, *Chem. Commun.*, **2004**, 2608–2609.
24. Milandnić, S.; Frkanec, L.; Meić, Z. and Žinić, M., Photoinduced Gelation by Stilbene Oxalyl Amide Compounds, *Langmuir*, **2005**, *21*, 2754–2760.
25. Milandnić, S.; Frkanec, L.; Meić, Z. and Žinić, M., Gelation Ability of Novel Oxamide-Based Derivatives Bearing a Stilbene as a Photo-Responsive Unit, *Eur. J. Org. Chem.*, **2006**, *2006*, 1323–1334.

26. Jiang, Y.; Zeng, F.; Gong, R.; Guo, Z.; Chen, C.-F. and Wan, X., A multi-stimuli responsive organogel based on a tetrapeptide –dithienylcyclopentene conjugate, *Soft Matter*, **2013**, *9*, 7538–7544.

27. Aryal, P.; Morris, J.; Adhikari, S. B.; Bietsch, J. and Wang, G., Synthesis and Self-Assembling Properties of Carbohydrate- and Diarylethene-Based Photoswitchable Molecular Gelators, *Molecules*, **2023**, *28*, 6228.

28. Akazawa, M.; Uchida, K.; Jong, J. J. D. de; Areephong, J.; Stuart, M.; Caroli, G.; Browne, W. R. and Feringa, B. L., Photoresponsive dithienylethene-urea-based organogels with "reversed" behavior, *Org. Biomol. Chem.*, **2008**, *6*, 1544–1547.

29. van Herpt, J. T.; Stuart, M. C. A.; Browne, W. R. and Feringa, B. L., A Dithienylethene-Based Rewritable Hydrogelator, *Chem. – Eur. J.*, **2014**, *20*, 3077–3083.

30. Qiu, Z.; Yu, H.; Li, J.; Wang, Y. and Zhang, Y., Spiropyran-linked dipeptide forms supramolecular hydrogel with dual responses to light and to ligand–receptor interaction, *Chem. Commun.*, **2009**, 3342–3344.

31. Chen, Q.; Feng, Y.; Zhang, D.; Zhang, G.; Fan, Q.; Sun, S. and Zhu, D., Light-Triggered Self-Assembly of a Spiropyran-Functionalized Dendron into Nano-/Micrometer-Sized Particles and Photoresponsive Organogel with Switchable Fluorescence, *Adv. Funct. Mater.*, **2010**, *20*, 36–42.

32. Yabuuchi, K.; Matsuo, N.; Maeda, H. and Moriyama, M., Photoinduced reinforcement of supramolecular gels based on a coumarin-containing gelator, *Polym. J.*, **2018**, *50*, 1093–1097.

33. R. Draper, E.; O. McDonald, T. and J. Adams, D., Photodimerisation of a coumarin-dipeptide gelator, *Chem. Commun.*, **2015**, *51*, 12827–12830.

34. Yu, H.; Mizufune, H.; Uenaka, K.; Moritoki, T. and Koshima, H., Synthesis and properties of coumarin-derived organogelators, *Tetrahedron*, **2005**, *61*, 8932–8938.

35. Tanaka, K., Supramolecular Photodimerization of Coumarins, *Molecules*, **2012**, *17*, 1408–1418.

36. Kim, S. H.; Sun, Y.; Kaplan, J. A.; Grinstaff, M. W. and Parquette, J. R., Photo-crosslinking of a self-assembled coumarin-dipeptide hydrogel, *New J. Chem.*, **2015**, *39*, 3225–3228.

37. Becker, H. Dieter., Unimolecular photochemistry of anthracenes, *Chem. Rev.*, **1993**, *93*, 145–172.

38. Dawn, A.; Shiraki, T.; Haraguchi, S.; Sato, H.; Sada, K. and Shinkai, S., Transcription of Chirality in the Organogel Systems Dictates the Enantiodifferentiating Photodimerization of Substituted Anthracene, *Chem. – Eur. J.*, **2010**, *16*, 3676–3689.

39. Ayabe, M.; Kishida, T.; Fujita, N.; Sada, K. and Shinkai, S., Binary organogelators which show light and temperature responsiveness, *Org. Biomol. Chem.*, **2003**, *1*, 2744–2747.

40. Wang, C.; Zhang, D.; Xiang, J. and Zhu, D., New Organogels Based on an Anthracene Derivative with One Urea Group and Its Photodimer: Fluorescence Enhancement after Gelation, *Langmuir*, **2007**, *23*, 9195–9200.

41. Sako, Y. and Takaguchi, Y., A photo-responsive hydrogelator having gluconamides at its peripheral branches, *Org. Biomol. Chem.*, **2008**, *6*, 3843–3847.

42. George, M. and Weiss, R. G., Low Molecular-Mass Gelators with Diyne Functional Groups and Their Unpolymerized and Polymerized Gel Assemblies, *Chem. Mater.*, **2003**, *15*, 2879–2888.

43. Kim, C.; Lee, S. J.; Lee, I. H.; Kim, K. T.; Song, H. H. and Jeon, H.-J., Stabilization of Supramolecular Nanostructures Induced by Self-Assembly of Dendritic Building Blocks, *Chem. Mater.*, **2003**, *15*, 3638–3642.

44. Liu, J.; Kang, W. and Wang, W., Photocleavage-based Photoresponsive Drug Delivery, *Photochem. Photobiol.*, **2022**, *98*, 288–302.

45. Haines, L. A.; Raandgopal, K.; Ozbas, B.; Salick, D. A.; Pochan, D. J. and Schneider, J. P., Light-Activated Hydrogel Formation via the Triggered Folding and Self-Assembly of a Designed Peptide, *J. Am. Chem. Soc.*, **2005**, *127*, 17025–17029.

46. Muraoka, Takahiro; Koh, Chung-Yan; Cui, Honggang and Stupp, Samuel I., Light-Triggered Bioactivity in Three Dimensions, *Angew. Chem. Int. Ed.*, *2009*, 5946–5949.

47. Liu, Q.; Wang, H.; Li, G.; Liu, M.; Ding, J.; Huang, X.; Gao, W. and Huayue, W., A photocleavable low molecular weight hydrogel for light-triggered drug delivery, *Chin. Chem. Lett.*, **2019**, *30*, 485–488.

48. Babu, S. S.; Prasanthkumar, S. and Aandyaghosh, A., Self-Assembled Gelators for Organic Electronics, *Angew. Chem. Int. Ed.*, **2012**, *51*, 1766–1776.

49. Jenifer, V. R. and Das, T. M., Smart supramolecular photoresponsive gelator with long-alkyl chain azobenzene incorporated sugar derivatives for recycling aromatic solvents and sequestration of cationic dyes, *Soft Matter*, **2022**, *18*, 9017–9025.

50. Babu, S. S.; Praveen, V. K. and Aandyaghosh, A., Functional π-Gelators and Their Applications, *Chem. Rev.*, **2014**, *114*, 1973–2129.

51. Tomatsu, I.; Peng, K. and Kros, A., Photoresponsive hydrogels for biomedical applications, *Adv. Drug Deliv. Rev.*, **2011**, *63*, 1257–1266.

52. Jia, S.; Fong, W.-K.; Graham, B. and Boyd, B. J., Photoswitchable Molecules in Long-Wavelength Light-Responsive Drug Delivery: From Molecular Design to Applications, *Chem. Mater.*, **2018**, *30*, 2873–2887.

53. Pianowski, Z. L.; Karcher, J. and Schneider, K., Photoresponsive self-healing supramolecular hydrogels for light-induced release of DNA and doxorubicin, *Chem. Commun.*, **2016**, *52*, 3143–3146.

54. Leistner, A.-L.; Most, M. M. and Pianowski, Z. L., Molecular Syringe for Cargo Photorelease: Red-Light-Triggered Supramolecular Hydrogel, *Chem. – Eur. J.*, **2023**, *29*, e202302295.

55. Li, F.-Z.; Yin, J.-F. and Kuang, G.-C., BODIPY-based supramolecules: Construction, properties and functions, *Coord. Chem. Rev.*, **2021**, *448*, 214157.

56. Sun, N.; Xiao, X.; Li, W. and Jiang, J., Multistimuli Sensitive Behavior of Novel Bodipy-Involved Pillar[5]arene-Based Fluorescent [2]Rotaxane and Its Supramolecular Gel, *Adv. Sci.*, **2015**, *2*, 1500082.

57. Camerel, F.; Bonardi, L.; Schmutz, M. and Ziessel, R., Highly Luminescent Gels and Mesogens Based on Elaborated Borondipyrromethenes, *J. Am. Chem. Soc.*, **2006**, *128*, 4548–4549.

58. Rubinstein, N.; Liu, P.; Miller, E. W. and Weinstain, R., meso-Methylhydroxy BODIPY: a scaffold for photo-labile protecting groups, *Chem. Commun.*, **2015**, *51*, 6369–6372.

59. Das, T.; Häring, M.; Haldar, D. and Díaz, D. D., Phenylalanine and derivatives as versatile low-molecular-weight gelators: design, structure and tailored function, *Biomater. Sci.*, **2017**, *6*, 38–59.

60. See, E.; Korhonen, E.; Nissinen, M. and Pettersson, M., Non-covalent attachment of BODIPY-caged amines to graphene and their localized photocleavage, *New J. Chem.*, **2024**.

61. Chevigny, R.; Rahkola, H.; Sitsanidis, E. D.; Korhonen, E.; Hiscock, J. R.; Pettersson, M. and Nissinen, M., Solvent-Induced Transient Self-Assembly of Peptide Gels: Gelator–Solvent Reactions and Material Properties Correlation, *Chem. Mater.*, **2024**, *36*, 407–416.

62. Adams, E. R. and Adams, D. J., Photochromic and electrochromic compounds, 2006.01, 5.3.2020.

Appendices

APPENDIX 1

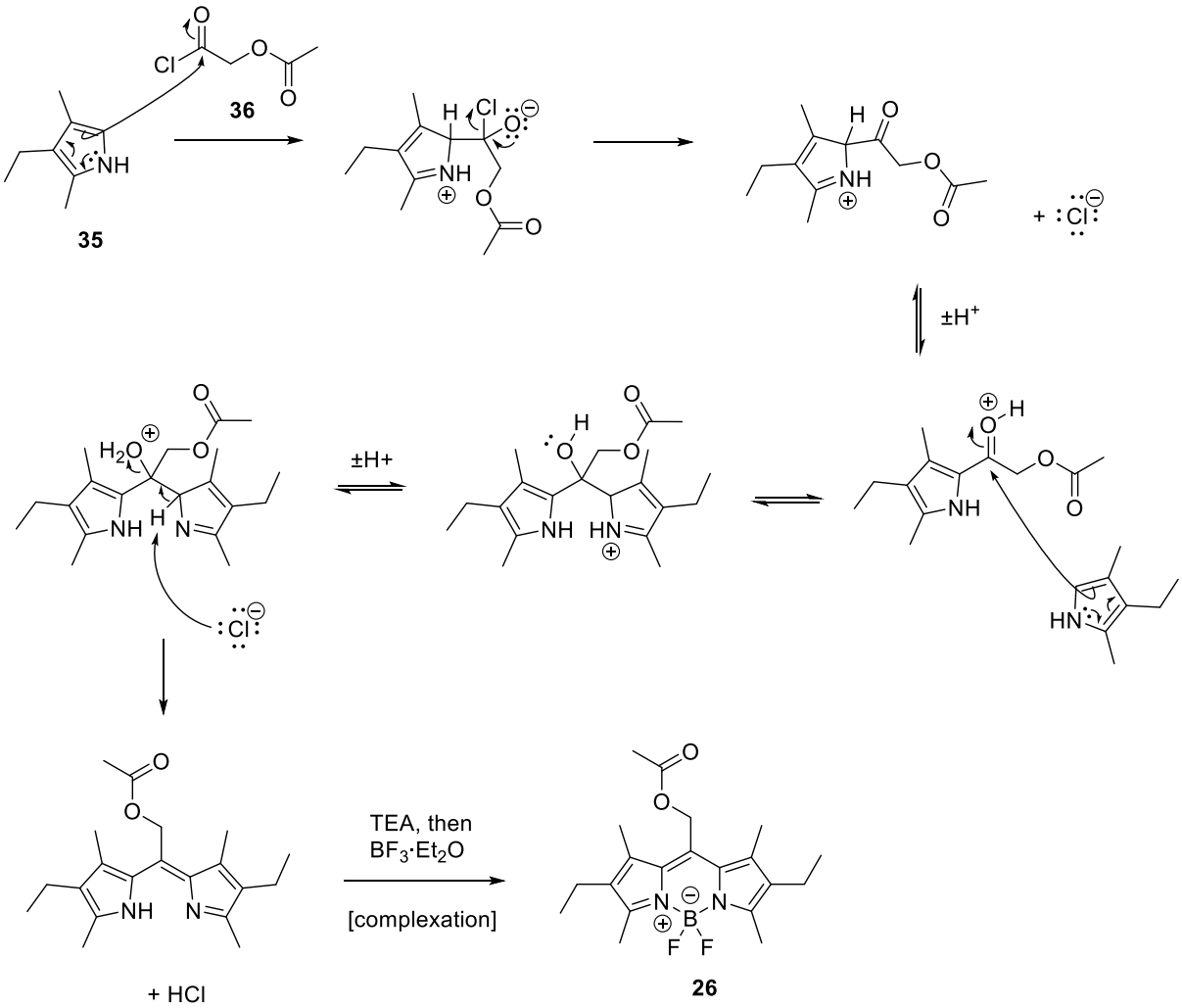

Scheme A1. A suggested mechanism for the formation of EtBODIPYOAc (**26**).

APPENDIX 2

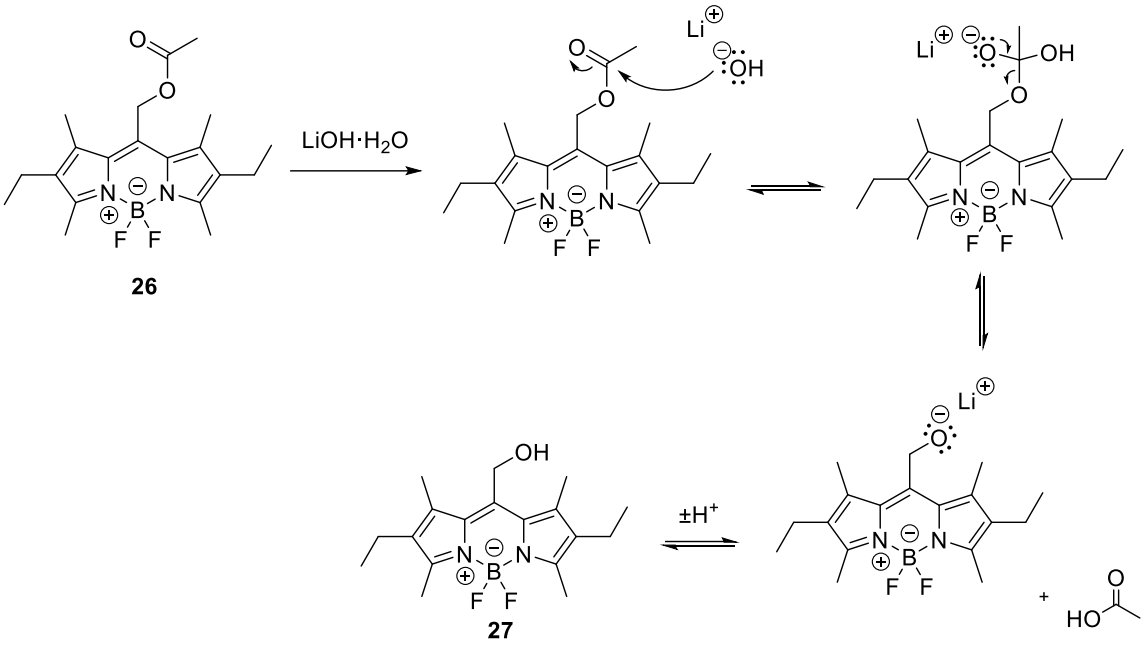

Scheme A2. A suggested mechanism for the formation of EtBODIPYOH (**27**).

APPENDIX 3

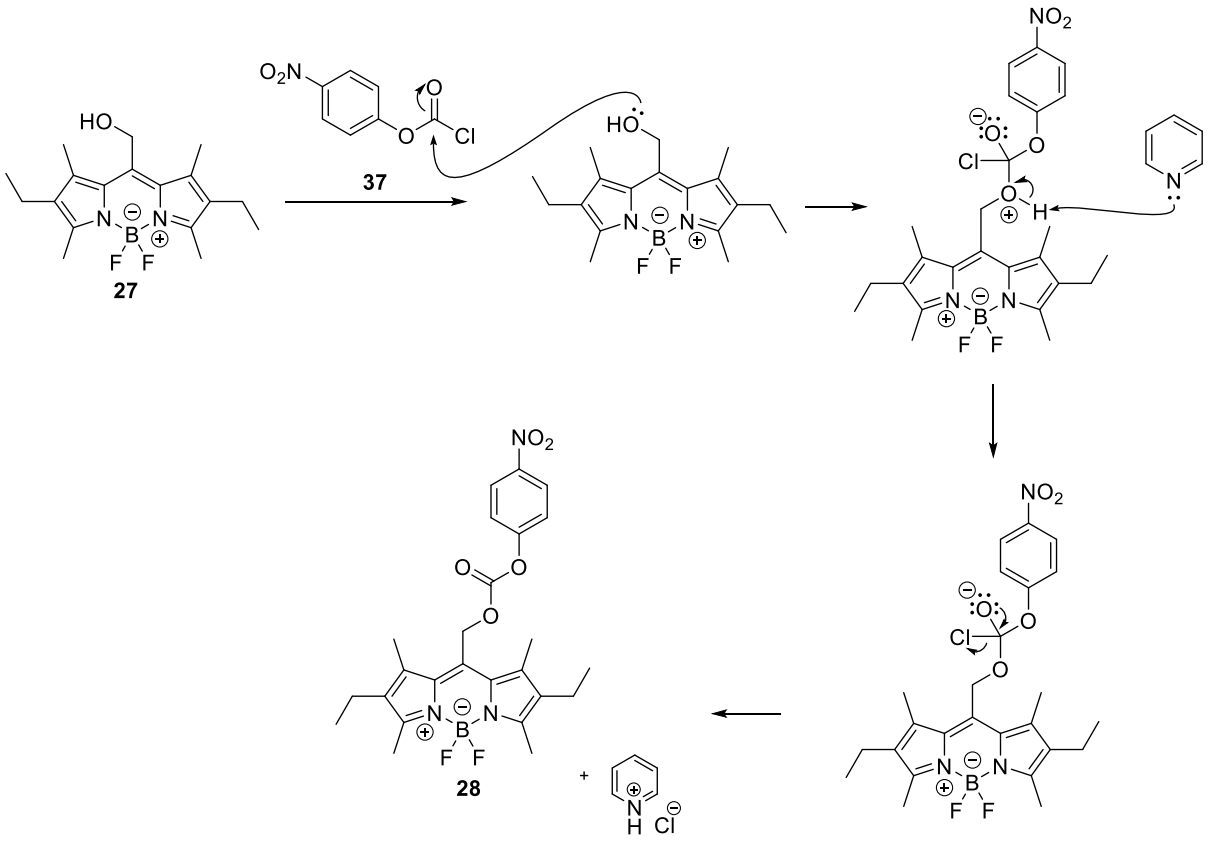

Scheme A3. A suggested mechanism for the formation of EtBODIPYPNP (**28**).

APPENDIX 4

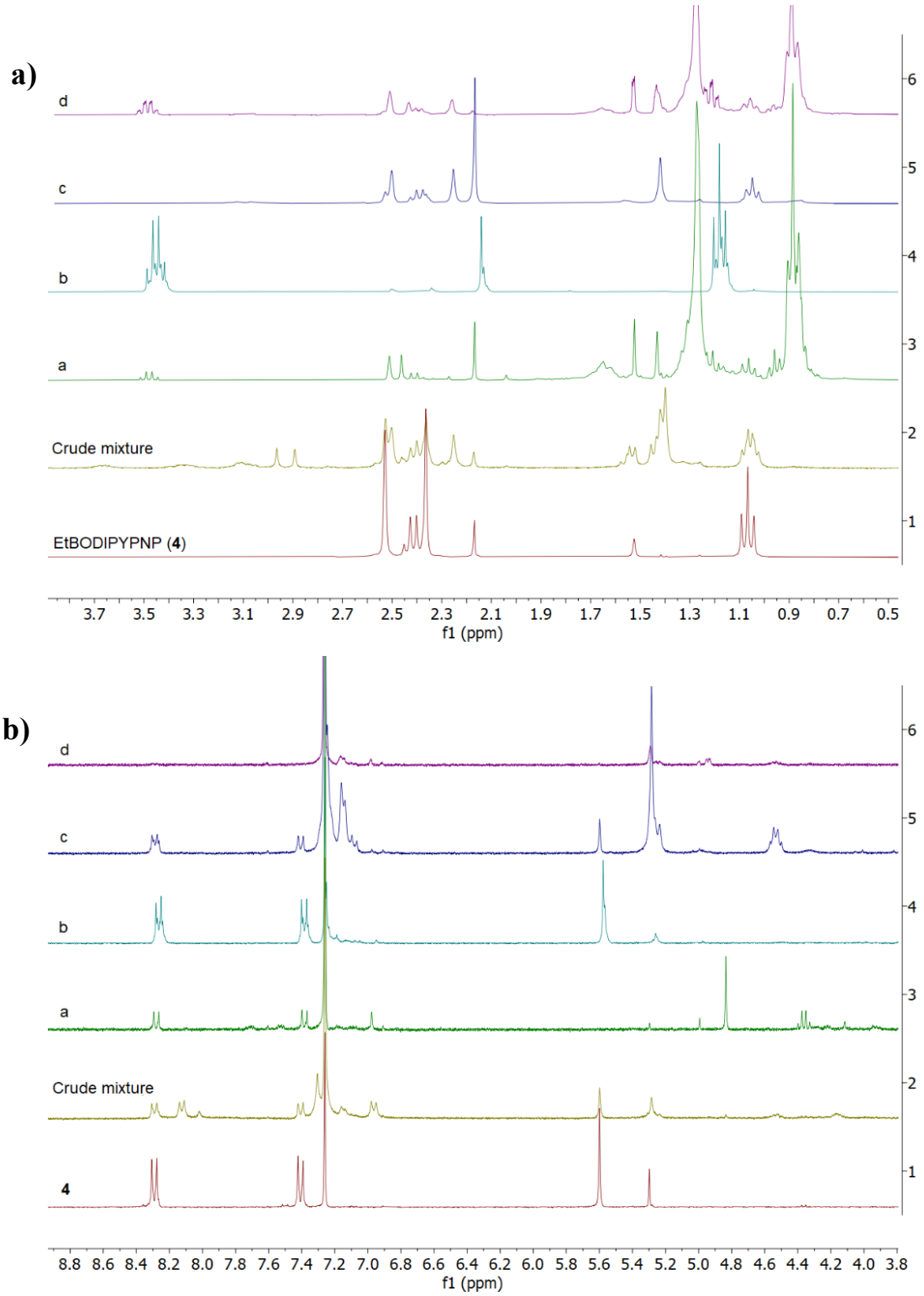

Figure A1. ^{1}H NMR spectra between a) 0-4 ppm and b) 4-9 ppm of the sections a-d obtained from the chromatographic purification of EtBODIPYPheO*t*Bu (**33A**). ^{1}H NMR spectra recorded at 300 MHz in $CDCl_3$.

APPENDIX 5

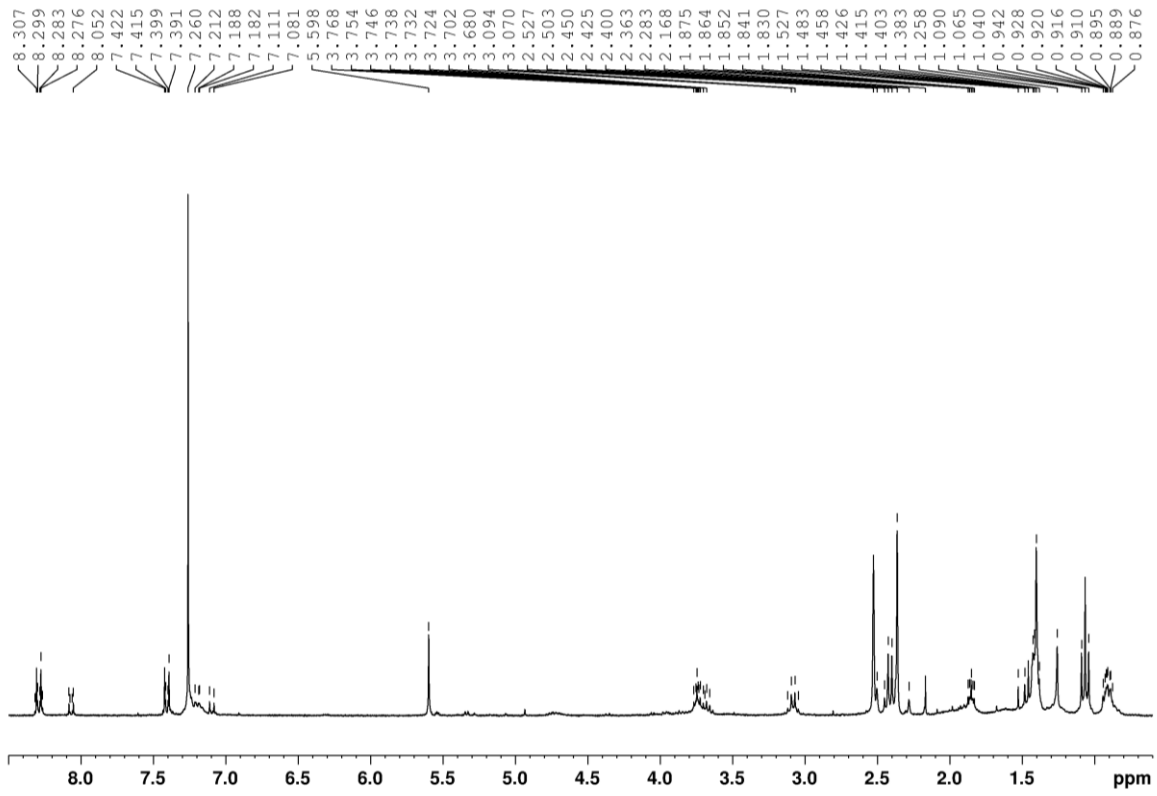

Figure A2. The crude mixture of the synthesis of EtBODIPYLeuPheO*t*Bu (**34A**). ^{1}H NMR spectrum recorded at 300 MHz in $CDCl_3$.

APPENDIX 6

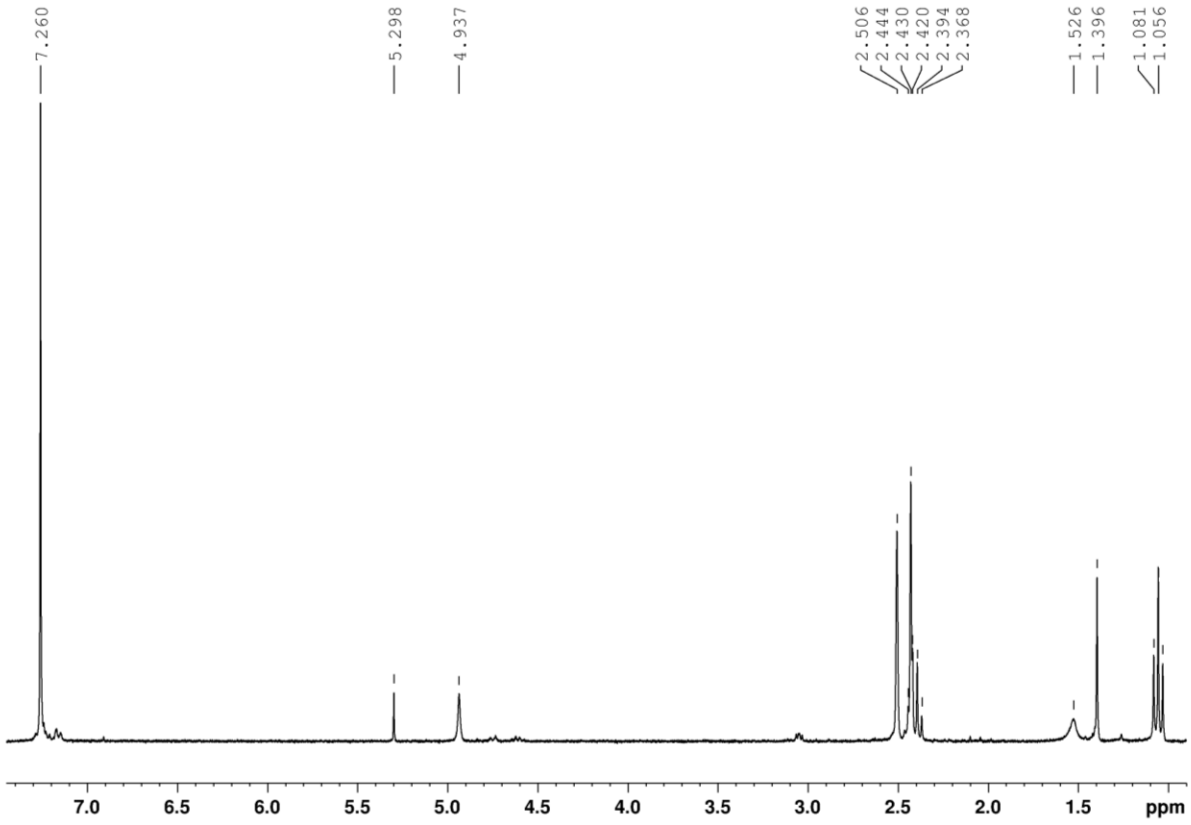

Figure A3. The crude mixture of the synthesis of EtBODIPYPheO*t*Bu (**33B**). ^{1}H NMR spectrum recorded at 300 MHz in $CDCl_3$.

APPENDIX 7

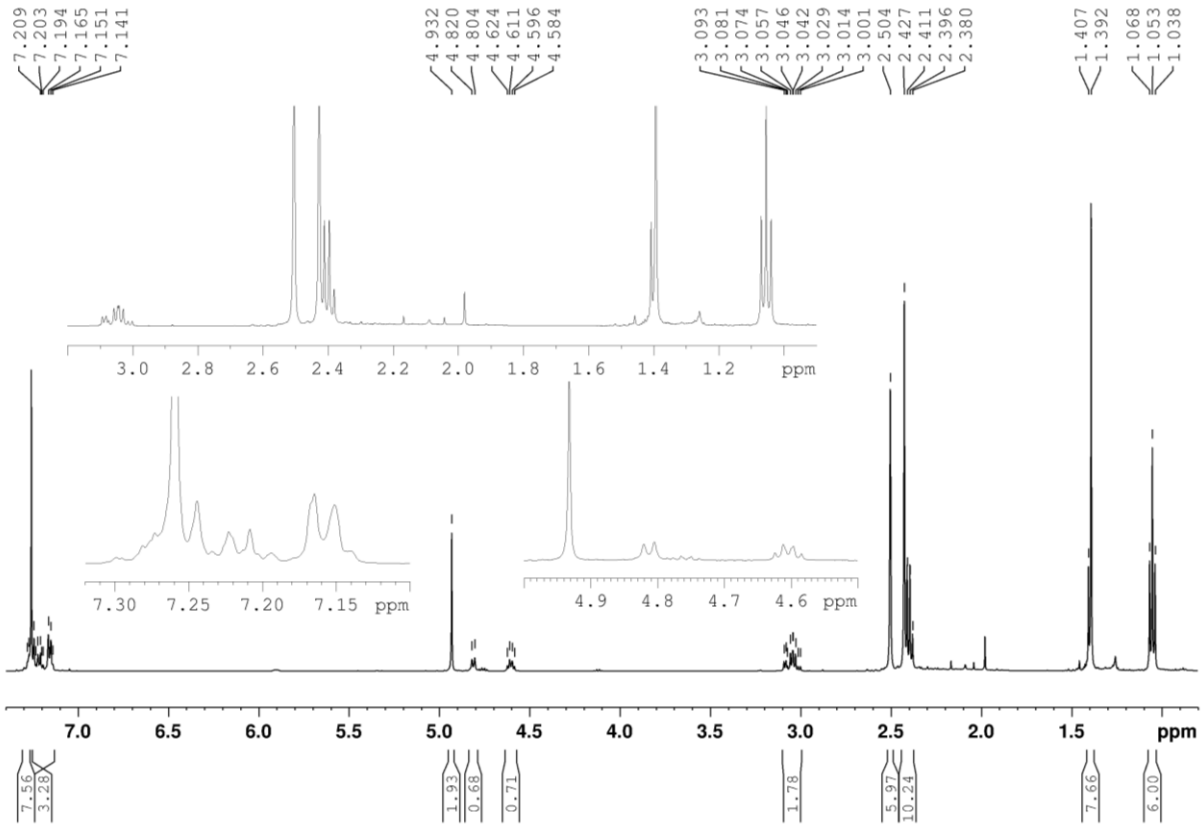

Figure A4a. EtBODIPYPheO*t*Bu (**33B**) ^{1}H NMR spectrum at 500 MHz in $CDCl_3$.

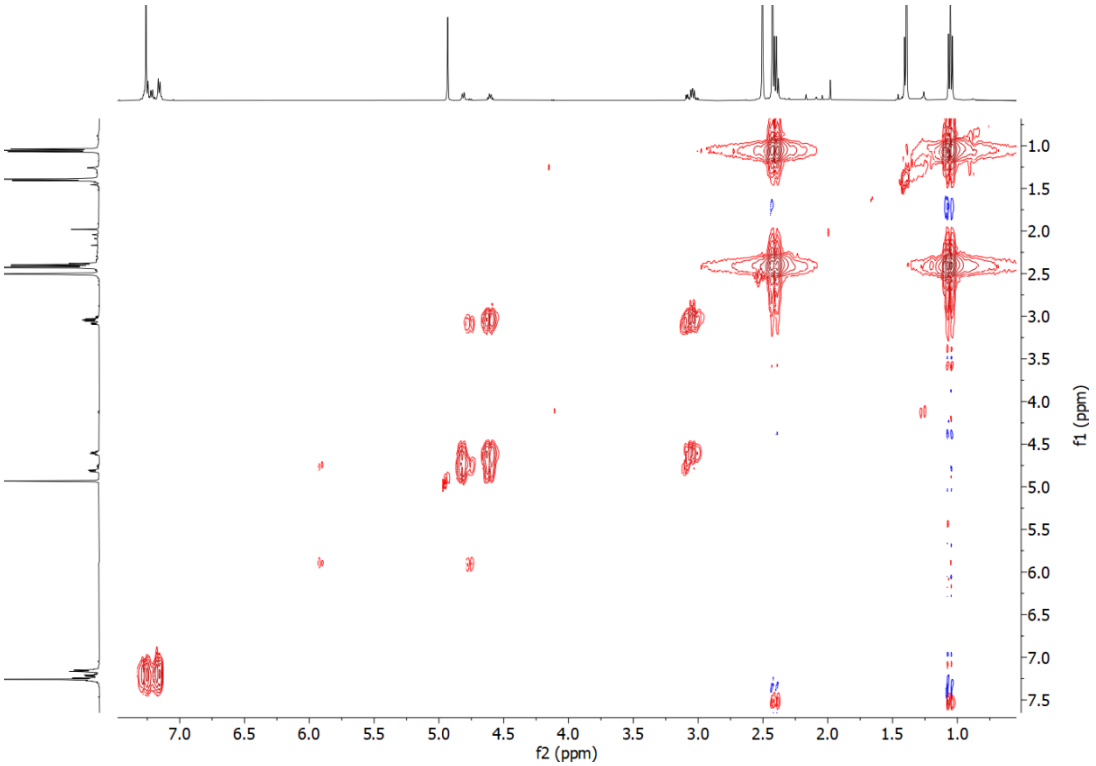

Figure A4b. EtBODIPYPheO*t*Bu (**33B**) H-H COSY NMR spectrum at 500 MHz in $CDCl_3$.

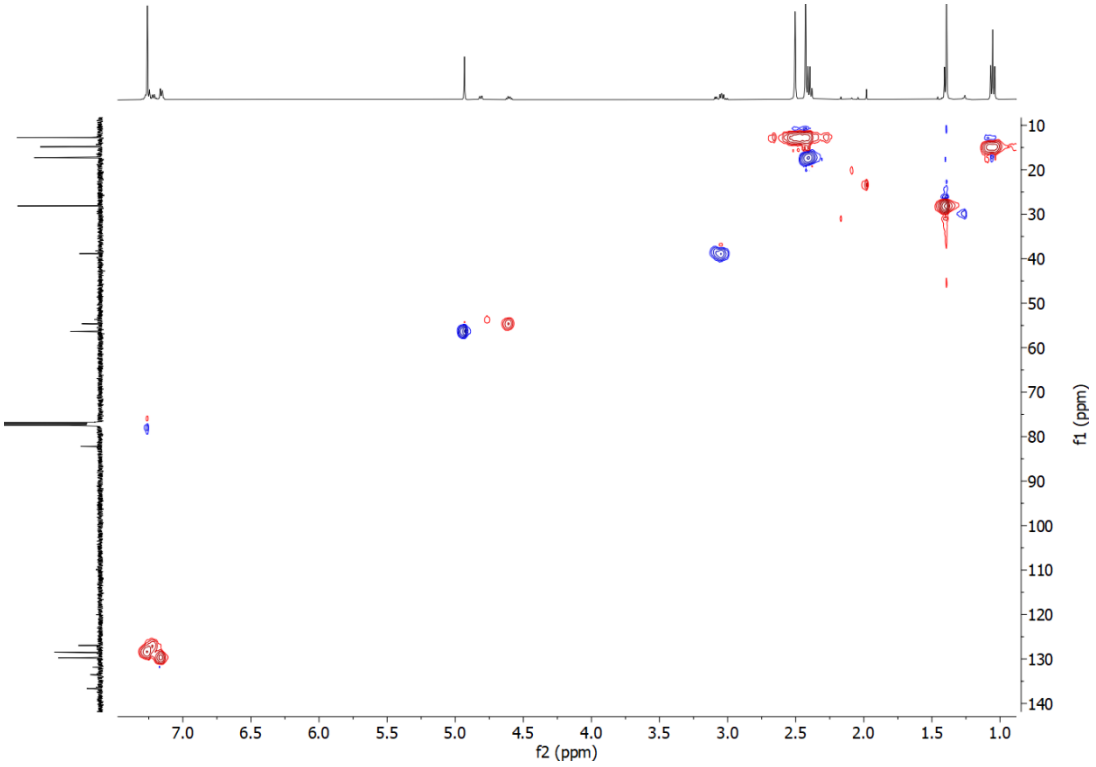

Figure A4c. EtBODIPYPheOtBu (**33B**) edited HSQC NMR spectrum at 500 MHz in $CDCl_3$. CH and CH_3 are denoted with red and CH_2 denoted with blue.

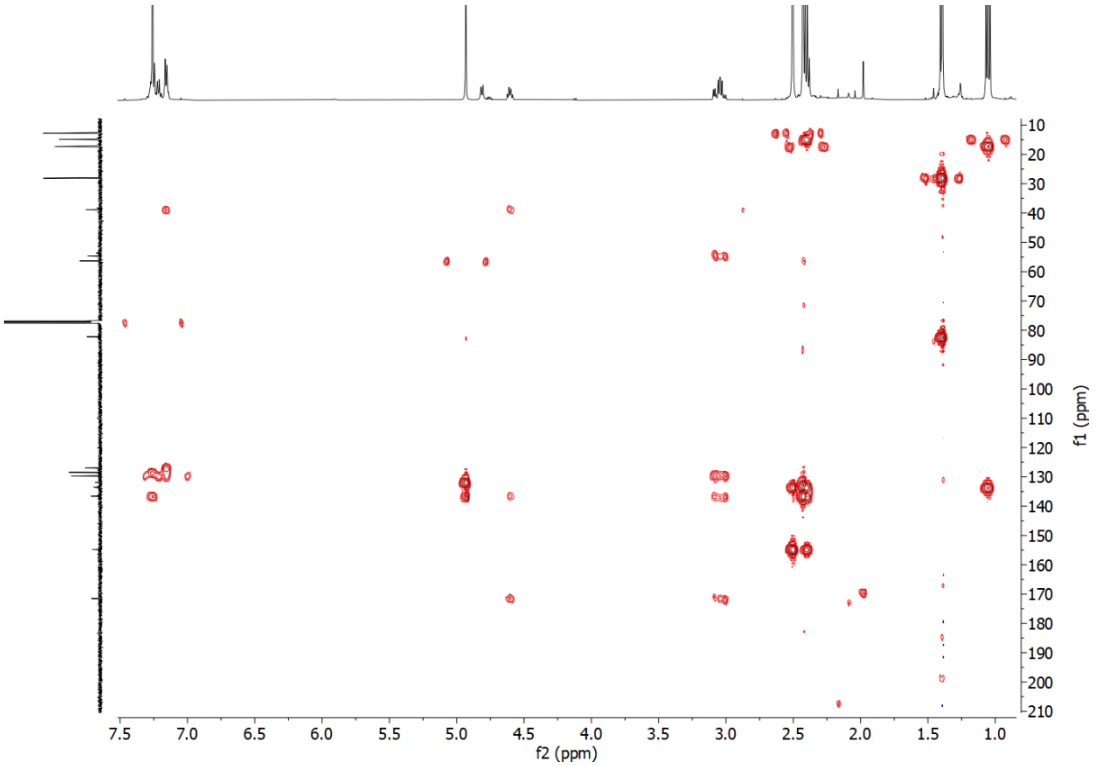

Figure A4d. EtBODIPYPheOtBu (**33B**) HMBC NMR spectrum at 500 MHz in $CDCl_3$.

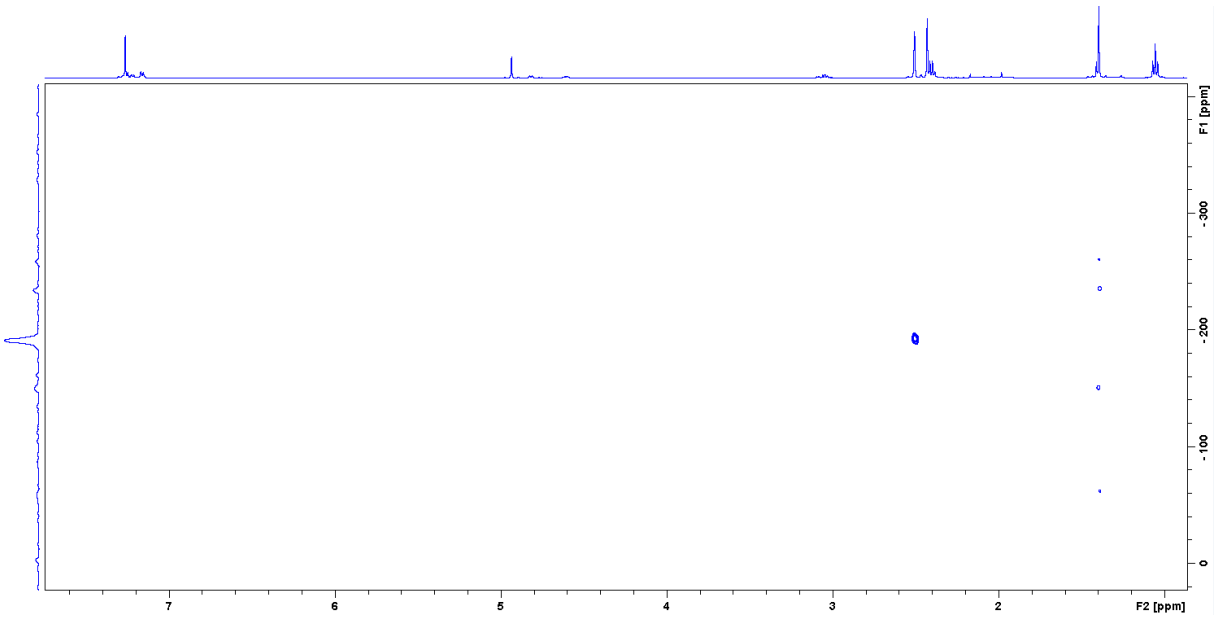

Figure A4e. EtBODIPYPheOtBu (**33B**) N-H correlation NMR spectrum at 500 MHz in $CDCl_3$.

APPENDIX 8

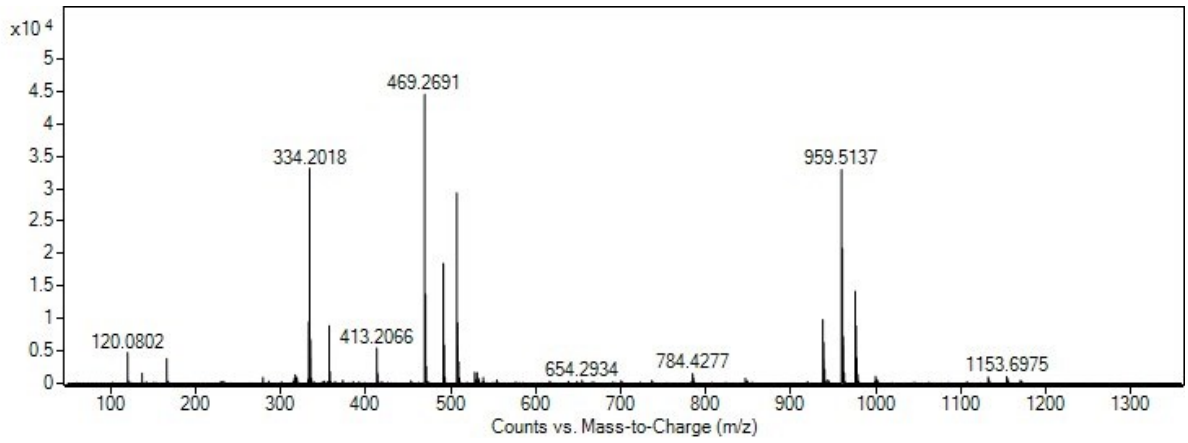

Figure A5. (+)-ESI-MS spectrum of the sample from the synthesis of compound **33B**.

Table A1. Ions of the identified compounds observed in (+)-ESI-MS spectrum

	Ion	**Molecular formula**	m/z_{theory}	m/z_{exp}
M=EtBODIPYOH (27)				
	$[M]^+$	$(C_{18}H_{25}BF_2N_2O)^+$	334.2023	334.2017
	$[M+Na]^+$	$(C_{18}H_{25}BF_2N_2ONa)^+$	357.1920	357.1438
M=PheO*t*Bu (40)	$[M-C_5H_9O_2]^+$	$(C_8H_{10}N)^+$	120.0808	120.0802
	$[M-C_4H_8]^+$	$(C_9H_{12}NO_2)^+$	166.0868	166.0857

APPENDIX 9

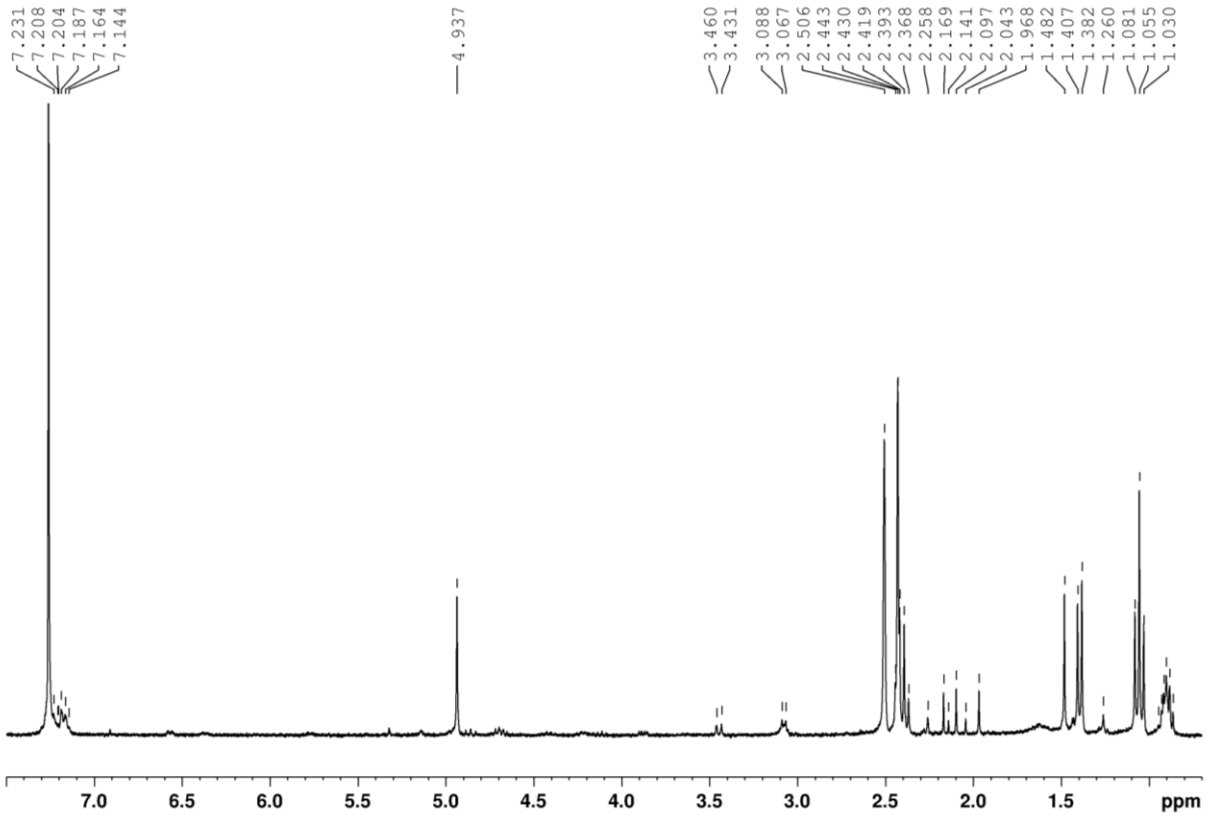

Figure A6. The crude mixture of the synthesis of EtBODIPYLeuPheO*t*Bu (**34B**). ^{1}H NMR spectrum recorded at 300 MHz in $CDCl_3$.

APPENDIX 10

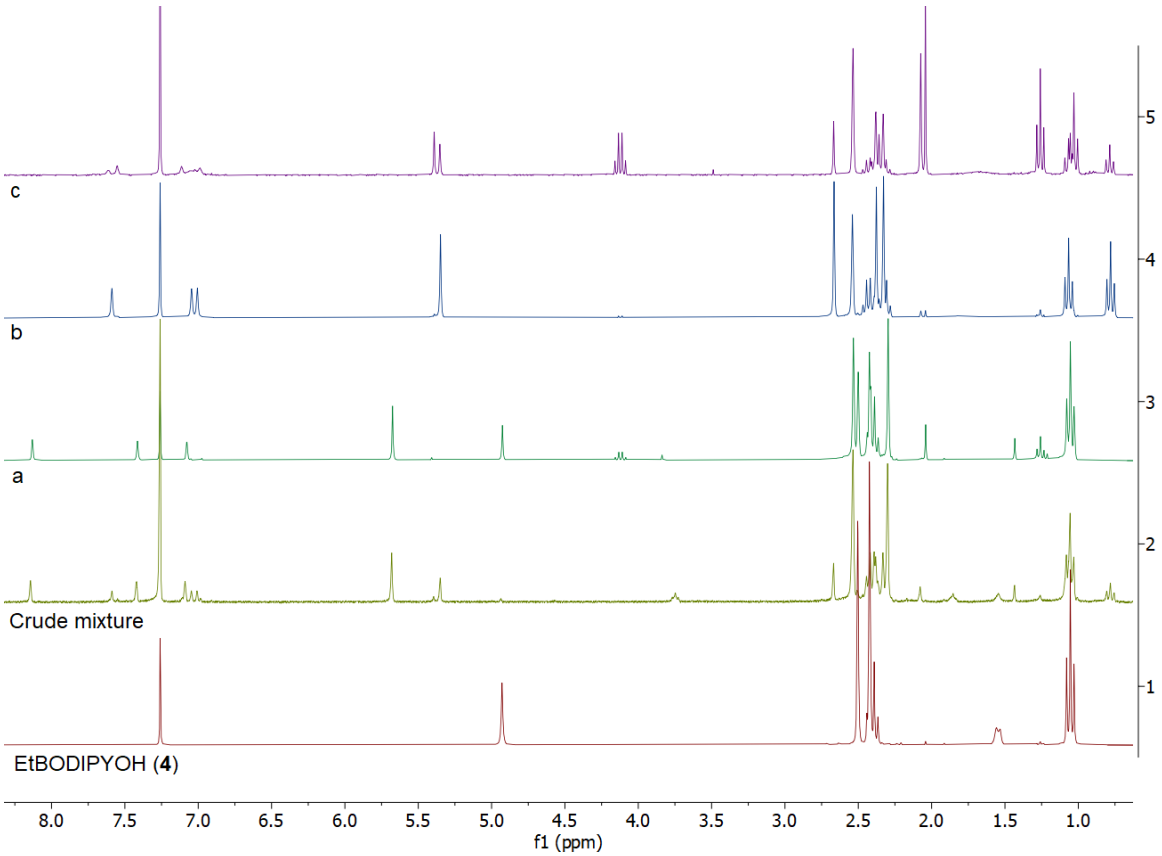

Figure A7. ^{1}H NMR spectra of the sections obtained from the chromatographic purification of the alkoxycarbonylimidazole compound **41**. ^{1}H NMR spectra recorded at 300 MHz in $CDCl_3$.